الجمهورية الجزائرية الديمقراطية الشعبية

République Algérienne Démocratique et Populaire
Ministère de L'Enseignement Supérieur et de la Recherche Scientifique

UNIVERSITÉ SETIF 1, Ferhat ABBAS

FACULTÉ DE TECHNOLOGIE

THÈSE

Présentée au Département de Génie des Procédés

Pour l'obtention du diplôme de

DOCTORAT

Domaine: Sciences et Technologie

Filière : Génie des Procédés **Option : Génie Chimique**

Par

BERAFTA MARIA

THÈME

Préparation et caractérisation des biomatériaux pour l'application à la dépollution des eaux usées.

Soutenue le 25/04/2026 devant le jury :

OUARI Kamel	**Professeur**	**Univ. Sétif 1-Ferhat ABBAS**	**Président**
KHELILI Hinda	**Professeur**	**Univ. Sétif 1-Ferhat ABBAS**	**Directeur de thèse**
GUELLAL Messaoud	**Professeur**	**Univ. Sétif 1-Ferhat ABBAS**	**Co-directeur**
KAABI Ilhem	**MCA**	**Univ. Sétif 1-Ferhat ABBAS**	**Examinateur**
OUNOKI Samira	**Professeur**	**Univ. Biskra-Mohamed khider**	**Examinateur**
ADAIKA Kaltoum	**MCA**	**Univ. Biskra-Mohamed khider**	**Examinateur**

الجمهورية الجزائرية الديمقراطية الشعبية

DEMOCRATIC AND POPULAR REPUBLIC OF ALGERIA
MINISTRY OF HIGHER EDUCATION AND SCIENTIFIC RESEARCH

Setif 1 University-Ferhat ABBAS

Faculty of technology

Thesis submitted to the Process Engineering Department for a Doctorate Degree

Domain : Science and Technology

Section: Process Engineering **Option : Chemical Engineering**

BY

BERAFTA MARIA

TITLE OF THE THESIS

Preparation and characterization of biomaterials for application in wastewater treatment.

Defended on 25/04/2026 in front of the Jury:

OUARI Kamel	**Professor**	**SETIF 1 University-Ferhat ABBAS**	**Chairman**
KHELILI Hinda	**Professor**	**SETIF 1 University-Ferhat ABBAS**	**Supervisor**
GUELLAL Messaoud	**Professor**	**SETIF 1 University-Ferhat ABBAS**	**Co-Supervisor**
KAABI Ilhem	**MCA**	**SETIF 1 University-Ferhat ABBAS**	**Examiner**
OUNOKI Samira	**Professor**	**Univ. Biskra-Mohamed khider**	**Examiner**
ADAIKA Kaltoum	**MCA**	**Univ. Biskra- Mohamed khider**	**Examiner**

Scientific publications

M. BERAFTA, H. KHELILI, M. GUELLAL, S. ACHOUR, K. KONAN, Sustainable Methylene Blue Removal Using Rosemary-Derived Activated Carbon and Green Nanoparticles. Larhyss 62 (2025) 215-241.

National Communications

M. BERAFTA, H. KHELILI, M. GUELLAL, Removing anionic dye from distilled water using a bioadsorbent, national seminar on Green Chemical Processes, Impact on the Environment and Sustainable Development GCPIESD'24.

M. BERAFTA, H. KHELILI, M. GUELLAL, Comparing the Adsorption Performance of Activated and Calcinated Fish Bone for Congo Red Removal, National Conference on Materials, Energy Environment February 13-14, 2024.

M. BERAFTA, H. KHELILI, M. GUELLAL, Decolorization of Wastewater Using Adsorbent Prepared from Fish Bone Waste, National Seminar on Bioindicators and Environmental Health May 3 – 4, 2024.

International Communications

M. BERAFTA, H. KHELILI, M. GUELLAL, Study of the kinetics and pH of the removal of Congo Red dye from aqueous media using raw and activated fish bones, International Workshop on Chemical Engineering dedicated to Catalysis (IWCE'23) December 09-10, 2023 Sétif, Algeria.

M. BERAFTA, H. KHELILI, M. GUELLAL, The effect of various factors on the removal of Congo red from water by the adsorption process using a biosorbent, International Workshop on Chemical Engineering dedicated to Catalysis (IWCE'23) December 09-10, 2023 Sétif, Algeria.

M. BERAFTA, H. KHELILI, M. GUELLAL, Effect of pH and adsorbent mass of raw fish bone on the removal of Congo red from distilled water, International Conference on Materials for Renewable Energies (ICMRE'23)

M. BERAFTA, H. KHELILI, M. GUELLAL, Study of the effect of the mass of a material adsorbing calcined fish bones on the elimination of Congo red from wastewater, International Conference on Sustainable Water Treatment Technologies and Environment, SUST-WATER2023, UDES, Algeria, 27-28th November 2023.

M. BERAFTA, H. KHELILI, M. GUELLAL, Removing cationic dye from distilled water using an activated rosemary, International Conference on Electrochemical, Sciences and Technology (ICEST2024), May 7 to 9, 2024, Setif, Algeria.

M. BERAFTA, H. KHELILI, M. GUELLAL, An iron nanoparticle (Fe-P)-derived adsorbent was utilized in an adsorption process to decolorize aqueous media, International Conference on Technological Application of Materials (ICTAM'24), October 30th and 31st, 2024, Setif , Algeria.

M. BERAFTA, H. KHELILI, M. GUELLAL, The adsorption kinetics and pH effects on Methylene blue dye removal from aqueous solutions were examined using iron nanoparticles (Fe-P) as the adsorbent material, International Conference on Chemical Engineering for Oil and Gas Industry ICCE "24-OGI

November 26-27,2024, Setif, Algeria.

Acknowledgements

First and foremost, I would like to express my deepest gratitude to Allah Almighty, whose guidance, mercy, and blessings have granted me the strength, patience, and determination to complete this research work. Without His divine support, none of this would have been possible.

I would also like to extend my sincere appreciation to my thesis supervisor, ***Pr. Hinda Khelili****, for her continuous guidance, valuable advice, and unwavering support throughout every stage of this study. Her insightful supervision and expertise have been instrumental in the successful completion of this thesis.*

I would like to express my sincere gratitude to my co-supervisor and laboratory manager,

Pr. Messaoud GUELLAL*, for his valuable guidance, insightful suggestions, and continuous encouragement throughout the preparation and completion of this thesis. His support and supervision have been greatly appreciated.*

I am particularly honored by the acceptance of ***Pr. Kamel OUARI*** *to chair the jury for my defense. I warmly thank him for the time he has generously dedicated to evaluating this work and for the thoroughness and care he brings to this role*

I would like to sincerely thank all the members of the jury: ***Pr. Samira OUNOKI, Dr. Ilham KAABI****, and* ***Dr. Kaltoum ADAIKA****. I am deeply grateful for your careful review, constructive feedback, and insightful comments, which will undoubtedly enhance the quality of this research*

I would also like to express my sincere appreciation to the laboratory engineers of the Process Engineering Department for providing the necessary equipment and materials required to carry out the experimental work of this research.

I would like to extend my heartfelt thanks to the entire team of the Chemical Process Engineering Laboratory (LGPC) at the University of Sétif 1 for their valuable collaboration

and technical assistance, which greatly contributed to the successful completion of my experimental work.

I wish to convey my deepest gratitude to my beloved parents, ***Bachir*** *and* ***Hasina****, whose unconditional love, constant encouragement, and countless sacrifices have been the foundation of all my achievements. Their support has been an endless source of strength and inspiration throughout my academic journey.*

*I would also like to express my heartfelt appreciation to my sisters, Asma****, Basmala, and Tasnim****, and to my brother* ***Aymen*** *and his wife* ***Roea****, for their constant encouragement, affection, and uplifting presence. Your love and support have been a true source of comfort and motivation throughout this journey.*

I would like to express my deep gratitude to my husband ***Mohamed*** *for his constant support and encouragement throughout this journey.*

I would also like to express my heartfelt appreciation to my parents-in-law, ***Djamel and Khaira****, for their constant encouragement and unwavering support throughout this journey.*

I would also like to express my heartfelt gratitude to my ***family, friends, and colleagues*** *for their unwavering support, encouragement, and trust throughout this journey. Each of you has played an important role in the realization of this work, and I am deeply thankful for your presence and belief in me.*

Thank you to all

Dedication

With deep gratitude to God for His guidance and blessings,

I dedicate this work to all those who are dear to me and to everyone who, directly or indirectly, contributed to the realization of this work.

List of figures

List of Tables

Abbreviations List

ACRu Activated calcinated Ruta graveolens

AFB Activated fish bone

AR Activated rosemary

CFB Calcinated fish bone

CR Congo Red

EDX Energy-dispersive X-ray spectroscopy

$FeCl_3 \cdot 6H_2O$ Iron (III) chloride hexahydrate

Fe-P Iron nanoparticles

FTIR Fourier transform infrared

HCl Hydrochloric acid

H_3PO_4 Phosphoric acid

MB Methylene blue

NaOH Sodium hydroxide

pH_{pzc} Point of zero charge

R Rosemary powder

RFB Raw fish bone

Ru Ruta graveolens

SEM Scanning electron microscopy

TGA Thermogravimetric Analysis

XRD X-ray diffraction

$Zn(CH_3COO)_2 \cdot 2H_2O$ Zinc acetate dihydrate

ZnO-ACRu Zinc oxide-modified activated calcinated Ruta graveolens

Chapter I: Bibliographic Study

Chapter II: Preparation and Characterization Methods

Chapter III: Sustainable Methylene Blue Removal Using Rosemary -Derived Activated Carbon and Green Nanoparticles

Chapter IV: Activated and Zinc Oxide-Modified Ruta graveolens Adsorbents for Congo Red Dye Removal

Chapter V: Preparation and Characterization of Fish Bone -Based Adsorbents for Congo Red Dye Removal

General introduction

General introduction

The widespread use of synthetic dyes across numerous industries such as textiles, food, cosmetics, and pharmaceuticals has led to significant environmental challenges due to the discharge of dye-laden industrial effluents into natural water bodies [1]. These dyes, known for their vibrant color and stable, non-biodegradable aromatic structures, pose serious threats to aquatic ecosystems and human health even at low concentrations [2]. At the same time, the growing global population and increasing agricultural and industrial activities have escalated the demand for freshwater, placing immense pressure on natural water resources [3]. As a result, the preservation of water quality and the development of innovative wastewater treatment technologies have become critical environmental priorities to ensure sustainable development and safeguard public health [4].

Although significant progress has been made in wastewater treatment technologies, a substantial portion, approximately 40%, of contaminated water, still bypasses proper treatment and is released directly into natural ecosystems [5]. This untreated discharge contributes to the buildup of persistent and non-biodegradable pollutants [6]. Traditional treatment approaches, whether based on physical, chemical, or biological methods, often fall short of completely removing contaminants and tend to shift pollutants from one form to another, such as concentrating them into sludge [7]. Rather than eliminating the problem, this merely relocates it, raising environmental and sustainability concerns [8]. One of the most critical issues in this context is the treatment of dye-contaminated effluents, as synthetic dyes are notably toxic and resistant to breakdown [9]. Various methods such as oxidation, membrane filtration, coagulation-flocculation, and adsorption have been proposed to address this challenge [10]. Among these, adsorption is particularly valued for its operational simplicity, cost-effectiveness, and capacity to remove even low concentrations of dyes without creating harmful residues [11]. Activated carbon, widely used in adsorption processes for its excellent removal capabilities, is nonetheless constrained by high production costs linked to its reliance on non-renewable resources like coal [12]. As a result, there has been growing interest in the development of alternative adsorbents that are not only low-cost and readily available but also environmentally friendly and efficient. Recent research has increasingly focused on utilizing waste-derived or natural materials as promising substitutes for commercial activated carbon, aiming to offer sustainable and affordable options for wastewater treatment [13].

In this study, we investigate the potential of Rosemary (Rosmarinus officinalis) and Rue (Ruta graveolens) as low-cost adsorbents. These two plants are aromatic medicinal species

traditionally used for their diverse therapeutic properties. Rosemary is well known for its antioxidant, antimicrobial, and neuroprotective effects [14,15], while Rue has been employed for its antispasmodic, anthelmintic, and anti-inflammatory activities [16,17]. Both plants are rich in bioactive compounds such as essential oils, flavonoids, alkaloids, and tannins, which contribute to their biological efficacy [18]. In recent years, increasing attention has been directed towards the application of plant-based materials in wastewater treatment, particularly as eco-friendly and cost-effective alternatives to conventional chemical treatments. Extracts of R. officinalis and R. graveolens have shown promising potential in this context, due to their ability to degrade organic pollutants, inhibit pathogenic microorganisms, and adsorb heavy metals [15,16, 19].

In parallel with plant-based solutions, this study also explores the use of fish bones as another abundant and low-cost biosorbent. Fish bones are a type of biowaste generated by the seafood processing industry, primarily composed of calcium phosphate in the form of hydroxyapatite ($Ca_{10}(PO_4)_6(OH)_2$) [20]. Due to their high surface area, porosity, and ion-exchange capacity, fish bones have gained attention as a sustainable and economical adsorbent for wastewater treatment applications, particularly in the removal of heavy metals such as lead (Pb^{2+}), cadmium (Cd^{2+}), and zinc (Zn^{2+}), as well as phosphate, nitrate, and dyes from contaminated water [21,22]. Their effectiveness can be further enhanced through thermal or chemical activation, which improves adsorption efficiency and material stability in aqueous environments [23]. The valorization of fish bones not only contributes to pollution control but also supports circular economy principles by converting waste into valuable materials for environmental remediation [24].

This work was conducted at the Chemical Process Engineering Laboratory (LGPC), Sétif-1 University, with the objective of valorizing selected agricultural and animal waste materials through the synthesis of novel adsorbents, aiming to efficiently remove the cationic dye Methylene Blue and the anionic dye Congo Red from wastewater.

This thesis is organized into four chapters.

Chapter I presents a comprehensive overview of water pollution, exploring its primary sources and key contaminants, with a specific focus on dye-related pollution. Particular attention is given to the various treatment technologies available, highlighting adsorption as a promising and widely studied method for pollutant removal.

Chapter II presents the main methods used for the preparation of adsorbent materials and dye solutions, along with the principal characterization techniques (FTIR, XRD, SEM, EDX, TGA, and pH_{pzc}) and UV–Visible analysis.

Chapter III examines the effectiveness of adsorbents derived from rosemary, including phosphoric-acid-activated rosemary (AR) and iron–polyphenol nanoparticles (Fe-P), for the removal of Methylene Blue (MB) dye from wastewater.

Chapter IV examines the removal efficiency of Congo Red dye from aqueous solutions using Ruta graveolens-based adsorbents, namely activated calcinated Ruta graveolens (ACRu) and zinc oxide-modified ACRu (ZnO-ACRu).

Chapter V investigates the effectiveness of raw fish bone (RFB), phosphoric acid-activated fish bone (AFB), and calcined fish bone (CFB) as adsorbents for the removal of Congo Red dye from aqueous solutions.

Finally, the general conclusion summarizes the main findings of this work.

Bibliographic references

[1] C. Arora, P. Kumar, S. Soni, J. Mittal, A. Mittal, B. Singh, Efficient removal of malachite green dye from aqueous solution using Curcuma caesia-based activated carbon. Desalination and Water Treatment, 195 (2020) 341–352.

[2] M. Yagub, T.K. Sen, S. Afroze, Dye and its removal from aqueous solution by adsorption: a review. Advances in Colloid and Interface Science, 209 (2014) 172–184.

[3] UN Water, World Water Development Report: Water and Climate Change. La Houille Blanche (2020).

[4] G. Ssekyanzi, M.J. Ahmad, K.-S. Choi, Sustainable solutions for mitigating water scarcity in developing countries: A comprehensive review of innovative rainwater storage systems. Water, 16 (2024) 2394.

[5] H. Trabelsi, Étude de la dégradabilité et de la toxicité des colorants par ozonation et photocatalyse, PhD Thesis, Yahia Fares University of Medea, Medea, Algeria, (2014).

[6] B. Rani, S. Kumar, S. Bisht, Wastewater generation and treatment: A review. International Journal of Environmental Sciences, 10(1) (2020) 1–8.

[7] N. Sharma, A. Singh, N. Batra, Modern and emerging methods of wastewater treatment. In: V. Achal, A. Mukherjee (Eds.), Ecological Wisdom Inspired Restoration Engineering, Springer Singapore, Singapore, (2019) 223–247.

[8] L.K. Wang, Y.T. Hung, N.K. Shammas, Physicochemical Treatment Processes, 3 (2005) 3141–3197.

[9] S. Rahmani, B. Zeynizadeh, S. Karami, Removal of cationic methylene blue dye using magnetic and anionic-cationic modified montmorillonite: kinetic, isotherm and thermodynamic studies. Applied Clay Science, 184 (2020) 105391.

[10] M. Nasrullah, L. Singh, A.W. Zularisam, A review on recent developments in the removal of synthetic dyes from wastewater. Journal of Environmental Chemical Engineering, 11(2) (2023) 109224.

[11] J. Mittal, R. Ahmad, A. Mittal, Kahwa tea (Camellia sinensis) carbon — a novel and green low-cost adsorbent for the sequestration of titan yellow dye from its aqueous solutions. Desalination and Water Treatment, 227 (2021) 404–411.

[12] A. Mittal, R. Jain, J. Mittal, S. Varshney, S. Sikarwar, Removal of Yellow ME 7 GL from industrial effluent using electrochemical and adsorption techniques. International Journal of Environment and Pollution, 43 (2010) 308–323.

[13] Y. Zhou, J. Lu, Y. Zhou, Y. Liu, Recent advances for dye removal using novel adsorbents: a review. Environmental Pollution, 252 (2019) 352–365.

[14] R. Ahmad, et al., Phytochemical-assisted removal of organic pollutants using Rosmarinus officinalis extracts. Environmental Technology & Innovation, 21 (2021) 101275.

[15] Y. Zhang, et al., Plant polyphenols as green agents for wastewater treatment: mechanisms and applications. Journal of Cleaner Production, 395 (2023) 136382.

[16] X. López-Martínez, et al., Potential of Ruta graveolens for phytoremediation: uptake of heavy metals and antimicrobial properties. Journal of Environmental Chemical Engineering, 8(4) (2020) 103873.

[17] P. Sharma, M. Khan, A review on traditional medicinal uses and pharmacological properties of Ruta graveolens. Biomedicine & Pharmacotherapy, 150 (2022) 113053.

[18] M.A. Khan, et al., Phytochemical composition and bioactivities of Rosmarinus officinalis: a comprehensive review. Arabian Journal of Chemistry, 14(3) (2012) 102901.

[19] N.E. El-Hefny, et al., Utilization of natural plant extracts for the treatment of industrial wastewater: efficacy and mechanisms. Ecotoxicology and Environmental Safety, 242 (2022) 113922.

[20] Y. Wang, et al., Efficient removal of heavy metals from aqueous solutions using modified fish bone-derived hydroxyapatite. Journal of Environmental Management, 317 (2022) 115406.

[21] I. Ali, et al., Valorization of fish waste: hydroxyapatite-based adsorbents for wastewater remediation. Environmental Research, 215 (2023) 114378.

[22] L. Chen, et al., Adsorptive removal of phosphate and nitrate from wastewater using thermally treated fish bone. Journal of Cleaner Production, 278 (2021) 123875.

[23] A. El-Sayed, H. Hassan, Biogenic hydroxyapatite derived from fish bones as a sustainable adsorbent for dye and metal ion removal. Environmental Science and Pollution Research, 27(24) (2020) 30318–30329.

[24] O.S. Ayanda, et al., Circular economic approach to fish bone waste utilization in water purification: a review. Sustainable Chemistry and Pharmacy, 32 (2023) 100947.

Chapiter I

Bibliographic Study

Sommaire

1. Introduction

Water pollution, particularly from industrial dyes and colored effluents, represents a critical challenge in our global environmental crisis. As industries continue to expand worldwide, the discharge of colored wastewater has become an increasingly urgent environmental threat requiring innovative and effective treatment.

This chapter provides a comprehensive overview of Water Contamination, with a specific focus on dye-related pollution, we explore various treatment methodologies, focusing primarily on adsorption technology as a promising solution. We also present the different pollutants and adsorbents used in this work.

2. Definition of wastewater

Wastewater is water that has undergone unfavorable modification of its physicochemical and biological properties, produced directly or indirectly by human activities, making it unsuitable for established normal use [1]. Wastewater includes all water from domestic, agricultural, and industrial activities loaded with toxic substances that reach the sewage systems. Wastewater also encompasses rainwater and its pollutant load, causing all kinds of pollution and nuisance to the receiving environment [1,2].

2.1. Foundation of Water Contamination Problems

Amid accelerating economic development and demographic surge, safeguarding aquatic resources has emerged as a critical imperative [3]. The escalating water consumption needs, intensified by swift metropolitan expansion and industrial proliferation, are exerting tremendous strain on existing supplies [4]. Daily discharge of roughly 2 million tons of contaminants from diverse manufacturing, farming, and household origins flows into water systems [5]. These unregulated releases encompass poisonous substances, biodegradable matter [6], metallic toxins [7], and additional pollutants that drastically undermine water purity. Such deterioration of potable water sources results in catastrophic health implications, with water-related illnesses claiming thousands of lives each day, particularly affecting the world's most disadvantaged areas [8]. The crisis proves especially severe across emerging nations, where purification facilities frequently lack adequate capacity to address mounting contamination levels. Nevertheless, industrialized regions face similar challenges; aggressive manufacturing operations and farming methods equally threaten both underground aquifers and open water sources [9]. Confronting this predicament demands immediate reform and reinforcement of aquatic resource governance frameworks, prioritizing contamination avoidance, effluent processing, and ecosystem conservation. Such frameworks require holistic and coordinated approaches, engaging governmental bodies alongside industrial sectors, community groups, and global institutions. Within the extensive array of water contamination sources, synthetic colorants [10] utilized across textile manufacturing and additional production sectors present an especially pernicious hazard. These pigments, frequently resistant to natural decomposition, remain active within environmental systems for prolonged durations [11], transforming water appearance while blocking crucial solar radiation needed for underwater plant metabolism [12]. Their accumulation threatens marine life through toxic exposure, destabilizing natural habitats and enabling hazardous materials to concentrate throughout biological networks [13]. Synthetic colorants may harbor cancer-causing and gene-altering substances, thus elevate human health dangers when infiltrate potable supplies. Addressing such contamination necessitates sophisticated purification methods coupled with rigid controls governing application and environmental release of these materials.

3. Environmental Release and Impact of Synthetic Dyes

The widespread manufacturing and utilization of synthetic dyes inevitably leads to their release into environmental systems through various pathways. Industrial discharge represents the

primary source of dye contamination, with manufacturing facilities and processing plants releasing these compounds through their wastewater streams [14]. Current estimates indicate that production losses typically range from 1-2%, while application processes result in 1-10% waste generation. The textile sector, particularly in reactive dye applications, experiences approximately 4% loss rates during processing operations.

The environmental presence of synthetic dyes creates both aesthetic and ecological concerns. Water bodies can exhibit visible discoloration at concentrations as low as 1 mg/dm³, fundamentally altering the visual characteristics and transparency of affected waters. This threshold demonstrates the potent coloring capacity of these compounds and their ability to impact aquatic environments even at relatively low concentrations.

The extensive scale of dye production and consumption translates into significant environmental burden beyond mere aesthetic degradation. These synthetic compounds pose substantial health risks to both human populations and ecological systems. While contemporary industrial practices increasingly emphasize environmental stewardship [15] and implement water conservation strategies with reduced wastewater generation [16,17], the continued release of substantial quantities of synthetic dyes into natural systems remains a persistent challenge.

The environmental fate and toxicological effects of these pollutants have been subject to comprehensive investigation [18-21]. Despite extensive research efforts, our understanding of the complete spectrum of biological effects remains limited. The carcinogenic potential, mutagenic properties, and antimicrobial activities of many dye compounds require further elucidation, particularly given the vast array of chemical structures currently in commercial use.

This knowledge gap presents ongoing challenges for environmental scientists and regulatory bodies, as the diversity of synthetic dye formulations continues to expand with technological advancement. The development of comprehensive risk assessment frameworks requires detailed understanding of each compound's environmental behavior and biological interactions, a task complicated by the chemical complexity and variety of modern dye formulations [14].

3.1. Types of Synthetic Dyes

Manufactured chromophores represent chemically engineered compounds synthesized through industrial processes, finding extensive application across diverse sectors including textile manufacturing, personal care products, and food processing [22]. These laboratory-produced colorants demonstrate enhanced luminosity and chemical resilience when compared to their

naturally occurring counterparts. The fundamental categorization of these compounds depends on their electronic charge distribution and substrate interaction mechanisms, dividing them into charged and neutral molecular species [23]. Charged colorant molecules function through electrostatic mechanisms, existing in either electron-deficient (cationic) [24] or electron-rich (anionic) [25] states. Electron-deficient colorants, characterized by their positive charge distribution, demonstrate particular affinity for substrates bearing negative surface charges, including synthetic acrylic materials and specialized paper formulations [26]. The binding mechanism involves coulombic attraction between the positively charged dye molecules and negatively charged substrate functional groups, resulting in robust molecular adhesion. These compounds achieve substrate attachment through electrostatic coupling, establishing durable associations with oppositely charged material surfaces [27].

Conversely, electron-rich colorants maintain negative charge characteristics and exhibit selective binding to positively charged substrate surfaces, particularly natural protein and cellulose fibers such as cotton and wool materials. The attachment process occurs through electrostatic bridging between the negatively charged dye molecules and positively charged substrate sites [28]. Charge-neutral colorant molecules operate without net electrical charge distribution across their molecular structure [29]. These compounds depend on secondary intermolecular forces including London dispersion forces, hydrogen bonding networks, and hydrophobic association mechanisms for substrate adhesion [30]. Electroneutral dyes find particular utility in treating substrates with neutral surface characteristics or materials that resist interaction with charged molecular species. Their molecular design provides exceptional adaptability regarding substrate compatibility, enabling application across diverse material categories with varying surface properties [31].

Table I.1. Types and Categories of Synthetic Dyes.

Chromophore		**Auxochrome**
Anionic	Cationic	*Azo
*Acide	*Basic	*Disperse
*Reactive		*Sulphur
*Direct		*Vat
*Mordent		*Solvent

3.2. The studied dye molecules

Our research concentrates on examining two essential dyes: Congo Red and Methylene Blue. Given the limited available data and research gaps concerning these specific dyes, we have systematically evaluated and summarized the current scientific understanding of both molecules.

3.2.1. Background information about Congo Red (CR)

Congo Red (CR) is a significant anionic dye used in various industries. It is highly toxic. Direct skin contact can cause dermatological issues and severe allergic reactions. If inhaled, it can lead to respiratory problems and chest pain. Ingestion causes gastrointestinal distress, vomiting, and in severe cases, can be carcinogenic. Its chemical structure contains a benzidine base, which makes it particularly hazardous to human health. CR can also cross the blood-brain barrier, potentially causing neurological complications [32]. Congo red contains two azo-type chromophores, consisting of double-bonded nitrogen pairs with various substituents. As an anionic dye, it has a strong affinity for basic substrates and forms stable ionic bonds. Some chemical and physical properties of Rouge Congo are presented in Table I.2.

Table I.2. Chemical and physical properties of Rouge Congo [33]

Molecular structure	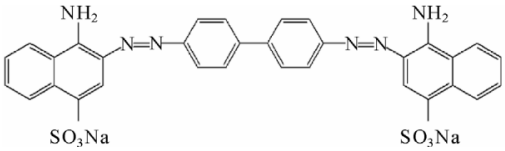
Molecular formula	$C_{32}H_{22}N_6Na_2O_6S_2$
Molecular weight (g/mol)	696.66
Family	Azo dyes
Synonyms	Bis-1-naphthylamine-4-sulfonic acid sodium salt diazo benzidine
Melting point (°C)	360
Solubility in water	At a rate of 25 g/L
Field of use	Textile
Appearance	Powder
Smell	Odorless

3.2.2. Background information about Methylene blue (MB)

Methylene blue (MB) is a widely used cationic dye selected as our model pollutant for this study. This compound exhibits significant toxicity. Its contact with eyes can result in severe burns and permanent damage. When inhaled, MB causes respiratory distress and cardiac arrhythmia [34]. Oral exposure leads to various symptoms including burning sensations, nausea, vomiting, and profuse sweating [35,36].

Methylene Blue contains a thiazine-type chromophore, consisting of a heterocyclic aromatic ring system with sulfur and nitrogen atoms. As a cationic dye, it has a strong affinity for acidic substrates and forms stable ionic bonds. The molecule features dimethylamine groups attached to the aromatic ring system, contributing to its characteristic blue color. Some chemical and physical properties of Methylene Blue are presented in Table I.3.

Table I.3. Chemical and physical properties of Methylene Blue [37]

Molecular structure	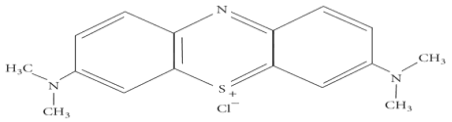
Molecular formula	$C_{16}H_{18}N_3SCl$
Molecular weight (g/mol)	319.85
Family	Phenothiazine dyes
Synonyms	Basic Blue 9, Methylthioninium chloride, Swiss Blue
Melting point (°C)	180
Solubility in water	At a rate of 35.5 g/L
Field of use	Textile, Medical applications
Appearance	Powder
Smell	Odorless

3.3. Techniques for the treatment of dye-contaminated wastewater

To enhance public health and safeguard the environment, dye users, industries, and government authorities should implement effective measures for treating colored wastewater. Various physical, chemical, and biological techniques [38], such as coagulation, ion exchange, adsorption, advanced oxidation, and membrane filtration, are employed for wastewater treatment. However, each method has certain limitations when it comes to large-scale applications. Table I.4 outlines different water treatment techniques along with their respective benefits and drawbacks. Among these, adsorption is considered a cost-effective and efficient approach for dye removal due to its simplicity, high effectiveness, and the availability of affordable adsorbents [39].

Table I.4. Pros and cons of different dye-contaminated water treatment technologies [40]

Technologies	Advantages	Disadvantages
Advanced oxidation	Under ambient conditions of pressure and temperature, dyes undergo efficient degradation, resulting in the conversion of organic contaminants to CO2.	Elevated operational and upkeep expenses.
Chemical Precipitation	An integrated physicochemical process combines multiple physical and chemical treatment methods to effectively address environmental contamination. It is simple to implement, reasonably priced compared to alternative technologies	Contains a large amount of chemicals and generates a lot of sludge.
Ion exchange	producing no sludge, offering shorter treatment time, and yielding water with higher purity degrees.	The process is highly sensitive to pH levels, which substantially impacts production efficiency
Electrochemical	This method operates with minimal to no chemical additives, delivering rapid processing times. It demonstrates versatility by effectively accommodating both water-soluble dye compounds and those that do not dissolve in aqueous solutions.	Entails substantial operational expenditures, escalating power consumption charges, sediment accumulation, environmental contamination through chlorine-based organic substances, and toxic metal infiltration resulting from secondary oxidation processes.
Oxidation	The coloring agent undergoes comprehensive decomposition, with the entire transformation process occurring within a brief timeframe	The process necessitates continuous pH monitoring and regulation; a catalytic agent is essential for achieving maximum efficiency in the treatment procedure; and high cost.
Coagulation – Flocculation	The remediation of colored effluents employs various physicochemical techniques; introduction of coagulant substances facilitates total elimination of pigments from the purified discharge water; this approach demonstrates both efficacy and straightforward implementation, achieving comprehensive chromatic neutralization.	The generation of a significant amount of sludge, increased operating costs ,and has a negative impact on the environment.
Ultrafiltration and Nanofiltration	Works efficiently with all dye types.	High cost, sludge buildup, and limited lifespan.
Biological techniques (aerobic and anaerobic)	Safe, affordable, and eco-friendly	Dyes have low biodegradability, requiring a large land area and more time for color removal.
Adsorption	Highly efficient, user-friendly, and adaptable to various pollutants; excellent at removing diverse impurities; cost-effective; adsorbents can be produced from waste and have the potential for regeneration.	

4. Adsorption

4.1 Adsorption mechanism

Adsorption is a surface phenomenon where solutes (gases or liquids) form an atomic film or molecular layer (adsorbate) on a solid surface (adsorbent). This process is widely implemented in water treatment and various other applications for contaminant removal, including organic compounds, metal ions, and microorganisms. The efficacy of adsorption is highly dependent on selecting appropriate adsorbent material for the targeted contaminants. The fundamental terminology of adsorption processes is depicted in Figure I.1 [41]. The classification of adsorption types is based on the nature of interactions between adsorbates and adsorbents, primarily categorized as physical adsorption (physisorption) and chemical adsorption

(chemisorption). Physical adsorption involves multiple intermolecular forces between the dissolved molecules (adsorbates) and the solid surface (adsorbent), including electrostatic interactions, hydrogen bonding, van der Waals forces, diffusion mechanisms, and hydrophobic interactions (particularly π-π interactions). A key characteristic of physisorption is its reversibility and relatively straightforward implementation. In contrast, chemical adsorption involves the formation of chemical bonds between adsorbate molecules and the adsorbent surface, resulting in an irreversible process [42]. Recent technological advances in adsorption processes have focused on understanding and utilizing the chemical mechanisms involved. These developments emphasize the role of covalent and ionic bonding in creating robust interactions between the adsorbent surface and adsorbate molecules, leading to more effective and selective adsorption systems [43].

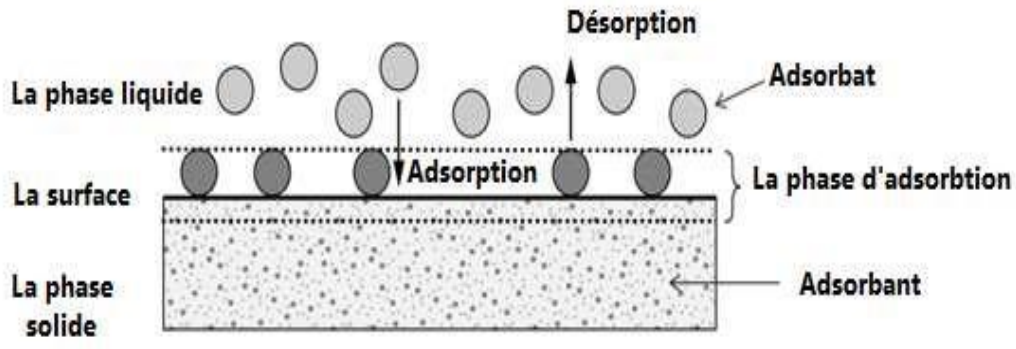

Figure I.1. Foundational terms for understanding adsorption [41].

4.2. Pollutant Trapping Substances

Activated carbon is a widely used adsorbent for removing organic and inorganic pollutants from contaminated water [44, 45]. However, this material can be expensive, which limits its application in large-scale treatment systems [46]. Consequently, researchers are increasingly focusing on various alternative, eco-friendly, cost-effective, naturally available adsorbents that are both efficient and easily regenerable [47]. Biomass materials, including agricultural and animal waste, have emerged as promising alternatives in water treatment technologies [48,49]. These natural adsorbents offer several advantages: they are abundant, renewable, and often have complex structural characteristics that enhance pollutant removal [50].

4.3.1. Origin of the investigated adsorbent materials

The selection of an appropriate adsorbent for pollutant removal is a complex process governed by multiple critical factors, including cost-effectiveness, material properties, and accessibility [51]. As global population growth and rapid urbanization continue to escalate, the annual production of agricultural and animal by-products has reached unprecedented levels, creating significant waste management challenges [52]. Traditional waste disposal methods like landfilling have proven increasingly unsustainable, prompting researchers to explore innovative waste valorization strategies [53]. Recent scientific investigations have revealed the potential of transforming agricultural and animal solid waste into valuable, low-cost adsorbent materials for environmental remediation [54].

4.3.1.1. Agricultural waste

Agricultural residues present a remarkable opportunity in environmental remediation. These materials - from fruit peels to crop stalks - possess inherent characteristics that make them excellent candidates for dye removal from contaminated water. Their molecular architecture, dominated by cellulose, hemicellulose, and lignin, creates a natural framework for pollutant capture. What makes these materials particularly effective is their rich surface chemistry, featuring an array of functional groups including hydroxyl, carbonyl, amino, carboxyl, and methyl moieties [55]. The interaction between these materials and synthetic dyes occurs through multiple mechanisms. The functional groups on their surfaces facilitate various binding processes, from ion exchange to complexation and hydrogen bonding [56]. Extensive research has validated their effectiveness, demonstrating that these once-discarded materials can serve as powerful tools in environmental protection, either in their natural state or after strategic modifications [57, 58].

4.3.1.2. Animal waste

Animal waste consists of a diverse range of organic and inorganic compounds essential for various applications. The primary components of animal waste include nitrogen-rich compounds such as urea and proteins, along with significant concentrations of phosphorus and potassium compounds [59]. Animal waste also contains carbon-based materials including cellulose, lignin, and various metabolic byproducts, along with important micronutrients such as calcium, magnesium, iron, zinc, and copper [60,61]. These materials demonstrate remarkable

capabilities in binding with synthetic dyes through diverse mechanisms including ion exchange, where charged functional groups like $–NH_3^+$, $–COO^–$, and –OH interact with charged dye molecules [57,58]. Such findings demonstrate that animal waste-derived materials can serve as powerful tools in environmental protection, especially in wastewater treatment applications.

5. Conclusion

This portion studies wastewater and dye pollutants and their major implications for environmental and public health. We then explore various water treatment methods, with special attention to adsorption of a cost-effective and efficient technique for removing contaminants from wastewater. The following section will provide a detailed review of previous research, particularly focusing on how pollutants interact with different surfaces during the adsorption process at solid-liquid interfaces.

Bibliographic references

[1] G. Tchobanoglous, F. Burton, H.D. Stensel, Wastewater engineering: treatment and reuse. American Water Works Association Journal, 95(5) (2003) 201.

[2] Angélique Léonard, Study of convective drying of sewage treatment plant sludge. Monitoring of texture by X-ray microtomography. PhD thesis, University of Liège, 2007.

[3] W.J. Cosgrove, D.P. Loucks, Water management: Current and future challenges and research directions. Water Resources Research, 51 (2015) 4823–4839.

[4] M. Afutuzumab, A.A. Rahman, Sustainable water demand management in the face of rapid urbanization and groundwater depletion for social-ecological resilience building. Global Ecology and Conservation, 10 (2017) 9–22.

[5] H. Kumari, S. Suman, R. Ranga, S. Chahal, S. Devi, S. Sharma, S. Kumar, P. Kumar, S. Kumar, A. Kumar, R. Parmar, A review on photocatalysis used for wastewater treatment: Dye degradation. Water, Air, and Soil Pollution, 234 (2023) 349.

[6] N. Akhtar, M.I. Syakir Ishak, S.A. Bhawani, K. Umar, Various natural and anthropogenic factors responsible for water quality degradation: A review. Water, 13 (2021) 2660.

[7] K. Sardar, S. Ali, S. Hameed, S. Afzal, S. Fatima, M.B. Shakoor, S.A. Bhawana, H.M. Tauqeer, Heavy metals contamination and their impacts on living organisms. Greener Journal of Environmental Management and Public Safety, 2 (2013) 172–179.

[8] K.R. Bhattarai, M. Bhasin, Water pollution is the main problem for human health. Journal of Algebraic Statistics, 13 (2022) 2812–2817.

[9] United States Environmental Protection Agency, Office of Water Regulations. National Water Quality Inventory: Report to Congress. The Office, 1996.

[10] S. Devi, S. Chahal, S. Singh, P. Kumar, S. Kumar, A. Kumar, V. Kumar, Magnetic Fe_2O_3/CNT nanocomposites: Characterization and photocatalytic application towards the degradation of Rose Bengal dye. Ceramics International, 49 (2023) 20071–20079.

[11] K. Maheshwari, M. Agrawal, A.B. Gupta, Dye pollution in water and wastewater. In: S.S. Muthu, A. Khadir (Eds.), Novel Materials for Dye-Containing Wastewater Treatment, Springer Singapore, (2021) 1–25.

[12] R. Al-Tohamy, S.S. Ali, F. Li, K.M. Okasha, Y.A.-G. Mahmoud, T. Elsamahy, H. Jiao, Y. Fu, J. Sun, A critical review on the treatment of dye-containing wastewater: Ecotoxicological and health concerns of textile dyes and possible remediation approaches for environmental safety. Ecotoxicology and Environmental Safety, 231 (2022) 113160.

[13] S. Dutta, S. Adhikary, S. Bhattacharya, D. Roy, S. Chatterjee, A. Chakraborty, D. Banerjee, A. Ganguly, S. Nanda, P. Rajak, Contamination of textile dyes in aquatic environment: Adverse impacts on aquatic ecosystem and human health, and its management using bioremediation. Journal of Environmental Management, 353 (2024) 120103.

[14] T. Robinson, G. McMullan, R. Marchant, P. Nigam, Remediation of dyes in textile effluent: A critical review on current treatment technologies with a proposed alternative. Bioresource Technology, 77(3) (2001) 247–255.

[15] S.D. Desphande, Indian Journal of Fibre & Textile Research, 26 (2001) 136–142.

[16] G.A. Montero, C.B. Smith, W.A. Hendrix, D.L. Butcher, Supercritical fluid technology in textile processing: An overview. Industrial & Engineering Chemistry Research, 39(12) (2000) 4806–4812.

[17] S.S. Kumar, K. Joseph, Waste minimisation in hosiery textile dyeing – A case study. Journal of Industrial Pollution Control, 22(2) (2006) 345–352.

[18] T. Platzek, C. Lang, G. Grohmann, U.S. Gi, W. Baltes, Formation of a carcinogenic aromatic amine from an azo dye by human skin bacteria in vitro. Human & Experimental Toxicology, 18(9) (1999) 552–559.

[19] G. Oros, T. Cserhati, E. Forgacs, Strength and selectivity of the fungicidal effect of diazo benzene dyes. (2001) 319–322.

[20] S. Tsuda, M. Murakami, N. Matsusaka, K. Kano, K. Taniguchi, Y.F. Sasaki, DNA damage induced by red food dyes orally administered to pregnant and male mice. Toxicological Sciences, 61(1) (2001) 92–99.

[21] A. Ahmad, M. Alam, Arsenic and heavy metal contamination of vegetables grown in Samta village, Bangladesh. Science of the Total Environment, 308(1–3) (2003) 83–96.

[22] H.B. Slama, A. Chenari Bouket, Z. Pourhassan, F.N. Alenezi, A. Silini, H. Cherif-Silini, T. Oszako, L. Luptakova, P. Golińska, L. Belbahri, Diversity of synthetic dyes from textile industries, discharge impacts and treatment methods. Applied Sciences, 11 (2021) 6255.

[23] E. Gurr, Synthetic Dyes in Biology, Medicine and Chemistry. Elsevier, (2012).

[24] M.A.M. Salleh, D.K. Mahmoud, W.A.W.A. Karim, A. Idris, Cationic and anionic dye adsorption by agricultural solid wastes: A comprehensive review. Desalination, 280 (2011) 1–13.

[25] M.M. Hassan, C.M. Carr, Biomass-derived porous carbonaceous materials and their composites as adsorbents for cationic and anionic dyes: A review. Chemosphere, 265 (2021) 129087.

[26] S.A. Shapovalov, Cation–anionic interactions of dyes in aqueous solutions: Bromocresol Purple in the processes of dissimilar association. Colorants, 1 (2021) 5–19.

[27] A. Safavi, H. Abdollahi, N. Maleki, S. Zeinali, Interaction of anionic dyes and cationic surfactants with ionic liquid character. Journal of Colloid and Interface Science, 322 (2008) 274–280.

[28] R.J. Aguado, A. Mazega, Q. Tarrés, M. Delgado-Aguilar, The role of electrostatic interactions of anionic and cationic cellulose derivatives for industrial applications: A critical review. Industrial Crops and Products, 201 (2023) 116898.

[29] Q. Li, Q.-Y. Yue, H.-J. Sun, Y. Su, B.-Y. Gao, A comparative study on the properties, mechanisms, and process designs for the adsorption of non-ionic or anionic dyes onto cationic polymer/bentonite. Journal of Environmental Management, 91 (2010) 1601–1611.

[30] M.D. Garcia, A. Sanz-Medel, Dye–surfactant interactions: A review. Talanta, 33 (1986) 255–264.

[31] W. Konicki, K. Cendrowski, G. Bazarko, E. Mijowska, Study on efficient removal of anionic, cationic, and nonionic dyes from aqueous solutions by means of mesoporous carbon nanospheres with empty cavity. Chemical Engineering Research and Design, 94 (2015) 242–253.

[32] N.A. Abdelwahab, F.M. Helaly, Simulated visible-light photocatalytic degradation of Congo red by TiO_2-coated magnetic polyacrylamide grafted carboxymethylated chitosan. Journal of Industrial and Engineering Chemistry, 50 (2017) 162–171.

[33] S. Venkat, P.V. Vijay Babu, Kinetic and equilibrium studies on the removal of Congo red from aqueous solution using Eucalyptus globulus sawdust. Journal of the Taiwan Institute of Chemical Engineers, 44 (2013) 81–88.

[34] D. Hui, J. Lu, G. Li, G. Zhu, X. Wang, Adsorption of methylene blue on adsorbent materials produced from cotton stalk. Chemical Engineering Journal, 172 (2011) 326–334.

[35] Y. Arzu, O. Dursun, T. Ozlem, Removal of Chemazol Reactive Red 195 from aqueous solution by dehydrated beet pulp carbon. Journal of Hazardous Materials, 194 (2011) 303–311.

[36] M. Gholamreza, R. Kh., The removal of cationic dyes from aqueous solutions by adsorption onto pistachio hull waste. Chemical Engineering Research and Design, 89 (2011) 2182–2189.

[37] Z. Marzougui, Development of functionalized magnetic latex for wastewater treatment by adsorption. PhD thesis, University of Lyon; University of Sfax, Faculty of Sciences, 2016.

[38] C. Santhosh, V. Velmurugan, G. Jacob, S.K. Jeong, A.N. Grace, A. Bhatnagar, Role of nanomaterials in water treatment applications: A review. Chemical Engineering Journal, 306 (2016) 1116–1137.

[39] Md. T. Uddin, Md. A. Rahman, Md. Rukanuzzaman, Md. A. Islam, A potential low-cost adsorbent for the removal of cationic dyes from aqueous solutions. Applied Water Science, 7 (2017) 2831–2842.

[40] H.N. Hamad, S. Idrus, Recent developments in the application of bio-waste-derived adsorbents for the removal of blue methylene from wastewater: A review. Polymers, 14 (2022) 4.

[41] N.B. Singh, G. Nagpal, S. Agrawal, Rachna, Water purification by using adsorbents: A review. Environmental Technology & Innovation, 11 (2018) 187–240.

[42] R. Gusain, N. Kumar, S.S. Ray, Recent advances in carbon nanomaterial-based adsorbents for water purification. Coordination Chemistry Reviews, 405 (2020) 213111.

[43] A. Tripathi, M.R. Ranjan, Heavy metal removal from wastewater using low-cost adsorbents. Journal of Bioremediation & Biodegradation, 6 (2015) 315.

[44] S. Babel, T.A. Kurniawan, Low-cost adsorbents for heavy metals uptake from contaminated water: A review. Journal of Hazardous Materials, 97(1–3) (2003) 219–243.

[45] D. Mohan, C.U. Pittman Jr., Activated carbon and low-cost adsorbents for remediation of tri- and hexavalent chromium from water. Journal of Hazardous Materials, 137(2) (2006) 762–811.

[46] K.Y. Foo, B.H. Hameed, Insights into the modeling of adsorption isotherm systems. Chemical Engineering Journal, 156(1) (2010) 2–10.

[47] M. Ahmad, A.U. Rajapaksha, J.E. Lim, M. Zhang, N. Bolan, D. Mohan, Biochar as a sorbent for contaminant management in soil and water: A review. Chemosphere, 99 (2014) 19–33.

[48] A. Demirbas, Agriculturally based activated carbons for the removal of dyes from aqueous solutions: A review. Journal of Hazardous Materials, 167(1–3) (2009) 1–9.

[49] S. Wang, X. Guo, Adsorption of heavy metal ions from aqueous solutions: A review. Journal of Environmental Sciences, 110 (2020) 1–13.

[50] M. Inyang, B. Gao, Y. Yao, Y. Xue, A. Zimmerman, A. Mosa, X. Cao, A review of biochar as a low-cost adsorbent for aqueous heavy metal removal. Critical Reviews in Environmental Science and Technology, 46(4) (2016) 406–433.

[51] G. Crini, E. Lichtfouse, Advantages and disadvantages of techniques used for wastewater treatment. Environmental Chemistry Letters, 17 (2019) 145–155.

[52] R. Kumar, A. Singh, S. Gupta, Utilization of agricultural waste materials as sustainable adsorbents for heavy metal removal: A comprehensive review. Journal of Environmental Chemical Engineering, 11(5) (2023) 109873.

[53] S. Dutta, C. Bhattacharjee, S. Datta, Valorization of agricultural wastes for wastewater treatment: A review. Journal of Environmental Management, 297 (2021) 113316.

[54] J. Ma, Y. Liu, L. Chen, Green substitutes from agricultural wastes: A review of sustainable adsorption materials. Applied Surface Science Advances, 19 (2023) 100562.

[55] Y. Zhou, J. Lu, Y. Zhou, Y. Liu, Recent advances for dyes removal using novel adsorbents: A review. Environmental Pollution, 252 (2019) 352–365.

[56] G. Crini, E. Lichtfouse, L.D. Wilson, N. Morin-Crini, Adsorption-oriented processes using conventional and non-conventional adsorbents for dye removal from aqueous solutions. Environmental Chemistry Letters, 17 (2019) 195–213.

[57] M.M. Hasan, M.A. Rahman, M.S. Islam, Surface modification of biomass-based adsorbents for enhanced dye removal: A review. Environmental Technology & Innovation, 30 (2023) 103129.

[58] M.A. Al-Ghouti, M. Khraisheh, Recent advances in functionalized biosorbents for industrial dye wastewater treatment. Journal of Environmental Chemical Engineering, 12(2) (2024) 110456.

[59] A.E. Ghaly, K.N. MacDonald, Nutrient management of animal manure: Livestock and poultry manure. Journal of Environmental Science and Technology, 5(2) (2012) 67–82.

[60] J. Zhao, Y. Ma, Y. Sun, X. Zhang, Agricultural waste-based biochar for sustainable wastewater treatment: A review. Bioresource Technology, 351 (2022) 127046.

[61] Y. Liu, H. Zhang, L. Chen, Animal waste-derived adsorbents for water purification: Composition, surface chemistry, and applications. Journal of Environmental Management, 337 (2023) 117668.

Chapter II

Preparation and Characterization Methods

Chapter II: Preparation and Characterization Methods

Sommaire

1. Introduction

The efficiency of an adsorbent in removing pollutants from aqueous solutions largely depends on its physicochemical properties, which are closely linked to the methods employed in its preparation and characterization. Therefore, understanding these methods is essential to explain the adsorption mechanisms and to optimize the performance of the materials [1–3]. This chapter provides a general overview of the main approaches used for the preparation of adsorbent materials and the preparation of dye solutions. It also highlights the analytical techniques employed to characterize the structural, morphological, and surface properties of the adsorbents, such as Fourier Transform Infrared Spectroscopy (FTIR), Thermogravimetric Analyses (TGA), Scanning Electron Microscopy (SEM), X-ray Diffraction (XRD), and the determination of the point of zero charge (pH_{pzc}) [4]. In addition, UV–Visible spectroscopy is presented as a key tool for monitoring the adsorption process and evaluating dye removal efficiency [5]. Overall, this chapter aims to establish a theoretical and methodological framework that supports the interpretation of the experimental results discussed in the following sections.

2. General Preparation Methods of Adsorbents

The preparation of adsorbent materials represents a fundamental stage in the development of efficient systems for wastewater treatment and the removal of organic pollutants. The choice of raw material, along with the treatment conditions applied during preparation, plays a decisive role in determining the final physicochemical characteristics of the adsorbent, such as its surface

area, porosity, surface functionality, and structural stability [6,7]. In general, the preparation process involves several steps designed to purify, activate, and stabilize the precursor material. Initially, the raw biomass or mineral precursor is subjected to washing and drying to remove impurities, moisture, and volatile components. Subsequent grinding and sieving steps help to obtain a homogeneous particle size, which facilitates uniform heat and reagent distribution during later treatments [8]. The activation step is considered one of the most critical stages in adsorbent synthesis. Chemical activation typically uses activating agents such as acids, bases, or salts to introduce oxygen-containing functional groups that increase the material's affinity toward pollutants [9]. In certain cases, calcination at controlled temperatures is applied to eliminate residual organic matter and to improve the thermal and structural stability of the material. Moreover, modification or functionalization steps may be introduced through impregnation or doping with metal oxides, nanoparticles, or organic molecules. These additional treatments aim to enrich the surface with specific active sites capable of interacting with various dye molecules through electrostatic attraction, hydrogen bonding, or π–π interactions [10].

In the present study, the adsorbent materials were prepared according to these general principles. Each material was developed with the objective of optimizing its surface characteristics and adsorption potential, while the specific synthesis conditions and detailed experimental procedures were described in the preceding chapters.

Figure II.1. Typical Methods Used in Adsorbent Preparation

3. Preparation of Dye Solutions

For the adsorption experiments, stock solutions of methylene blue (MB) and Congo red (CR) dyes were prepared by dissolving an accurately weighed amount of each dye in distilled water to obtain a known concentration (1000 mg L^{-1}). Working solutions of the desired concentrations were then prepared by successive dilution of the stock solutions with distilled water [11]. The concentration of each dye in solution was determined spectrophotometrically using a UV–Visible spectrophotometer at their respective maximum absorption wavelengths, λ_{max} = 664 nm for methylene blue and 497 nm for Congo red [9]. To ensure precise quantification of dye removal, calibration curves (courbes d'étalonnage) were established for both dyes by measuring the absorbance of a series of standard solutions with known concentrations. The relationship between absorbance (A) and concentration (C) followed the Beer–Lambert law:

$$A = \varepsilon \times l \times C$$

where ε is the molar absorptivity and l the optical path length.

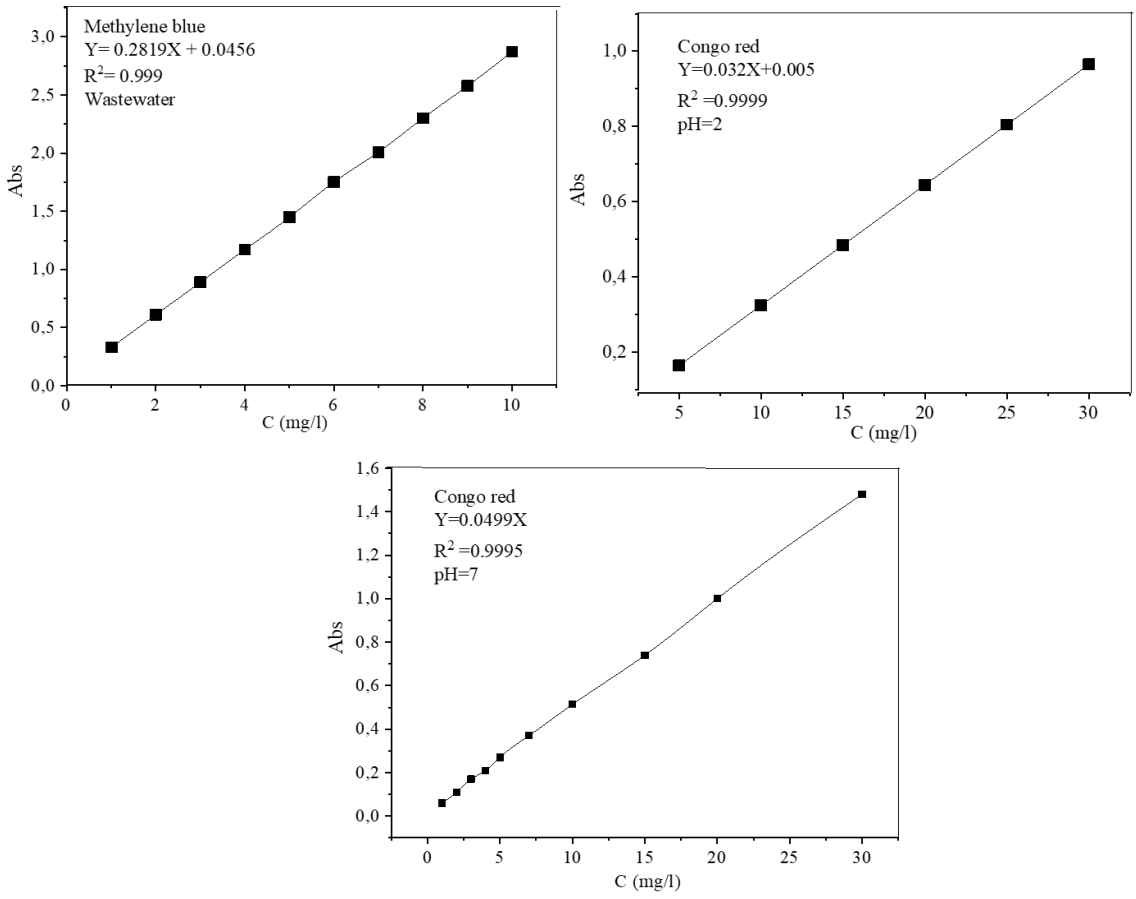

Figure II.2. Calibration curves

4. Characterization techniques

4.1. Fourier Transform Infrared (FTIR)

Fourier Transform Infrared (FTIR) spectroscopy is an essential analytical technique used to identify functional groups and investigate the molecular structure and composition of materials. In a typical FTIR spectrometer, infrared radiation from a source is divided into two beams that pass alternately through the sample and reference chambers. These beams are recombined by an optical system, and the resulting interference pattern known as an interferogram is processed mathematically using a Fourier Transform to produce the final spectrum [12]. During the analysis, one beam interacts with the sample while the other passes through a reference path. The resulting differences in intensity and phase provide information about the sample's vibrational modes and chemical bonds. The spectral resolution and sensitivity depend on factors such as slit width and detector performance; narrower slits improve frequency discrimination, while wider slits enhance light transmission and signal intensity [13].

In this study, an Agilent Technologies FTIR spectrophotometer was used to record the infrared spectra of the materials. The instrument was controlled by a microcomputer, and spectra were collected in the range of 4500-400 cm^{-1}, allowing identification of characteristic absorption bands associated with surface functional groups.

4.3.X-Ray Diffraction (XRD)

X-ray diffraction (XRD) is used to identify the crystalline phases present in a solid and to obtain information about its crystal structure. The technique is based on Bragg's Law:

$$n.\lambda = 2d\ sin\theta$$

n is the diffraction order,

λ is the wavelength of the X-ray radiation used (1.5418 Å),

d is the interplanar spacing (Å),

θ is the diffraction angle.

which describes the condition for constructive interference between X-rays scattered by atomic planes in a crystal lattice [14]. X-rays are produced when electrons emitted from a heated cathode are accelerated by an electric field and directed onto a metal anode, generating characteristic radiation. The diffracted beams are collected as a function of the diffraction angle (2θ), producing a diffractogram that represents the intensity of the diffracted X-rays versus 2θ [15]. Each crystalline phase exhibits a characteristic set of diffraction peaks corresponding to

specific interplanar spacings (d-values). Identification of the phases is performed by comparing the obtained patterns with standard reference data from the Joint Committee on Powder Diffraction Standards (JCPDS) or ASTM databases [16]. XRD can also provide information on grain size, crystalline, lattice parameters, and preferred orientation. The average crystallite size (D) can be estimated from the broadening of diffraction peaks using the Scherrer equation:

$$D = \frac{0.9\,\lambda}{\beta \cos(\theta)}$$

4.4. Scanning Electron Microscopy (SEM)

The working principle of Scanning Electron Microscopy (SEM) is based on the interaction between a focused beam of accelerated electrons and the surface of a specimen. During analysis, the primary electron beam is scanned systematically across the sample surface, enabling the observation of its microstructural features with high resolution. When the incident electrons interact with the surface, they generate secondary and backscattered electrons, which are detected and converted into signals. These signals are processed to form images on a cathode-ray screen or monitor, reproducing the scanned area with a pattern corresponding to the electron beam movement [17]. In solid materials, SEM effectively reveals the presence of pores, cracks, and variations in particle shape and size. It is particularly valuable for the characterization of monophase catalysts, as it allows for the evaluation of surface uniformity, preparation consistency, and elemental distribution across the material [18]. Within the sample, the interaction between electrons and atoms occurs in a defined “interaction volume,” often described as pear-shaped. This region produces a range of signals that can be utilized to obtain detailed morphological images or to conduct compositional analyses. The electron beam’s penetration depth and interaction depend on factors such as the beam energy and the angle of incidence, offering valuable insights into the arrangement of crystalline planes [19]. Overall, SEM serves as an indispensable tool for morphological characterization and surface analysis, especially in research focused on catalyst synthesis and structural optimization.

4.5. Energy Dispersive X-ray Spectroscopy (EDX)

Energy Dispersive X-ray Spectroscopy (EDX) is an essential analytical technique employed for both qualitative and quantitative determination of the elemental composition of materials. Typically coupled with Scanning Electron Microscopy (SEM), it enables simultaneous observation of surface morphology and chemical composition. When a focused electron beam

strikes the sample, the atoms within emit characteristic X-rays unique to each element. These emitted X-rays are detected and processed to identify and quantify the elements present in the analyzed region. Through this mechanism, EDX provides detailed information on the spatial distribution and relative concentration of elements, serving as a powerful tool for compositional and microstructural analysis in material science [20].

4.4. Thermogravimetric Analysis (TGA)

Thermogravimetric Analysis (TGA) is a thermal analytical technique used to determine the change in a material's mass as a function of temperature or time under a controlled atmosphere. During the analysis, the sample is gradually heated in an inert or reactive gas environment, and the resulting weight loss or gain is continuously recorded. These variations correspond to processes such as moisture evaporation, decomposition, oxidation, or reduction. The obtained thermogram provides valuable information about the material's thermal stability, composition, and degradation behavior. TGA is widely applied in material science and chemistry for assessing thermal resistance, determining volatile or filler content, and evaluating the stability and composition of catalysts, polymers, and other solid materials [21].

4.5. Measurement of the Isoelectric Point (pH_{pzc})

The isoelectric point (pH_{pzc}) represents the pH at which the surface of an adsorbent carries an equal number of positive and negative charges, resulting in a net zero surface charge. When the solution pH exceeds the pH_{pzc}, the surface functional groups become predominantly deprotonated due to the abundance of hydroxide ions (OH^-), leading to a negatively charged surface. Conversely, at pH values below the pH_{pzc}, the surface groups are protonated because of the excess of hydrogen ions (H^+), making the surface positively charged.

The determination of the point of zero charge (pH_{pzc}) for each material is essential for understanding the adsorption mechanism and the electrostatic interactions between the solid and liquid phases. The measurement was performed following a standard procedure: six beakers were prepared, each containing 20 mg of adsorbent and 20 mL of distilled water. The initial pH values of the suspensions were adjusted in the range of 2 to 11 using either HCl or NaOH solutions. The mixtures were continuously stirred for 24 h, after which the final pH of each sample was recorded. The obtained data were then plotted as $\Delta pH = f(pH_i)$, where the point at which ΔpH equals zero corresponds to the pH_{pzc} of the material.

Table II.1. Explanation of Equations Used in This Thesis

Equation	Parameter descriptions
$Qe = (C_0 - Ce) \times V/m$ $R(\%) = (C0 - Ce/Ce) \times 100$	C_0 represents the initial concentration of MB in mg/L, C_e represents the equilibrium concentration of MB in (mg/L), V denotes the volume of the solution being treated in L, and m denotes the mass of the adsorbents employed in g.
$R^2 = 1 - \frac{\sum_{i=1}^{N}(Q_{e,exp} - Q_{e,cal})^2}{\sum_{i=1}^{N}(Q_{e,exp} - Q_{e,mean})^2}$	R^2represent the coefficient of determination, $Q_{e,exp}$ is the equilibrium adsorption capacity obtained from experimental data, $Q_{e,cal}$ represents the value predicted by the model for the corresponding equilibrium concentration Ce.
$E_r = \frac{1}{n}\sum_{i=1}^{n}\frac{Q_{e,mod} - Q_{e,exp}}{Q_{e,exp}}$	E_r represent the chi-square, $Q_{e,mean}$ is the average of the experimental adsorption capacities, and N denotes the total number of experimental observations.
Kinetic models	
PFO :$Q_t = Q_e(1 - e^{-K_1 t})$	k_1 (min^{-1}) corresponds to the first-order kinetic constant.
PSO :$Q_t = (K_2 Q_e^2 t)/(1 + K_2 Q_e t)$	$K_2(g/mg.\min)$ corresponds to the second-order kinetic constant
Elovich :$Q_t = \frac{1}{B}\ln(ABt + 1)$	The variables A and B refer to the initial adsorption rate constant ($mg/g.min$) and the desorption constant associated with surface coverage and activation energy (g/mg), respectively.
Intra-particlediffusion : $Q_t = K_{int}\, t^{1/2} + C$	C (mg/g) corresponds to the intercept related to boundary layer effects, $k_{int}(mg/g.min^{1/2})$ is the intraparticle diffusion rate parameter.
Isotherm models	
Langmuir :$Q_e = (Q_{max}\, K_L C_e)/(1+K_L C_e)$	Q_{max} indicates the highest adsorption capacity achievable by the adsorbent material,K_L corresponds to the Langmuir adsorption constant.
Freundlich :$Q_e = K_f\, C_e^{\frac{1}{n}}$	K_f $(mg/g)/mg/L)^{\frac{1}{n}}$, n corresponds to the Freundlich adsorption coefficients .
Redlich-Peterson:$Q_e = (KC_e)/(1 + aC_e^{\beta})$	k (L/g) and α $[(mg/L)^{-\beta}]$ are Redlich-Peterson isotherm coefficients,β is the dimensionless exponent in the Redlich-Peterson model, with values constrained between 0 and 1.
Sips: $Q_e = Q_s\,(bC_e)^n/1 + (bC_e)^n$	Q_s represents the highest adsorption capacity, b (L/mg) is the Sips model equilibrium coefficient, n characterizes the adsorbent surface heterogeneity.
Thermodynamic	
$\Delta G = \Delta H - T\Delta S$	ΔG Gibbs Free Energy Change, ΔH Enthalpy Change, T absolute Temperature.

$\Delta G = -RT\ln(K_C)$	K_c dimensionless equilibrium constant , R Universal Gas Constant
$\ln K_C = -\frac{\Delta H^\circ}{R} \times \frac{1}{T} + \frac{\Delta S^\circ}{T}$	(8.314 $J{\cdot}mol^{-1}{\cdot}K^{-1}$)
$K_C = K_L \times M_{adsorbate} \times 55.5 \times 10^3$	K_L : Langmuir isotherm equilibrium constant
Crystallite size (Scherrer equation)	
$D = \frac{0.9\,\lambda}{\beta\cos(\theta)}$	D is the particle size (nm), λ is the X-ray wavelength represents the FWHM (full width at half maximum) of the diffraction peak, θ is Bragg angle (half of the diffraction angle, in radians).

5. Conclusion

This chapter presented the overall procedures related to the preparation of the adsorbent materials and dye solutions, as well as the different analytical methods used for their characterization. The adopted preparation techniques allowed the development of materials with suitable physicochemical properties for dye adsorption. The preparation of methylene blue and Congo red solutions, accompanied by calibration curves, ensured the accuracy of the quantitative analyses.

The characterization techniques, including FTIR, TGA, SEM, XRD, and pH_{pzc}, provided complementary information about the structural, morphological, thermal, and surface characteristics of the adsorbents. These results are essential for understanding the interaction mechanisms between dyes and the adsorbent surfaces.

Overall, this chapter established a solid methodological foundation for the interpretation of adsorption experiments and the discussion of results presented in the next chapters.

Bibliographic references

[1] M. Rafatullah, O. Sulaiman, R. Hashim, A. Ahmad. Adsorption of methylene blue on low-cost adsorbents: a review. Journal of hazardous materials, 177(2010),70-80.

[2] A.O. Dada, A.P. Olalekan, A.M. Olatunya, O. Dada. Langmuir, Freundlich, Temkin and Dubinin-Radushkevich isotherms studies of equilibrium sorption of Zn_2 unto phosphoric acid modified rice husk. Journal of Appl Chem, *3*.1(2012), 38-45.

[3] M.T. Yagub, T.K. Sen, S. Afroze, H.M. Ang. Dye and its removal from aqueous solution by adsorption: a review. Advances in colloid and interface science, 209(2014)172-184.

[4] J. Wu, X. Wang, Q. Wang, Z. Lou, S. Li, Y. Zhu, H. Wei. Nanomaterials with enzyme-like characteristics (nanozymes): next-generation artificial enzymes (II). Chemical Society Reviews, *48*.4(2019)1004-1076.

[5] A. Elzoghby, H. Fahmy, M. Taha, S. Ibrahim. Active carbon-based waste packaging materials for uranium sorption from aqueous solution. Environmental Science and Pollution Research, *30*.30(2023), 74726-74741.

[6] S. Babel, T.A. Kurniawan. Low-cost adsorbents for heavy metals uptake from contaminated water: a review. Journal of hazardous materials, 97(2003), 219-243.

[7] M.T. Yagub, T.K. Sen, S. Afroze, H.M. Ang.Dye and its removal from aqueous solution by adsorption: a review. Advances in colloid and interface science, 209(2014) 172-184.

[8] A.O. Dada, A.P. Olalekan, A.M. Olatunya, O. Dada. Langmuir, Freundlich, Temkin and Dubinin-Radushkevich isotherms studies of equilibrium sorption of Zn_2 unto phosphoric acid modified rice husk. J Appl Chem, *3*.1(2012), 38-45.

[9] M. Rafatullah, O. Sulaiman, R. Hashim, A. Ahmad. Adsorption of methylene blue on low-cost adsorbents: a review. Journal of hazardous materials, 177(2010), 70-80.

[10] C. Arora, P. Kumar, S. Soni, J. Mittal, A. Mittal, B. Singh, Desalination Water Treat. **195** (2020) 341–352.

[11] M. Yagub, T.K. Sen, S. Afroze, H.M. Ang. Dye and its removal from aqueous solution by adsorption: a review. Advances in colloid and interface science, *209*(2014)172-184.

[12] C. Berthomieu, R. Hienerwadel, Fourier transform infrared (FTIR) spectroscopy, Photosynth Res 101 (2009) 157–170.

[13] M.A. Mohamed, J. Jaafar, A.F. Ismail, M.H.D. Othman, M.A. Rahman, Fourier transform infrared (FTIR) spectroscopy, in: Membrane Characterization, Elsevier, (2017) 3–29.

[14] C.F. Holder, R.E. Schaak, Tutorial on Powder X-ray Diffraction for Characterizing Nanoscale Materials, ACS Nano 13 (2019) 7359–7365.

[15] J. Epp, X-ray diffraction (XRD) techniques for materials characterization, in: Materials Characterization Using Nondestructive Evaluation (NDE) Methods, Elsevier, (2016)81–124.

[16] W. Wong-Ng, H.F. McMurdie, C.R. Hubbard, A.D. Mighell, JCPDS-ICDD research associateship (cooperative program with NBS/NIST), Journal of Research of the National Institute of Standards and Technology 106 (2001) 1013.

[17] K. Akhtar, S.A. Khan, S.B. Khan, A.M. Asiri, Scanning Electron Microscopy: Principle and Applications in Nanomaterials Characterization, in: S.K. Sharma (Ed.), Handbook of Materials Characterization, Springer International Publishing, Cham, (2018)113–145.

[18] N.G. Yadav, N. Folastre, M. Bolmont, A. Jamali, M. Morcrette, C. Davoisne, Study of failure modes in two sulphide-based solid electrolyte all-solid-state batteries via in situ SEM, Journal of Materials Chemistry A 10 (2022) 17142–17155.

[19] B. Hafner, Scanning electron microscopy primer, Characterization Facility, University of Minnesota-Twin Cities (2007) 1–29.

[20] M. Abd Mutalib, M.A. Rahman, M.H.D. Othman, A.F. Ismail, J. Jaafar, Scanning electron microscopy (SEM) and energy-dispersive X-ray (EDX) spectroscopy, in: Membrane Characterization, Elsevier, (2017)161–179.

[21] J. Rouquerol, F. Rouquerol, P. Llewellyn, G. Maurin, K. Sing. Adsorption by powders and porous solids: principles, methodology and applications. Academic press,(2013).

Chapiter III

Sustainable Methylene Blue Removal Using Rosemary-Derived Activated Carbon and Green Nanoparticles

Summary

GRAPHICAL ABSTRACT

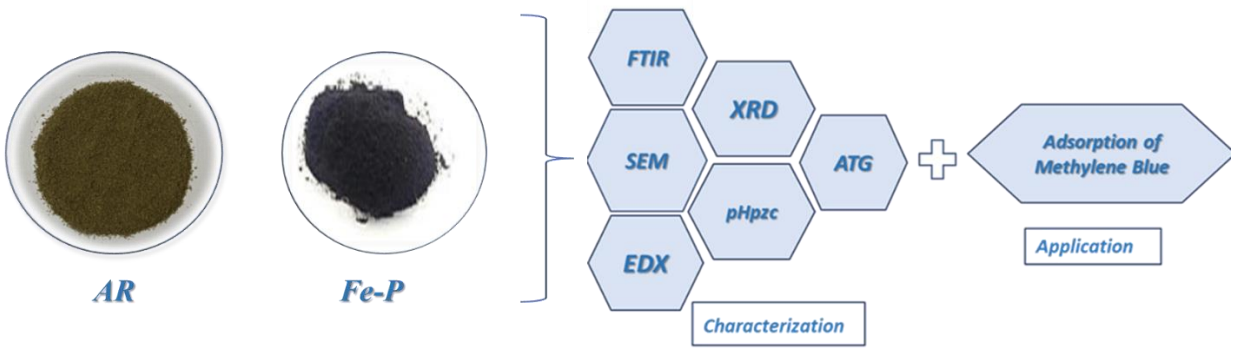

1. Introduction

The proliferation of dye-containing industrial waste has become a critical environmental concern. Recent studies investigate the use of dry spearmint sprigs as a low-cost, eco-friendly biosorbent for removing methyl violet 10B dye from aqueous solutions. The research highlights the adsorbent's high removal efficiency and potential for sustainable wastewater treatment applications [1]. Furthermore, many authors have explored the adsorption capacity of biosorbents prepared from mango seed kernels for the removal of methyl orange dye from aqueous solutions, emphasizing the effectiveness of using agricultural waste materials in dye wastewater treatment [2]. A previously conducted, highly pertinent study assessed the efficacy of biosorbents derived from Algerian date stones in adsorbing methylene blue dye from aqueous

solutions, highlighting the potential of utilizing local agricultural by-products in wastewater treatment processes [3]. These articles contribute valuable insights into sustainable and cost-effective methods for treating dye-laden industrial wastewater, addressing critical environmental concerns. Dyes as pollutants are particularly problematic because their chemical stability, while beneficial for their intended use, makes them extremely difficult to remove from wastewater. Environmental agencies worldwide have recognized this challenge, as these compounds not only disrupt aquatic ecosystems but also pose significant risks to human health [4]. Dyes are widely used in industries such as textiles, cosmetics, leather, rubber, pharmaceuticals, and food processing, which employ various dyes to manufacture diverse products. It is estimated that around 7 x 10^5 tons of dyes and pigments are consumed worldwide annually [5], with nearly 100 tons/year released into wastewater [6]. As a result, substantial coloured effluent from these industries is discharged into the natural environment. Their presence in water bodies poses serious risks to both humans and aquatic life [7]. Dyes can modify the colour characteristics of different products in various industries. They are typically defined as ionized and aromatic organic compounds [8]. Dyes can be broadly classified into anionic, cationic, and non-ionic types. Even at very low concentrations, dyes present serious pollution threats owing to their intense toxicity and high persistence in the environment [9]. Moreover, the chemicals in dyes and degraded dyes found in dye-containing wastewater are typically poisonous, mutagenic, or even carcinogenic, causing major harm to humans and aquatic life. For example, when dye-laden wastewater enters aquatic ecosystems, the toxic pollutants tend to accumulate in some fish tissues. Ultimately, these harmful substances may enter the human body through the food chain, resulting in many pathological issues [10]. Due to the large amounts and impacts, removing these pollutants is a major concern. Many physical, chemical, and biological treatment technologies (trickling filters, activated sludge, chemical coagulation, ion exchange, precipitation, carbon adsorption) have been extensively studied for eliminating dyes from wastewater effluents [11]. The adsorption method, which is of crucial interest in this study, has consistently demonstrated high efficiency in water treatment, effectively removing a wide range of pollutants, including heavy metals, dyes, organic compounds, and emerging contaminants from aqueous solutions [12]. Owing to its simplicity, cost-effectiveness, and high removal capacity, the adsorption method has been widely adopted and continuously developed in the water treatment field from the early 20th century to the present [13]. Moreover, as a versatile water treatment technique, adsorption has been successfully applied to treat industrial effluents, municipal wastewater, and groundwater,

making it one of the most adaptable methods in the field [14]. The adsorption method is preferred for removing dyes from industrial effluents over other techniques since it is efficient, cost-effective, and reusable. Researchers are also closely pursuing adsorption as a viable approach for eliminating dyes from wastewater due to its simplicity of fabrication, sensitivity to pollutants, and potential for industrial-scale application. To enhance adsorption efficiency, adsorbents have been continuously modified regarding pore structure and surface chemistry [15]. The use of adsorbents derived from biomass sources to remove dyes has recently garnered much interest owing to their renewable nature, low cost, and abundance. Nanotechnology involves the synthesis of nanoparticles with varying sizes, shapes, and chemical compositions that can have immense potential applications in diverse fields [16]. Metal nanoparticles, such as iron nanoparticles (Fe-P), have been found to possess wide functionality for purposes like wastewater treatment. Metal nanoparticles with desired properties like size and shape are typically synthesized using various physical and chemical processes with major drawbacks like high cost. Therefore, there is a clear need for a reliable, cost-effective, safe, and biocompatible system for nanoparticle production [17]. Activated carbon is renowned for its exceptional adsorption capabilities, making it a pivotal component in water and wastewater treatment processes. Its porous structure and extensive surface area enable the effective removal of a wide range of contaminants, including organic compounds, dyes, heavy metals, and other pollutants. Activated carbon can be derived from a wide range of natural and synthetic materials, with agricultural waste products such as coconut shells, rice husks, and orange peels being some of the most sustainable and cost-effective sources. Industrial by-products, including paper mill sludge, bagasse, and spent tea grains, offer an economical alternative for activating carbon production, transforming waste into valuable adsorbents. Coal-based activated carbon, derived from bituminous, sub-bituminous, and lignite coal, remains one of the most widely used forms of activated carbon due to its high adsorption capacity and availability. Activated carbon derived from lignite and peat is particularly effective for removing colour, taste, and odor from drinking water, making it a popular choice in municipal water treatment facilities. Relevant references supporting the aforementioned aspects are provided in [18].

The primary objective of this study was to evaluate the effectiveness of activated carbon derived from rosemary biomass (AR) and iron–polyphenol nanoparticles (Fe-P) for the removal of methylene blue (MB) dye from contaminated water. The contaminated water is wastewater sourced from Oued Bouslam, located in the city of Setif, Algeria. This work aimed to harness renewable agricultural waste and green synthesis methods to create cost-effective and

environmentally friendly solutions for dye pollution. To achieve this, the study involves several key stages: preparation and characterization of AR and Fe-P, optimization of adsorption parameters such as pH, adsorbent dosage, and contact time, and analysis of adsorption kinetics and isotherms to elucidate the adsorption mechanisms. Thermodynamic studies are conducted to assess the feasibility and spontaneity of the adsorption process, while the reusability of the adsorbents is evaluated through regeneration cycles. By combining renewable resources and green nanotechnology, this work contributes to the development of innovative and sustainable materials for water treatment.

2. Experimental Method

2.1. Method for preparing AR

Rosemary is a relatively drought-tolerant plant used in landscaping for hedges and rock gardens, especially during spring. After spring, the rosemary hedges are often burned or discarded, making this plant a potential waste resource for contaminant removal. The rosemary waste was collected, rinsed, dried overnight at 80°C, and crushed into powder (R). The powder was mixed with (6 M) phosphoric acid (H_3PO_4, 85%) in a (1:2) weight-to-volume ratio. The mixture was left under stirring for 24 h, which was washed with water until the pH reached 6.5. Finally, the mixture was dried, producing an activated rosemary material (AR).

Figure III.1. Preparation protocol for AR

2.2. Method for preparing Fe-P NPs

Aqueous rosemary extract was prepared by boiling 50 g of crushed leaves in 250 ml of distilled water at 80 °C for 1 h. The mixture was allowed to settle for 1 h [18], then vacuum filtered. Iron nanoparticles were synthesized using iron (III) chloride hexahydrate ($FeCl_3 \cdot 6H_2O$) as the iron precursor. A (0.10 M) solution of $FeCl_3 \cdot 6H_2O$ was made by

dissolving 1.62 g of $FeCl_3 \cdot 6H_2O$ in 100 ml of distilled water [19]. The 0.10 M $FeCl_3 \cdot 6H_2O$ solution was then added to the rosemary extract in a (2:1) volume ratio and heated at 80°C for 1 h with constant stirring at 540 rpm. This resulted in a black-colored solution with a pH of 4.40. After nanoparticle synthesis, (0.5 M) sodium hydroxide (NaOH) was incrementally introduced to the black iron nanoparticle solution, altering the pH from 4.40 to 11. The iron nanoparticle suspension was then agitated for 2 h. The final black nanoparticle dispersion was washed several times with distilled water and then subjected to drying in a 100°C oven for 17 h.

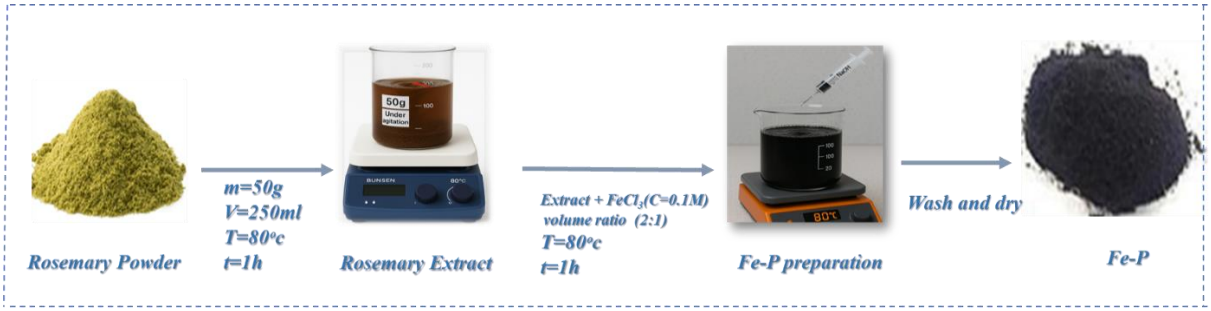

Figure III.2. Preparation protocol for Fe-P

3. Results

3.1. Characterization of AR and Fe–P adsorbents

3.1.1. X-Ray diffraction

X-ray diffraction (XRD) analysis was conducted to examine the crystalline of the prepared adsorbents AR and Fe-P (Figure III.3). The XRD pattern of AR shows the absence of sharp and well-defined diffraction peaks, indicating its predominantly amorphous nature. This behavior is evidenced by a high background signal and the presence of broad diffraction humps in the regions of 20°–30° and 35°–50°, which are characteristic of the disordered stacking of carbon layers in amorphous carbon materials. Such an amorphous structure is favorable for adsorption processes, as it promotes the formation of a heterogeneous surface rich in active sites, thereby enhancing the adsorption of dye molecules [20].

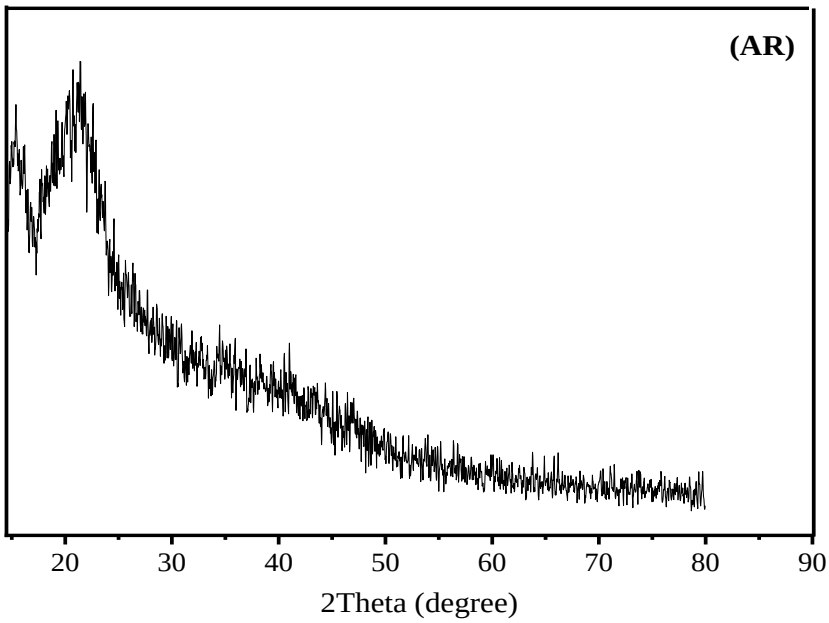

Figure III.3. X-ray Diffraction (XRD) patterns of AR

The XRD pattern of Fe-P (Figure III.4) exhibits sharp and well-defined diffraction peaks, confirming the crystalline nature of the synthesized material. The main diffraction peaks correspond to the hematite phase (α-Fe_2O_3) [21-23], indicating the successful formation of crystalline iron oxide. The average crystallite size calculated using the Scherrer equation is approximately 47.6 nm [24], confirming the nanocrystalline structure of the material.

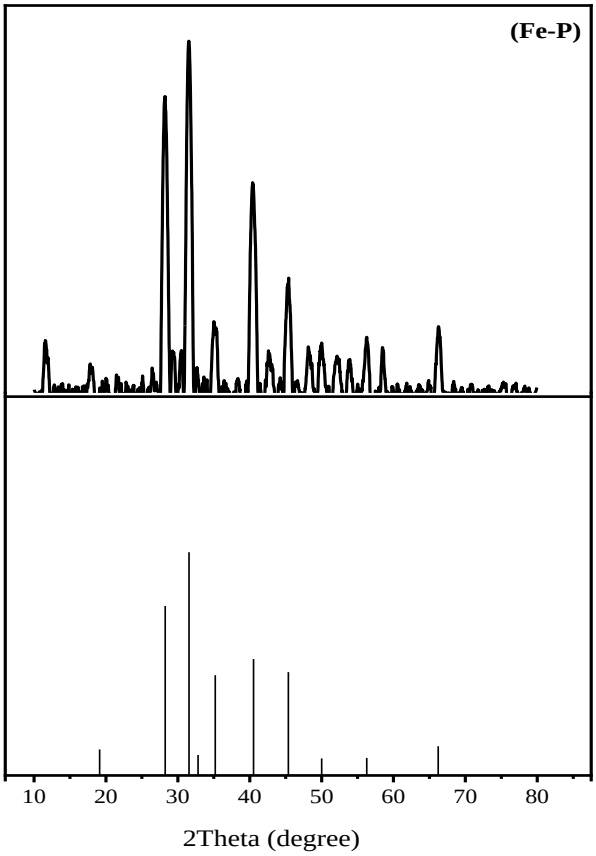

Figure III.4. X-ray Diffraction (XRD) patterns of Fe-P

3.1.2. Fourier-transform infrared spectroscopy

The FTIR spectra of AR and Fe-P samples (Figure III.5) reveal the presence of key functional groups on the adsorbent surface. A broad band around 3425 cm^{-1} is attributed to the stretching vibrations of O-H and N-H groups, indicating hydroxylated and phenolic surface sites as well as hydrogen bonding interactions [25]. The bands observed near 2923 cm^{-1} correspond to C-H stretching vibrations of aliphatic groups [26]. The absorption band at 1258 cm^{-1} is assigned to C-O stretching vibrations, while the appearance of bands around 600 cm^{-1} in the Fe-P sample is characteristic of Fe-O stretching, confirming the successful incorporation of iron oxide species onto the surface [27].

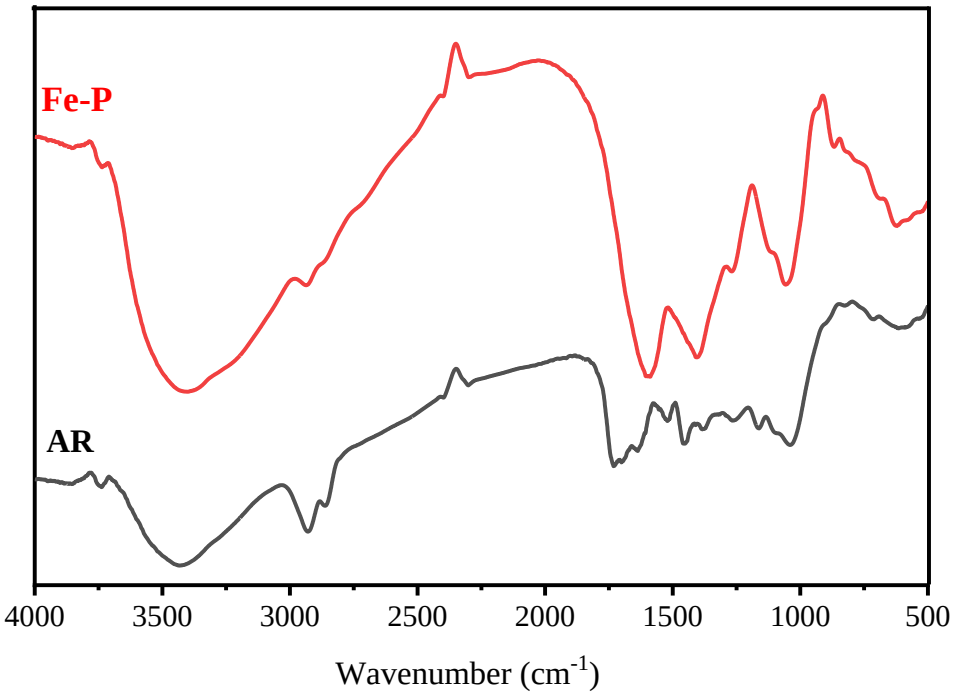

Figure III.5. Fourier-Transform Infrared spectroscopy profiles of AR and Fe-P

3.1.3. Scanning electron microscopy (SEM)

The micromorphology of the AR and Fe-P samples was examined using scanning electron microscopy (SEM), as presented in Figure III.6a and 6b. The SEM images of the AR sample reveal an irregular, and highly heterogeneous surface morphology, with developed and fragmented pore structures of varying sizes, suggesting a well-developed porous architecture conducive to adsorption. However, the outer surface also shows notable cracks, fissures, and surface fragmentation [20]. In contrast, the surface morphology of the Fe-P displays a dense distribution of agglomerated particles and self-assembled granular clusters, indicating successful deposition of iron-based species onto the carbon matrix. These modifications not only alter the surface texture but may also contribute to enhanced functional performance through increased surface reactivity and the presence of iron-active sites.

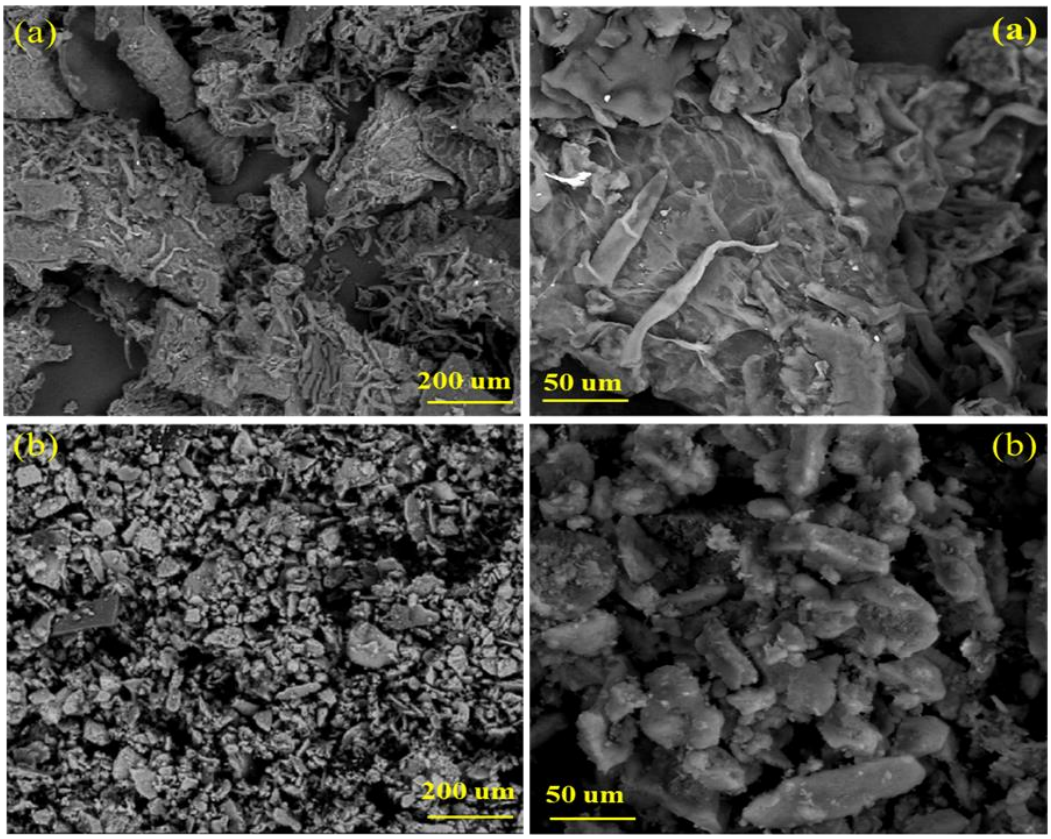

Figure III.6. SEM captures of (a) AR and (b) Fe-P

Particle size analysis based on image-derived histogram fitting shows a near-Gaussian size distribution, with an average particle diameter of approximately 49.40 nm, as illustrated in Figure III.7. This nanoscale particle size is expected to facilitate mass transfer and enhance the accessibility of adsorbate molecules to surface active sites, which may contribute to improved adsorption performance

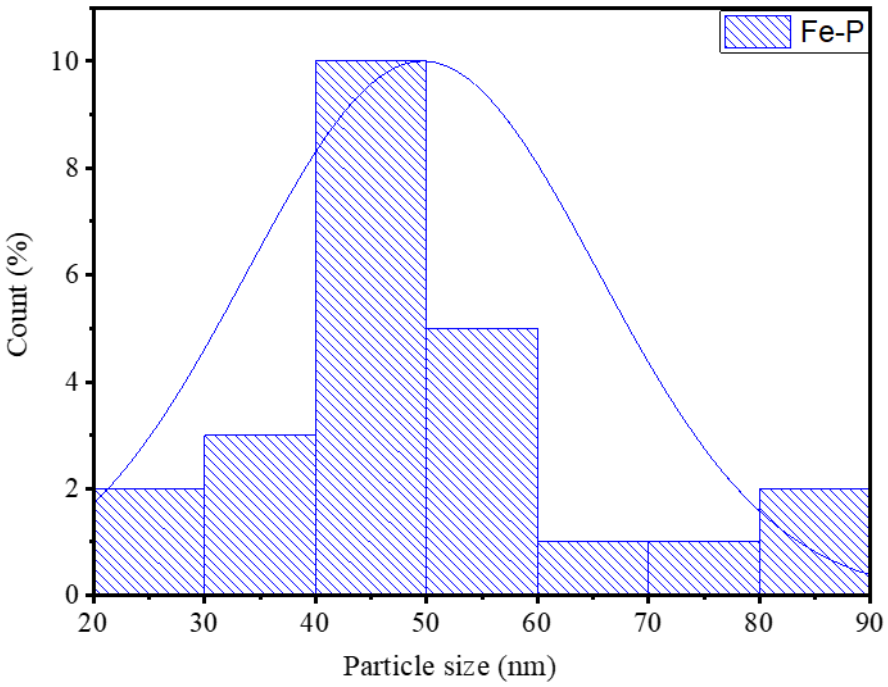

Figure III.7. The particle size average for (Fe-P)

3.1.4. Energy-dispersive X-ray spectroscopy (EDX)

Elemental analysis of the AR and Fe-P was conducted using energy-dispersive X-ray (EDX) spectroscopy (Figure III.8), providing crucial insights into the structural modifications occurring during synthesis. The AR material exhibits a typical carbonaceous structure with carbon and oxygen as predominant elements, along with trace amounts of Ca, Al, and Cl originating from the original biomass feedstock. In contrast, the Fe-P composite demonstrates a markedly different elemental profile with reduced carbon content (29.37 wt%) and successful Fe incorporation (11.79 wt%), while maintaining high oxygen content (40.22 wt%) indicative of iron oxide formation. Most notably, the Fe-P composite shows an expanded trace element composition including Mg, Al, Si, P, S, Na, K, Cl, and Ca, which can be attributed to NaOH-mediated immobilization mechanisms that retain these elements within the carbon framework through precipitation and complexation processes. This compositional transformation suggests enhanced functionality compared to AR material, where the introduction of catalytically active iron species and diverse trace elements may contribute to improved adsorption selectivity.

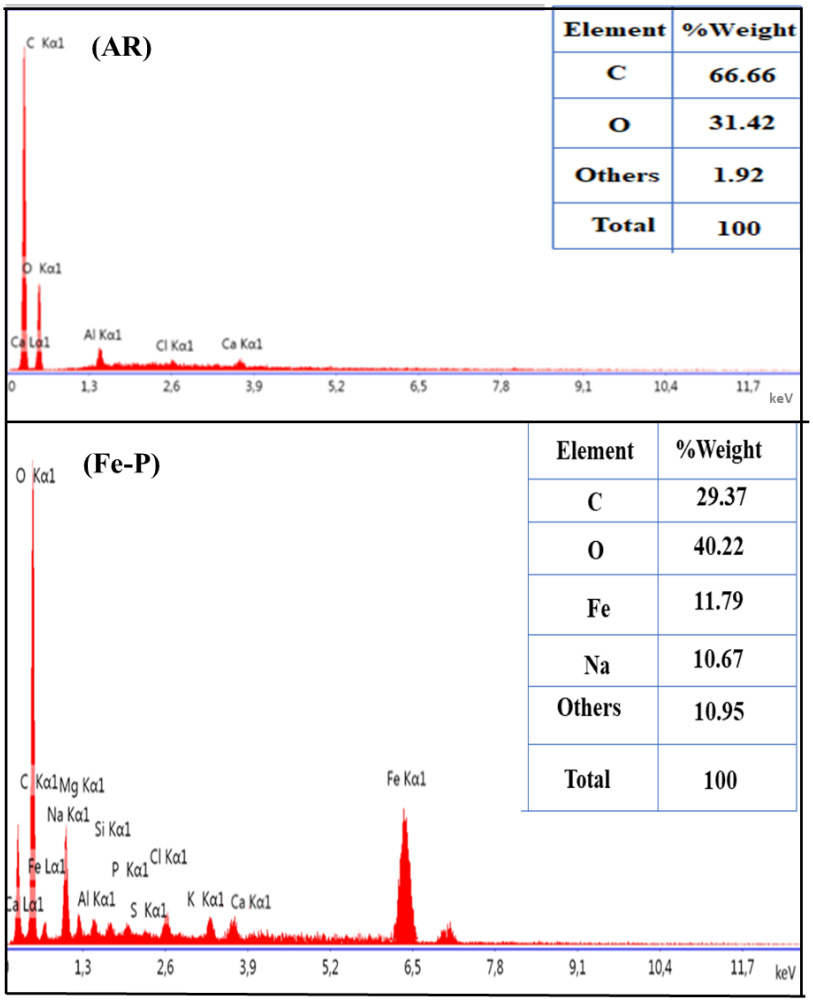

Element	%Weight
C	66.66
O	31.42
Others	1.92
Total	100

Element	%Weight
C	29.37
O	40.22
Fe	11.79
Na	10.67
Others	10.95
Total	100

Figure III.8. EDX spectra for the AR and Fe-P adsorbent materials

3.1.5. Thermogravimetric Analysis (TGA)

Thermogravimetric analysis was carried out on AR and Fe-P samples across a temperature range of 25 to 1000 °C, with the experimental data illustrated in Figure III.9. The thermal decomposition profile revealed three distinct stages: initially, from 25 °C to 200°C, the samples experienced weight losses of 4.43% for AR, and 19.84% for Fe-P, primarily attributable to the removal of adsorbed water and surface-bound volatile matter. The second stage, spanning 200 °C to 498 °C for AR and Fe-P, demonstrated significant mass reductions of 77.7% for AR, and 40% for Fe-P, which resulted from the decomposition of cellulosic elements. The final stage involved the gradual degradation of lignin, a component characterized by exceptional thermal stability compared to cellulose and hemicellulose polymers, progressively decomposing until reaching a stable residual mass [28].

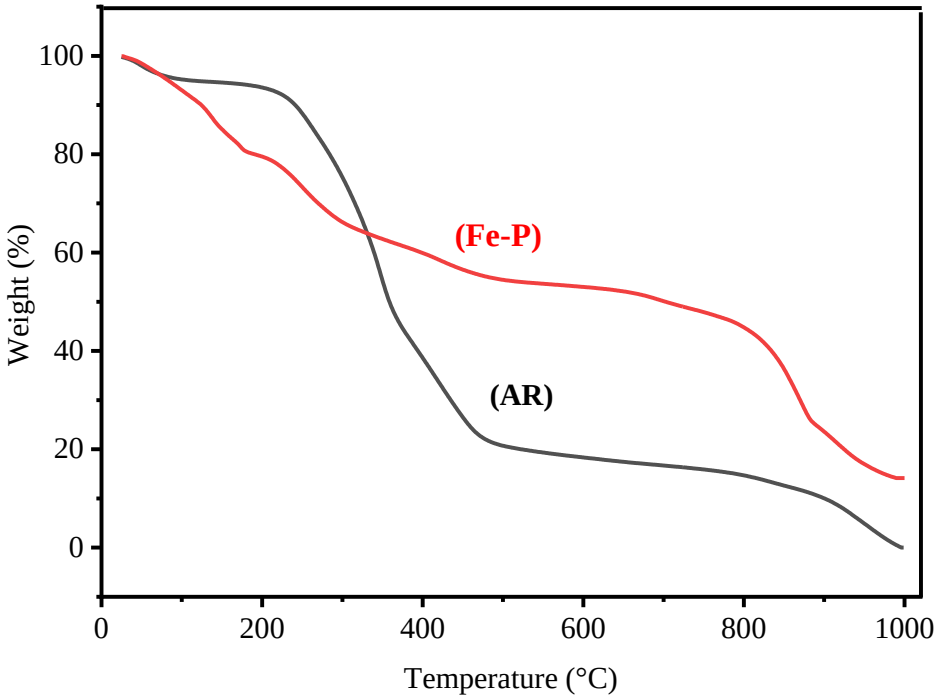

Figure III.9. TGA of AR and Fe-P

3.1.6. Point of zero charge (pH_{pzc})

The point of zero charge (pH_{pzc}) of the AR and Fe-P composite was experimentally determined and illustrated in Figure III.10. The measured pH_{pzc} values were 2.9 for AR and 7.9 for the Fe-P composite, respectively. These values are crucial for understanding the surface charge behavior of the adsorbents under different pH conditions. When the solution pH is lower than the pH_{pzc}, the surface of the adsorbent becomes positively charged due to the protonation of surface functional groups by H^+ ions. This favors the adsorption of negatively charged species. In contrast, at pH values above the pH_{pzc}, the surface acquires a negative charge because of deprotonation by OH^- ions, enhancing the adsorption of positively charged contaminants.

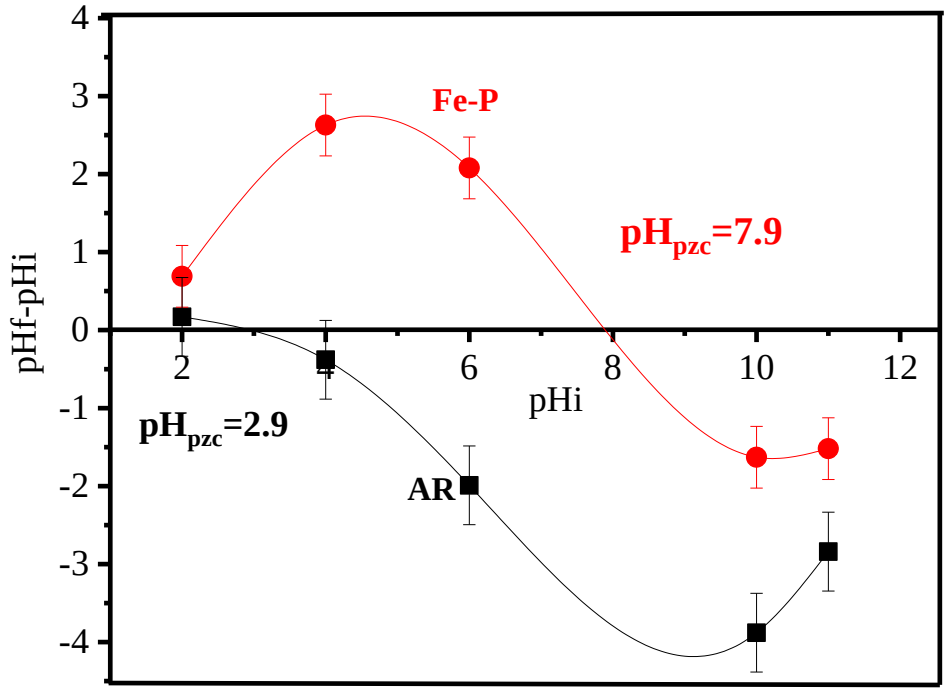

Figure III.10. Isoelectric points of AR, and Fe-P

3.2. Adsorption results

3.2.1. Effect of adsorbent dose

Figure III.11 plots the equilibrium adsorption capacity (mg/g) and percent dye removal against the adsorbent dosage (mg/L) for AR and Fe-P. As the dosage increased from 50 to 1000 mg/L, the adsorption density substantially decreased from 162.5 to 9.3 mg/g for AR, and 157.3 to 8.4 mg/g for Fe-P. This decline stems from the dilutive effect of higher sorbent levels on the dye concentration gradient, reducing the driving force for mass transfer onto each adsorbent binding site [29,30]. Conversely, the percentage of dye elimination rose with increasing dosage, from 81.2% to 93% for AR, and 78.6% to 84.3% for Fe-P over the same range.

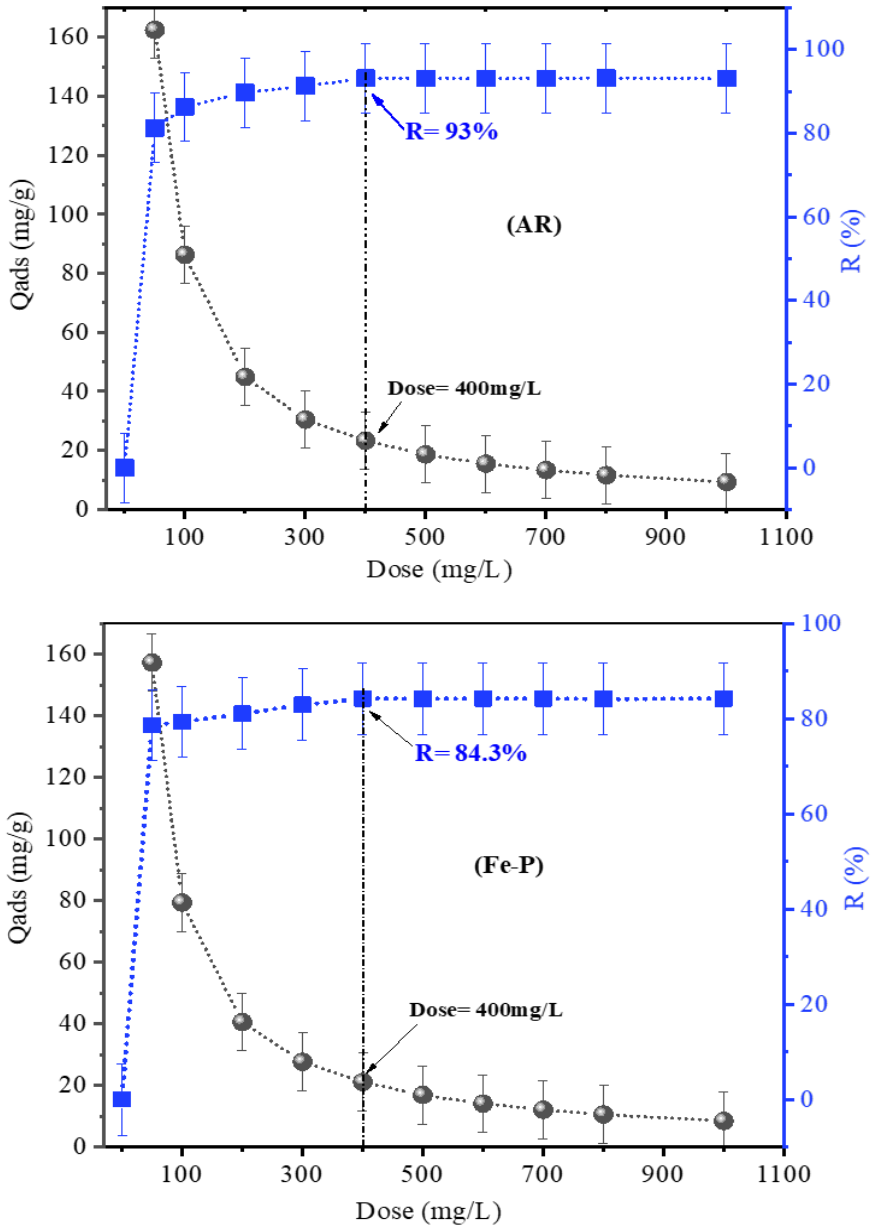

Figure III.11. Effect of AR, and Fe-P, mass on the amount of adsorption and percent removal of MB ($C_0 = 10\,mg/L\,;\ pH = 7.5\,;t = 24h$)

3.2.2. Initial pH effect

The results presented in Figure III.12 demonstrate the impact of initial pH on removing MB. For AR, adsorption efficiency increased under basic conditions and decreased in acidic media. This trend is attributed to the point of zero charge (pH_{pzc}) of AR (2.9). At higher pH values, the surface becomes negatively charged, and the presence of OH^- ions enhance electrostatic attraction with cationic MB molecules. Conversely, at lower pH values, the surface charge

becomes positive, leading to electrostatic repulsion and reduced adsorption. Interestingly, Fe-P exhibited an adsorption capacity of 16.96 mg/g in an acidic medium, despite its surface charge being positive like MB. This observation suggests that mechanisms beyond electrostatic interactions play a significant role in MB adsorption onto Fe-P.

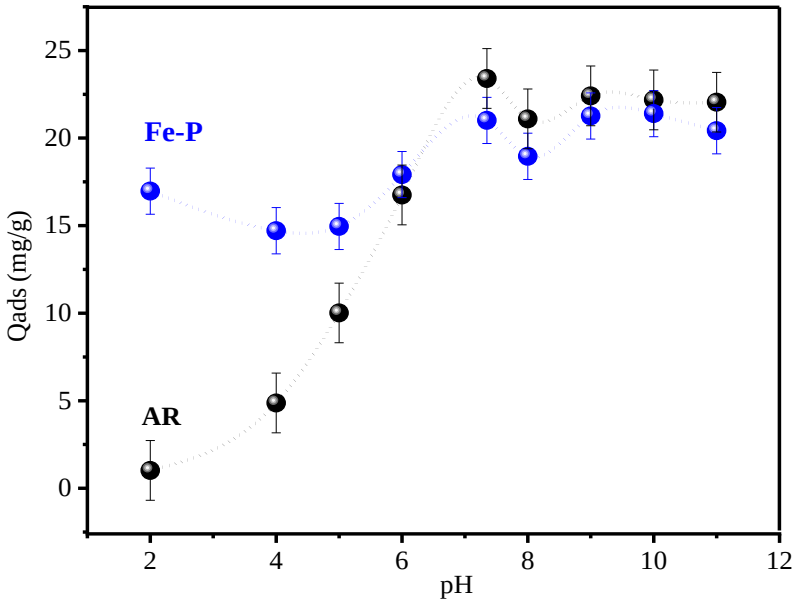

Figure III.12. Influence of pH on the adsorption of MB onto AR, and Fe-P

$(C_0 = 10\,mg/L\,;\ Dose_{(AR,Fe-P)} = 400mg/L\,;t = 24h)$

3.2.3. Kinetics of MB adsorption

* Impact of the MB initial concentration and the contact time

The adsorption kinetics shown in Figure III.13 demonstrate a two-stage uptake process for both AR and Fe-P. Initially, rapid dye uptake was observed within the first 40 min for AR, and 20 min for Fe-P as the MB molecules quickly diffused to occupy the readily accessible external surface sites. This fast stage was followed by a slower diffusion phase, where dye molecules penetrated deeper into the adsorbent pores and overcame boundary layer resistance to reach less accessible internal sites. As equilibrium approached, the adsorption rate decreased until saturation was achieved. Notably, the equilibrium adsorption capacities increased significantly with rising initial MB concentrations from 9.7 to 45.2 mg/g for AR and 6.8 to 45.0 mg/g for Fe-P reflecting the stronger concentration gradient that enhanced the driving force for mass transfer and adsorption efficiency.

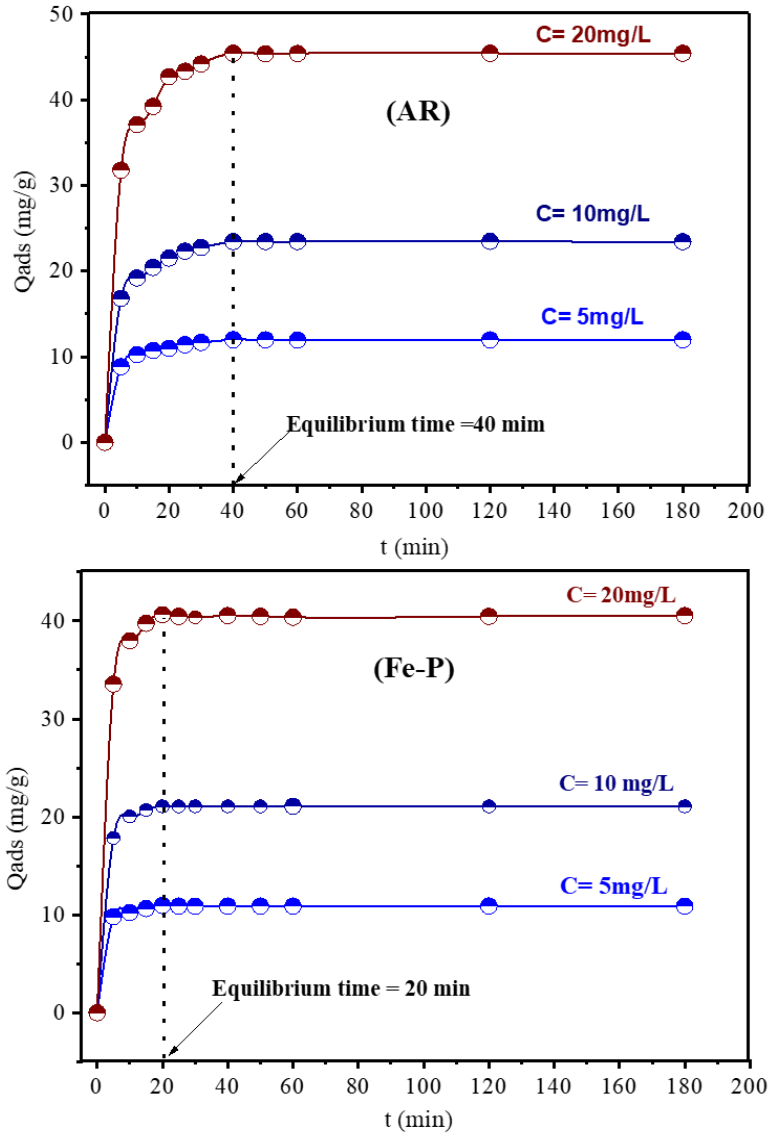

Figure III.13. Effect of MB concentration on the adsorption capacity of AR, and Fe-P ($pH = 7.5$; $Dose_{(AR,Fe-P)} = 400mg/L$)

***Modeling of kinetics**

Figure III.14 and Table III.1 present the results of three kinetic models. A comparison between the experimental adsorbed quantities and the theoretical values obtained from each revealed that the PSO model was the most suitable for describing the adsorption kinetics of MB onto AR, and Fe-P, outperforming the PFO and Elovich models. According to the literature, the pseudo-second-order kinetic model operates on the assumption that the rate- limiting step is chemical adsorption, involving the transfer of electrons between the

adsorbent and the adsorbate [31].

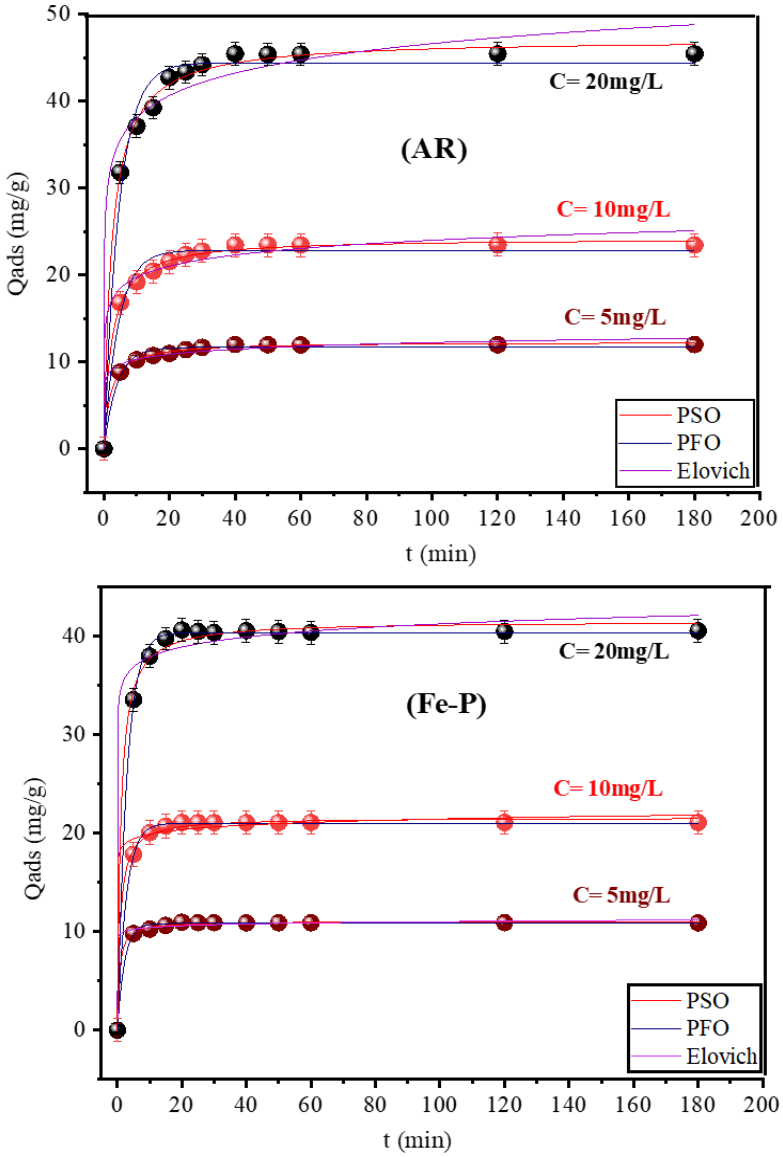

Figure III.14. PFO, PSO, and Elovich Kinetics model

Figure III.15 illustrates the intra-particle diffusion plots for AR and Fe-P. The multilinear nature of the curves, irrespective of initial dye concentration, suggests that MB adsorption proceeds through three distinct stages. In the first stage, MB molecules migrate from the bulk solution across the boundary layer to the external surface of the adsorbents. The second stage involves the gradual diffusion of dye molecules into the internal pores of the adsorbents, where intraparticle diffusion becomes the rate-limiting factor. Finally, the third stage corresponds to

the attainment of equilibrium, where the adsorption rate significantly slows as the available active sites become saturated [32].

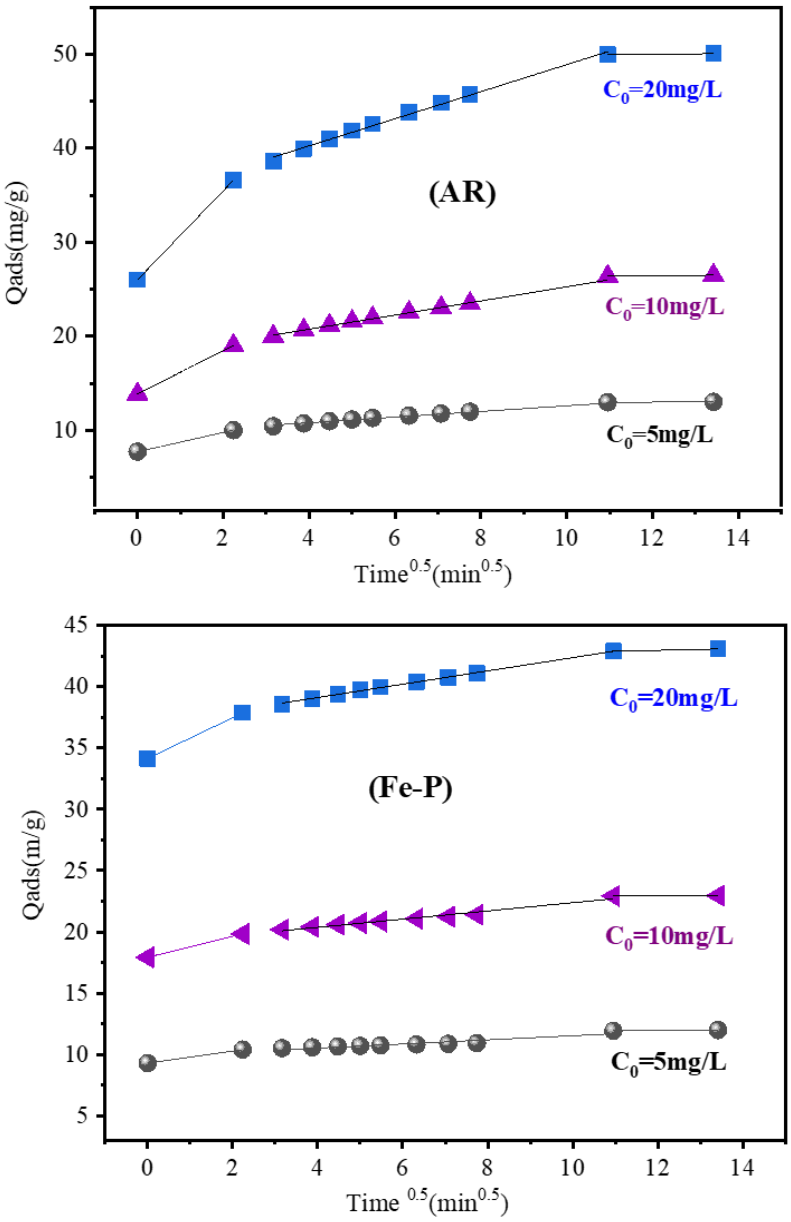

Figure III.15. Modeling of intraparticle diffusion of MB adsorption

Table III.1. Kinetics modeling parameters of PFO, PSO and Elovich models for MB adsorption onto AR, Fe-P

Materials	Models	Parameters	5mg/L	10 mg/L	20 mg/L
AR	PFO	Q_{exp}	11.98	23.44	45.43
		Q_e	11.65	22.82	44.39
		K_1	0.250	0.223	0.221
		R^2	0.985	0.981	0.984
		E_r	0.033	0.038	0.034
	PSO	Q_e	12.29	24.20	47.12
		K_2	0.040	0.017	0.008
		R^2	0.998	0.997	0.996
		E_r	0.010	0.015	0.015
	Elovich	A	17063.35	7761.08	10616.15
		B	1.188	0.539	0.269
		R^2	0.982	0.978	0.973
		E_r	0.202	0.090	0.048
	Intra-particle diffusion	K_{int}	1.529	3.448	7.085
		C	7.079	13.860	26.001
		R^2	0.822	0.804	0.779
		E_r	0.040	0.048	0.055
Fe-P	PFO	Q_{exp}	10.95	21.08	40.64
		Q_e	10.82	21.02	40.36
		K_1	0.451	0.368	0.344
		R^2	0.997	0.997	0.998
		E_r	0.011	0.006	0.006
	PSO	Q_e	11.04	21.56	41.53
		K_2	0.145	0.052	0.023
		R^2	0.998	0.999	0.999
		E_r	0.008	0.012	0.014
	Elovich	A	40592.6	46001	26808.4
		B	3.802	1.486	0.684
		R^2	0.998	0.988	0.985
		E_r	0.459	0.471	0.210
	Intra-particle diffusion	K_{int}	0.407	1.209	2.493
		C	9.787	18.028	34.145
		R^2	0.926	0.858	0.831
		E_r	0.019	0.028	0.033

3.2.4. Modeling of Adsorption Isotherms

To accurately describe the experimental equilibrium adsorption data, four models were employed: Langmuir, Freundlich, Redlich-Peterson, and Sips (Figure III.16). The Langmuir isotherm provided the best representation of the experimental data, indicating monolayer adsorption on homogeneous surfaces. The corresponding maximum adsorption capacities were 894.81 mg/g for AR and 603.96 mg/g for Fe-P, reflecting the higher affinity and availability of active sites in AR. The Freundlich model, which considers surface heterogeneity and multilayer adsorption, exhibited 1/n values lower than 1, suggesting favorable adsorption. Meanwhile, the

Redlich–Peterson and Sips models, which merge characteristics of Langmuir and Freundlich, provided additional flexibility in describing adsorption across different concentration ranges. Although all models showed a strong fit ($R^2 > 0.99$), the predominance of the Langmuir model implies that adsorption occurs primarily as a uniform monolayer rather than through heterogeneous multilayer coverage.

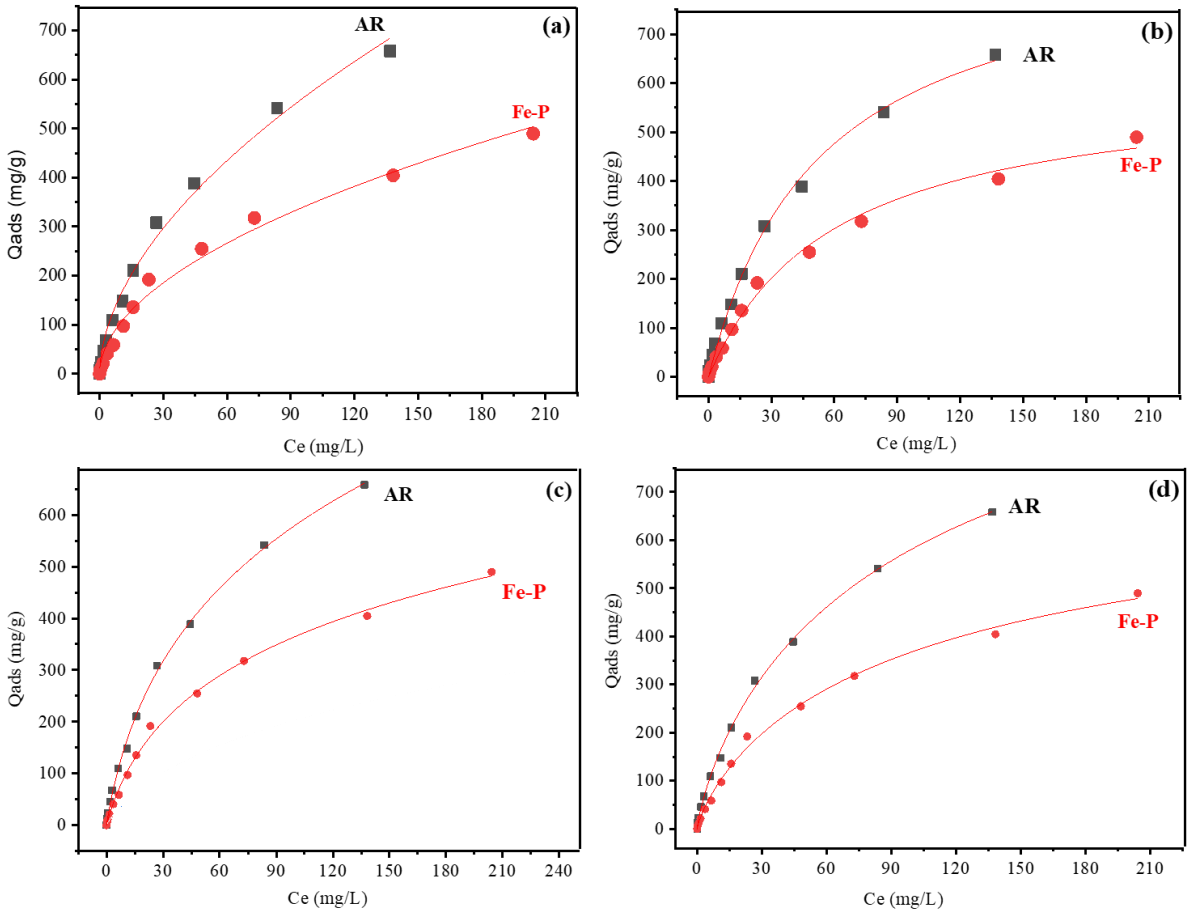

Figure III.16. The Freundlich (a); Langmuir (b); Redlich-Peterson (c); and Sips (d); models were applied to fit the equilibrium adsorption isotherms

Table III.2. Parameters of Adsorption Isotherms models on AR, and Fe-P

Models	Materials	Parameters				
Freundlich		K_f	n	R^2	E_r	
	AR	45.580	0.550	0.993	0.202	
	Fe-P	31.519	0.521	0.988	0.380	
Langmuir		K_L	Q_{max}	R^2	E_r	
	AR	0.0189	894.811	0.996	0.237	
	Fe-P	0.0167	603.968	0.995	0.143	
Redlich-Peterson		K	α	β	R^2	E_r
	AR	24.92	0.110	0.738	0.996	0.173
	Fe-P	14.807	0.091	0.763	0.993	0.382
Sips		Q_s	b	n	R^2	E_r
	AR	1222.36	0.022	0.799	0.995	0.107
	Fe-P	776.748	0.021	0.807	0.995	0.131

3.2.5. Thermodynamic study of adsorption

The evaluation of thermodynamic parameters, namely Gibbs free energy change (ΔG), enthalpy change (ΔH), and entropy change (ΔS), is essential to elucidate the adsorption mechanism of MB on AR and Fe-P. The Gibbs free energy change (ΔG) is a key indicator of the spontaneity of the adsorption process under standard conditions. A negative ΔG (ΔG < 0) denotes that adsorption is spontaneous and thermodynamically favorable, while a positive ΔG suggests a non-spontaneous process [33]. Similarly, the enthalpy change (ΔH) provides insights into the heat effect associated with adsorption. A positive ΔH indicates that the process is endothermic, implying that higher temperatures favor adsorption, whereas a negative ΔH indicates exothermic behavior, where adsorption is favored at lower temperatures. In this study, the negative ΔH values confirm that MB adsorption on AR and Fe-P is an exothermic process, suggesting stronger adsorbate–adsorbent interactions at lower temperatures [34]. Entropy change (ΔS) reflects the degree of randomness at the solid–liquid interface during adsorption. A positive ΔS suggests increased disorder and possible structural changes in the adsorbent or adsorbate molecules during adsorption. Conversely, a negative ΔS indicates decreased randomness, implying a more ordered system at the adsorbent surface [33]. The negative ΔS values observed in this study indicate that the adsorption process results in a more organized adsorbate layer on the adsorbent surface.

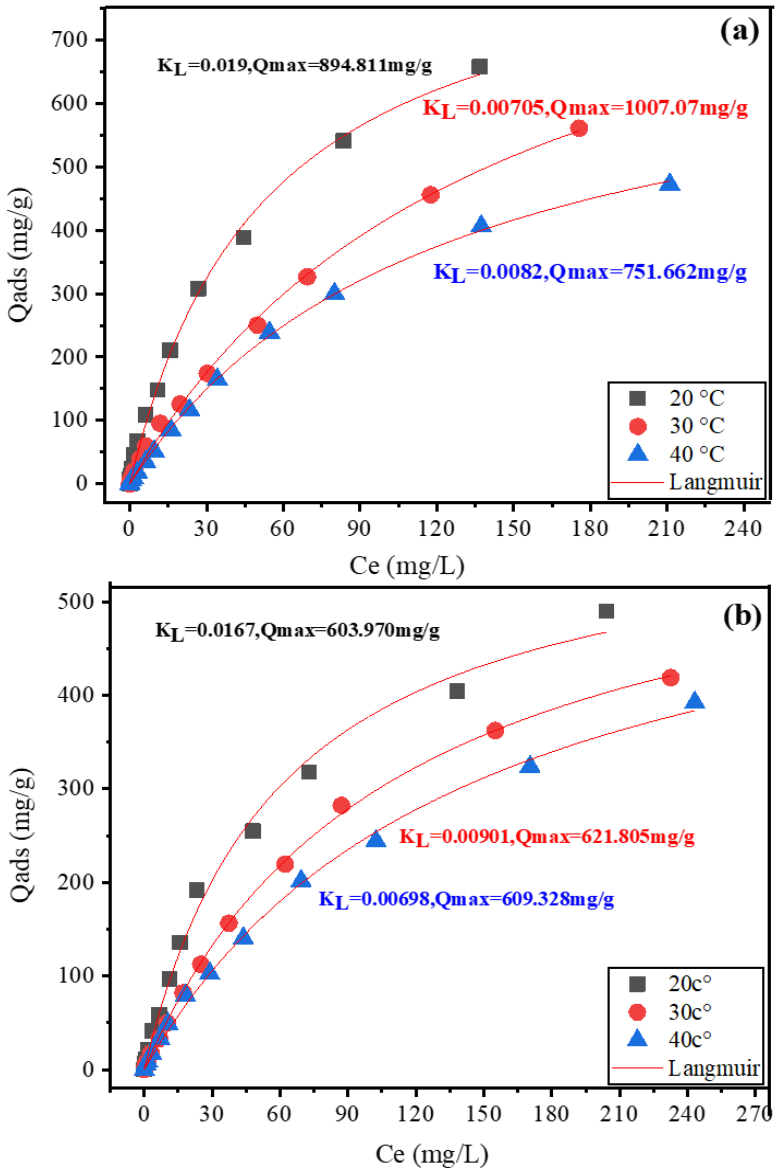

Figure III.17. Adsorption data obtained for AR (a) and Fe-P (b) at different temperatures were analyzed using the nonlinear Langmuir isotherm model.

Table III.3. Thermodynamics parameters of MB adsorption on AR, Fe-P

Adsorbent	*T* (K)	*ΔG°* (kJ/mol)	*ΔH°*(kJ/mol)	*ΔS°* (J/mol.K)
AR	293	-31.0082	-32.136	-5.358
	303	-30.963		
	313	-29.569		
Fe-P	293	-30.701	-33.510	-10.037
	303	-30. 519		
	313	-30.187		

3.2.6. Regeneration of AR

The ability to regenerate adsorbents offers both economic advantages and practical necessity for sustainable operation. Figure III.18 illustrates the reuse and regeneration performance of AR. The experimental results demonstrate that the adsorbent's efficiency gradually decreased over 7 consecutive cycles, with removal rates declining from 85.56% in the first cycle to 39.72% in the seventh cycle. This performance deterioration can be attributed to the progressive accumulation of MB molecules occupying the active sites on the AR surface. However, treatment with 0.1 M HCl effectively regenerated the adsorbent by promoting MB desorption and restoring the availability of active sites. These regeneration capabilities, combined with multiple reuse cycles, establish AR as a cost-effective and sustainable solution for MB removal from aqueous solutions.

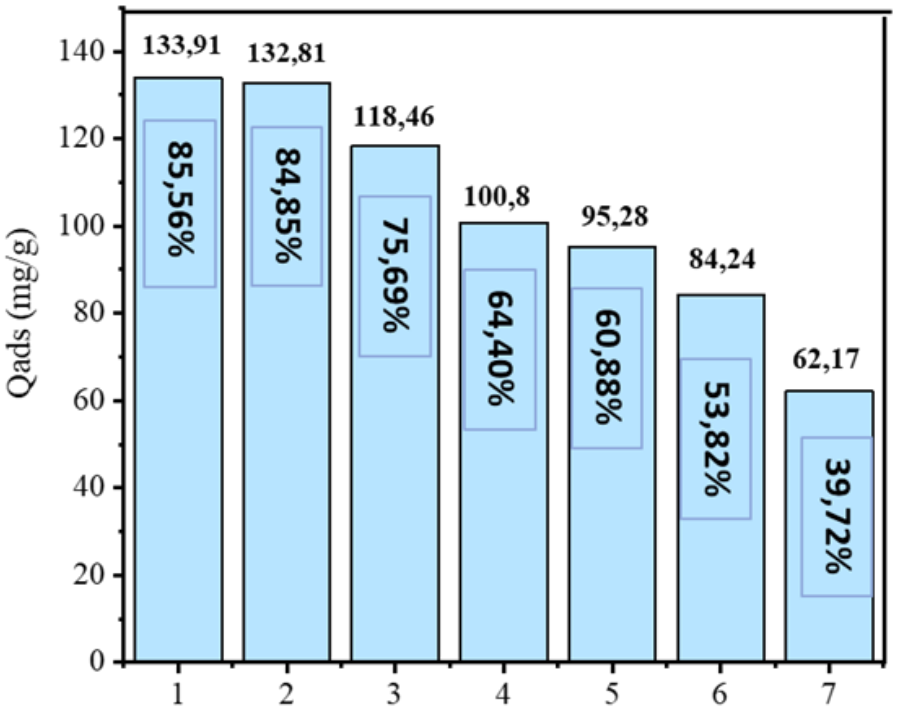

Figure III.18. Regeneration of AR($m = 300mg; V = 300mL; C_{MB} = 100mg/L$)

4. Conclusion

This study confirms the potential of rosemary-derived materials as efficient and eco-friendly adsorbents for dye removal from wastewater, addressing a critical environmental challenge while promoting sustainable resource utilization. The activated rosemary (AR) demonstrated exceptional adsorption capacity (894.81 mg/g) owing to its highly porous, amorphous structure, while the iron–polyphenol nanoparticles (Fe-P) exhibited faster kinetics and notable efficiency under acidic conditions due to their crystalline nature and surface reactivity. Thermodynamic evaluations revealed that adsorption on both materials was spontaneous and exothermic, and kinetic modeling confirmed that the process followed a pseudo-second-order mechanism, suggesting strong interactions at the active sites. The successful integration of plant-based carbon materials and green-synthesized iron oxide nanoparticles not only reduces dependence on conventionally activated carbon but also values agricultural waste, offering a promising alternative for potential large-scale wastewater treatment applications.

Bibliographic references

[1] A. Boudaoud, M. Djedid, M. Guermit, M. Benalia. Removal of azo toxic dye from aqueous solutions using dry spearmint sprigs, Larhyss Journal, 59(2024)29-51.

[2] O. Khelifi, I. Mehre, M. Younsi, M. Nacef, A.M. Affoune. Methyl orange adsorption on biosorbent derived from mango seed kernels, Larhyss Journal, 36(2018) 145-156.

[3] O. Khelifi, I. Mehrez, W. Ben Salah, F. Ben Salah, M. Younsi. Study of methylene blue (MB) adsorption from aqueous solutions on biosorbent prepared from Algerian date stones, Larhyss Journal, 28(2016) 135-148.

[4] A. Hamezadeh, Y. Rashtbari, S. Afshin, M. Morovati, M. Vosouchi . Application of low-cost material for adsorption of dye from aqueous solution. International Journal of Environmental Analytical Chemistry, 102(2022) 254-269.

[5] V.K. Gupta, R. Kumar, A. Nayak, A. Saleh, M.A. Barakat. Adsorptive removal of dyes from aqueous solution onto carbon nanotubes: a review, Advances in colloid and interface science, 193(2013) 24-34.

[6] N. Dizge, C. Aydiner, E. Demirbas, M. Kobya, S. Kara. Adsorption of reactive dyes from aqueous solutions by fly ash: kinetic and equilibrium studies, Journal of hazardous materials, 150(2008) 737-746.

[7] H. Khelili, S. Achour, K.G. Konan, M. Gulelil. Kinetic and isotherm study of Methylene blue adsorption on orange peel activated carbon, Larhyss Journal, 21(2024) 89-103.

[8] M.T. Yagub, T.K. Sen, S. Afroze, S.S. Afroze, M. Ang, H. Dye and its removal from aqueous solution by adsorption: a review, Advances in colloid and interface science, 209(2014)172-184.

[9] K. Hameed, M.P. Shahul, M.M. Sundaram. Adsorption of chromotrope dye onto activated carbons obtained from the seeds of various plants: equilibrium and kinetics studies, Arabian Journal of Chemistry, (2017) S2225-S2233.

[10] S. Afroze, T.K. Sen. A review on heavy metal ions and dye adsorption from water by agricultural solid waste adsorbents, Water, Air, Soil Pollution, (2018)1-50.

[11] D.H. Fadhil, A. AL-Hussin, E. Yousif. Removal of methylene blue dye from water using eco-friendly waste products (Eggshell) as an adsorbent and using the optimum adsorption conditions with real water sample from Tigris River, Al-Nahrain Journal of Science, (2019)9-14.

[12] H. Khelili, S. Achour. A. Rezeg. Effectiveness of aluminum sulfate and activated carbon against aromatic organic pollutants, Larhyss Journal, (2010) 99-110.

[13] L. Youcef, A. Ouakouak, D. Boulanouar, S. Achour. Study of the adsorbent power of powdered activated carbon for the elimination of phosphates from natural waters, Larhyss Journal, (2014) 35-46.

[14] A.A. Awang Nasrizal, W. Farzana, I. Saad, N. Bolong N. Carbonized coconut shell media applicability for stormwater pollution control, Larhyss Journal,(2023) 43-52.

[15] X. Zhang, S. Lin, Z. Chen. M. Mecharaj, R. Naidu. Kaolinite-supported nanoscale zero-valent iron for removal of $Pb^{2+}$from aqueous solution: reactivity, characterization and mechanism, Water Research , 45 (2011), 2911–2928.

[16] H. Kumar, K. Bhardwaj, K. Kuča, A. Kalia, E. Nepovimova, R. Verma, D. Kumar, Flower-based green synthesis of metallic nanoparticles: Applications beyond fragrance. Nanomaterials, 10 (2020).

[17] Z. Wang, Iron complex nanoparticles synthesized by eucalyptus leaves. ACS Sustainable Chemistry & Engineering, 1(2013), 1551–1554.

[18] R.U. Kanppe, D. Chapter 9 - Surface chemistry effects in activated carbon adsorption of industrial pollutants, Interface Science and Technology,10(2009)55-177.

[19] A. Naboulsi, I. Naboulsi, A. Regti, M. El Himri, El Haddad, the valorization of rosemary waste as a new biosorbent to eliminate the Rhodamine B dye. Microchemical Journal, 191 (2023), 108790.

[20] M. Zainuri, et al. Hematite from natural iron stones as microwave absorbing material on X-band frequency ranges. Materials Science in Semiconductor Processing, 71 (2017), 327–334.

[21] M. Anbukkarasi, et al. green synthesis: An eco-friendly route for the synthesis of iron oxide nanoparticles using aqueous extract of Thevetia peruviana and their biological activities. Scientific Reports, 15(2025)18316.

[22] P. Farshchi, et al. Eco-friendly synthesis of Fe_3O_4 nanoparticles using plant extracts: Rosemary and thyme. Iranian Journal of Chemistry and Chemical Engineering (2022).

[23] H.M. Nguyen, A.T. Tran, D.N.L. Nguyen, H.H. Lam, T.M. Tran-Thuy, L.Q. Nguyen, D.V. Nguyen. One-pot fabrication of zero-valent iron-embedded activated carbon from rosemary distillation residues for malachite green removal. Materials Research Express, 10(2023)085603.

[24] P. Tiwari, M.C. Vishwakarma, S.K. Joshi, Adsorption of Pb(II), Cu(II), and Zn(II) ions onto Urtica dioica leaves (UDL) as a low-cost adsorbent: Equilibrium and thermodynamic studies. Modern Chemistry, 5 (2017), 11–18.

[25] M.A. Nahil, P.T. Williams, Pore characteristics of activated carbons from the phosphoric acid chemical activation of cotton stalks. Biomass and Bioenergy, 37 (2012), 142–149.

[26] E. Sarala, N.M. Madhukara, M. Vinuth, R.Y.V. Rami, H.R. Sujatha, Green synthesis of Lawsonia inermis-mediated zinc ferrite nanoparticles for magnetic studies and anticancer activity against breast cancer (MCF-7) cell lines. Journal of Materials Science: Materials in Electronics, 31 (2020), 8589–8596.

[27] S.P. Yudha, S. Tekasakul, K. Phoungthong, L. Chuenchom, Green synthesis of low-cost and eco-friendly adsorbent for dye and pharmaceutical adsorption: Kinetic, isotherm, thermodynamic and regeneration studies. Materials Research Express, 6.12 (2019), 125526.

[28] A. Shukla, Y.H. Zhang, P. Dubey, J.L. Margrave, S.S. Shukla, The role of sawdust in the removal of unwanted materials from water. Journal of Hazardous Materials, 95.1–2 (2002), 137–152.

[29] M.A. Al-Ghouti, M.A.M. Khraisheh, M.N.M. Ahmad, S. Allen, Adsorption behaviour of methylene blue onto Jordanian diatomite: A kinetic study. Journal of Hazardous Materials, 165.1–3 (2009), 589–598.

[30] S. Sahnoun, M. Boutahala, Adsorption removal of tartrazine by chitosan/polyaniline composite: Kinetics and equilibrium studies. International Journal of Biological Macromolecules, 114 (2018), 1345–1353.

[31] G. Polat, Y.S. Açikel, Synthesis and characterization of magnetic halloysite–alginate beads for the removal of lead (II) ions from aqueous solutions. Journal of Polymers and the Environment, 27 (2019), 1971–1987.

[32] I. Anastopoulos, G.Z. Kyzas, Are the thermodynamic parameters correctly estimated in liquid-phase adsorption phenomena? Journal of Molecular Liquids, 218 (2016), 174–185.

[33] H.N. Tran, S.J. You, H.P. Chao, Thermodynamic parameters of cadmium adsorption onto orange peel calculated from various methods: A comparison study. Journal of Environmental Chemical Engineering, 4.3 (2016), 2671–2682.

Chapiter IV

Activated and Zinc Oxide-Modified Ruta graveolens Adsorbents for Congo Red Dye Removal

Summary

GRAPHICAL ABSTRACT

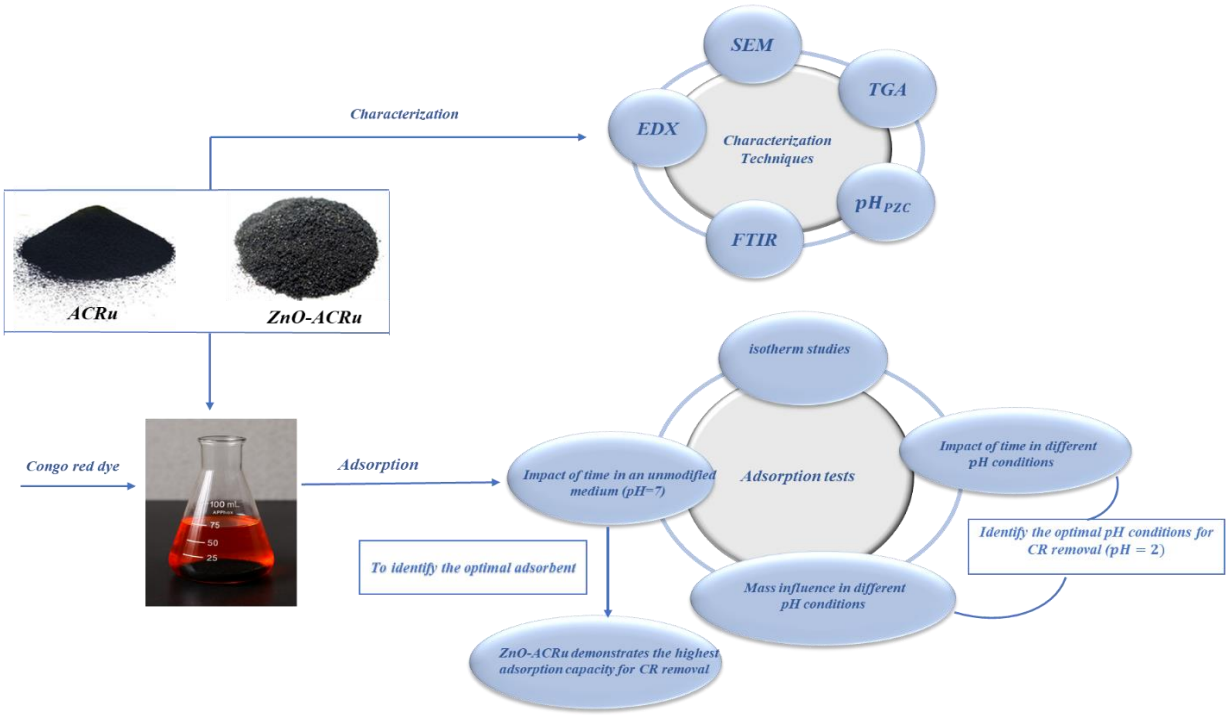

1. Introduction

Synthetic dyes are discharged in large volumes from textile dyeing, paper finishing, leather processing, and laboratory uses, and many persist because of complex aromatic structures, auxochromes, and strong chromophore bonds that resist conventional biological treatment.

Highly colored carcinogenic by-products introduced into receiving waters inhibit photosynthetic activity, interfere with aquatic food webs, and, upon chemical or biological transformation, can yield toxic or carcinogenic byproducts [1]. Among industrial colorants, anionic azo dyes bearing sulfonate groups are especially troublesome because their water solubility promotes transport and their structural stability limits degradation. Congo red (CR) is widely employed as a model pollutant for this dye class in adsorption and advanced treatment research because it is analytically tractable and strongly colored [2].

Unlike cationic species, anionic dyes often experience electrostatic repulsion at the surfaces of many carbonaceous materials, which assume net negative charge at neutral to alkaline pH. Effective removal thus depends on tailoring the surface chemistry of adsorbents, exploiting non-electrostatic interactions such as hydrogen bonding, and optimizing pore structure [3]. Hybrid carbon/metal-oxide systems have drawn attention because the inorganic phase can tune surface charge and reactivity while the carbon matrix supplies high area and mass-transfer pathways [4,5].

This research aimed to assess how effectively Ruta graveolens-based adsorbents, specifically activated and calcined Ruta graveolens (ACRu) and zinc oxide-modified activated calcinated Ruta graveolens (ZnO-ACRu) remove Congo red dye from aqueous solutions. The investigation followed a systematic approach: first preparing and characterizing both ACRu and ZnO-ACRu materials, then identifying ZnO-ACRu as the superior adsorbent and determining its optimal operating conditions. The study examined adsorption kinetics and isotherms to understand the underlying removal mechanisms. Additionally, thermodynamic parameters were analyzed to evaluate the process feasibility and spontaneity, while the economic viability of the adsorbent was assessed through multiple regeneration and reuse cycles

2. Method of the experiment

2.1. Method for preparing ACRu and ZnO-ACRu

The ACRu and its ZnO-ACRu composite were synthesized using Ruta graveolens as the precursor material, with the preparation steps summarized in Figure IV.1. Initially, the plant material was thoroughly washed with hot tap water and rinsed with distilled water to remove surface impurities, then dried at 105 °C for 12 h. To produce Ru, 2 g of dried Ruta graveolens powder was impregnated with concentrated phosphoric acid (H_3PO_4, 85%) at a solid-to-liquid ratio of 1:1.5 and kept at room temperature for 24 h. The impregnated mixture was neutralized

with 0.1 M NaOH, rinsed with distilled water until the filtration reached a stable pH, and subjected to thermal activation at 450 °C for 2 h (ACRu).

For the ZnO-ACRu composite, 0.5 g of ACRu was dispersed in 25 mL of zinc acetate solution (0.25 mol/L) under continuous magnetic stirring at 50 °C for 1 h. A 0.5 mol/L NaOH solution was added dropwise, followed by stirring for an additional 2 h. The suspension was then centrifuged, and the precipitate was repeatedly washed with distilled water until neutral pH was achieved. The final ZnO-ACRu composite was dried and stored in sealed containers, following a methodology like that reported in [6].

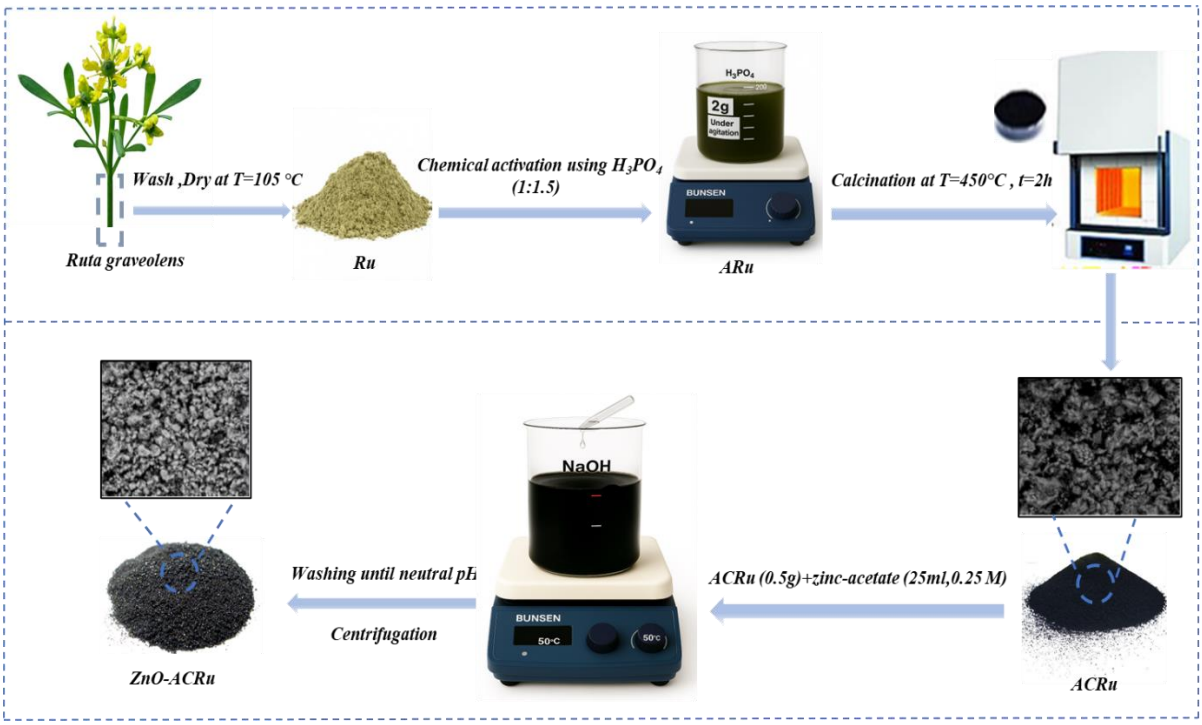

Figure IV.1. Preparation protocol for ACRu and ZnO-ACRu

3. Results

3.1. Characterization of ACRu and ZnO-ACRu

3.1.1. Fourier-transform infrared spectroscopy (FTIR)

Figure IV.2 compares the FTIR spectra of ACRu and ZnO-ACRu, highlighting clear spectral changes that accompany ZnO loading. The broad O-H stretching band centered near 3413 cm^{-1} becomes more intense in the ZnO-ACRu sample, suggesting an increase in surface hydroxylated or hydrogen-bonded functionalities. The aromatic C=C vibration at ~1575 cm^{-1} also gains intensity, consistent with modifications in the carbon matrix. A distinct new band

appears around 1375 cm^{-1}, which can be assigned to C-H bending modes. Additional absorption features observed in the 1035–600 cm^{-1} region, particularly below 600 cm^{-1}, are characteristic of Zn-O lattice stretching vibrations, providing clear spectroscopic evidence for the successful anchoring of ZnO nanoparticles onto the activated carbon surface. Overall, these spectral modifications confirm the effective incorporation of ZnO and the resulting evolution of surface chemistry in ZnO-ACRu [6].

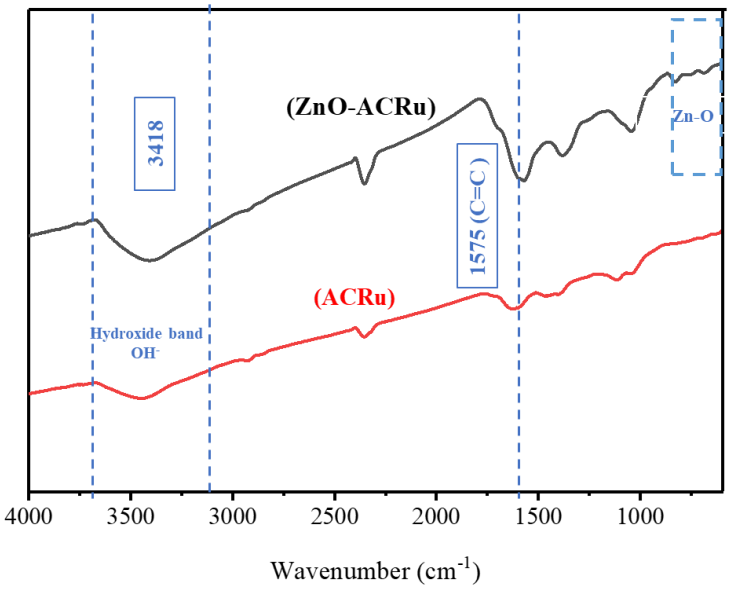

Figure IV.2. FTIR characterization of ACRu and ZnO-ACRu

3.1.2. Scanning electron microscopy (SEM)

Figure IV.3 presents the SEM micrographs of ACRu and ZnO-ACRu, highlighting notable differences in their surface morphology. The pristine ACRu displays an irregular and rough surface texture characterized by a heterogeneous distribution of pores, including interconnected macropores and some mesopores. Such a porous network is advantageous for adsorption, as it enhances the diffusion of adsorbate molecules and increases the active surface area available for interaction. In contrast, the ZnO-ACRu composite shows a surface uniformly decorated with quasi-spherical to slightly hexagonal ZnO nanostructures, firmly anchored onto the carbon framework. These nanoparticles not only increase surface roughness but may also introduce additional active sites due to the presence of ZnO, which can facilitate surface complexation and electrostatic interactions during adsorption. The well-dispersed ZnO nanostructures further

indicate successful nucleation and growth on the carbon matrix without causing pore blockage, thereby maintaining the accessibility of the carbon surface [6].

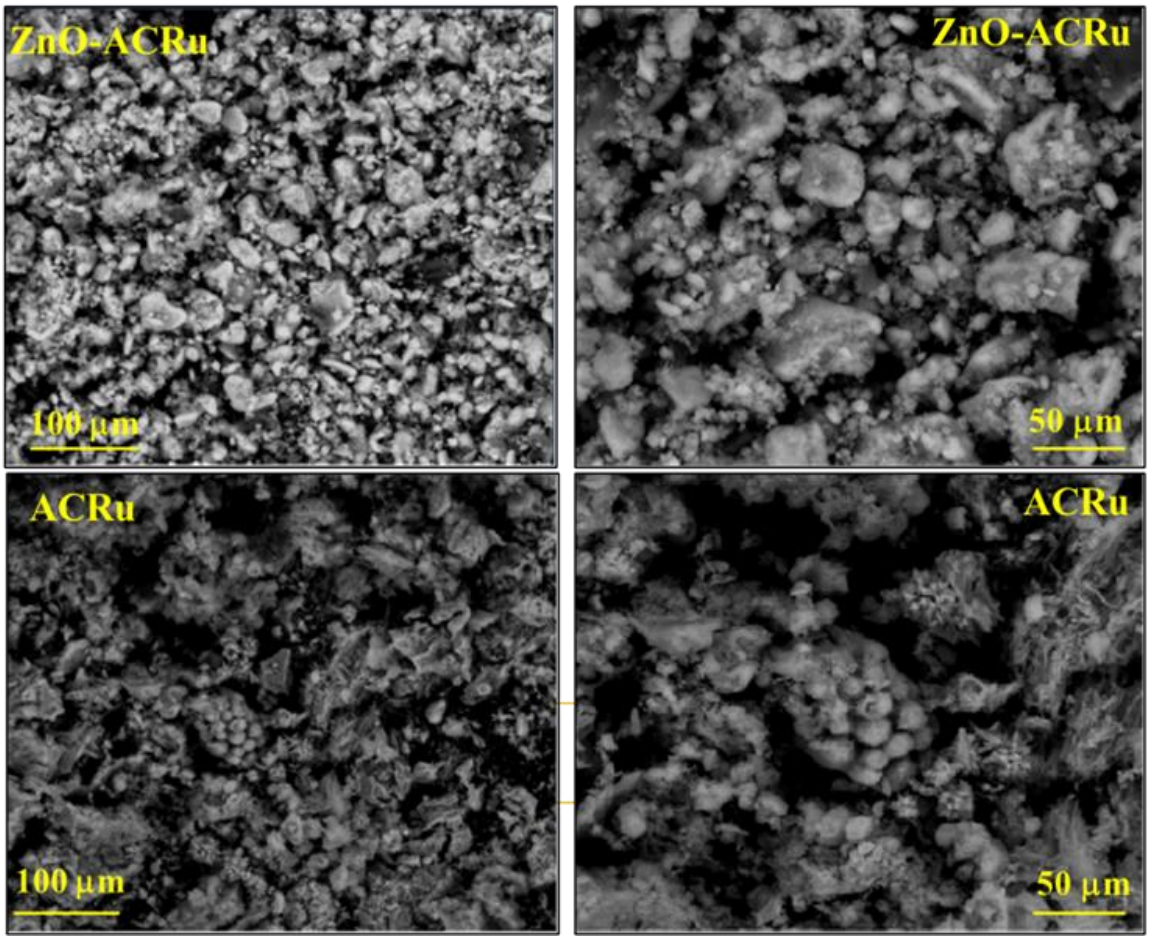

Figure IV.3. SEM captures of ACRu, and ZnO-ACRu

Particle size analysis based on image histogram fitting reveals a Gaussian distribution, with an average particle size of about 14.05 nm, as shown in Figure IV.4. This narrow and symmetric distribution indicates good control over the synthesis process. The obtained average size is also consistent with the values reported by other researchers [6].

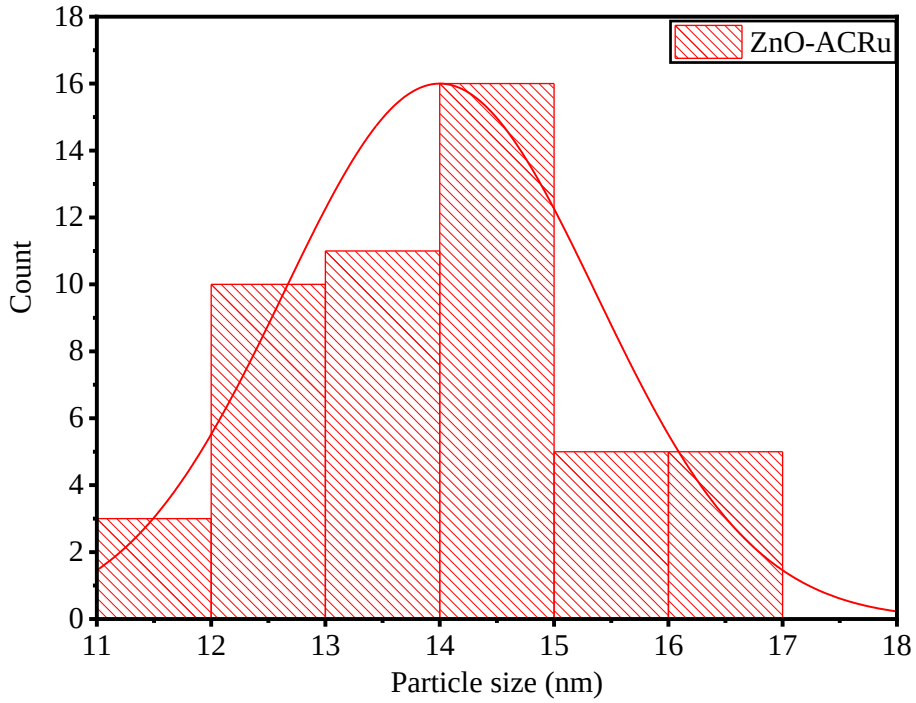

Figure IV.4. The particle size average for (ZnO-ACRu)

3.1.3. Energy-dispersive X-ray spectroscopy (EDX)

The EDX analysis of the adsorbent materials demonstrates notable compositional alterations following ZnO nanoparticle modification. Initially, the ACRu material was predominantly composed of oxygen (68%) and carbon (24%), with minor constituents such as Mg, Al, and Ca (3.7%), along with trace amounts of Zn (0.05%). After modification, the ZnO-ACRu composite exhibited a marked increase in zinc content to 11%, confirming the successful deposition of ZnO nanoparticles on the carbon matrix. This modification also led to an increase in oxygen content to 72.3% and a corresponding decrease in carbon content to 16%, which can be attributed to the incorporation of oxygen-rich ZnO. Additionally, the calcium content significantly declined from 3.7% to 0.41%, suggesting possible ion-exchange phenomena during synthesis, where zinc ions may have replaced calcium ions. These compositional variations collectively verify the successful formation of the ZnO-ACRu composite.

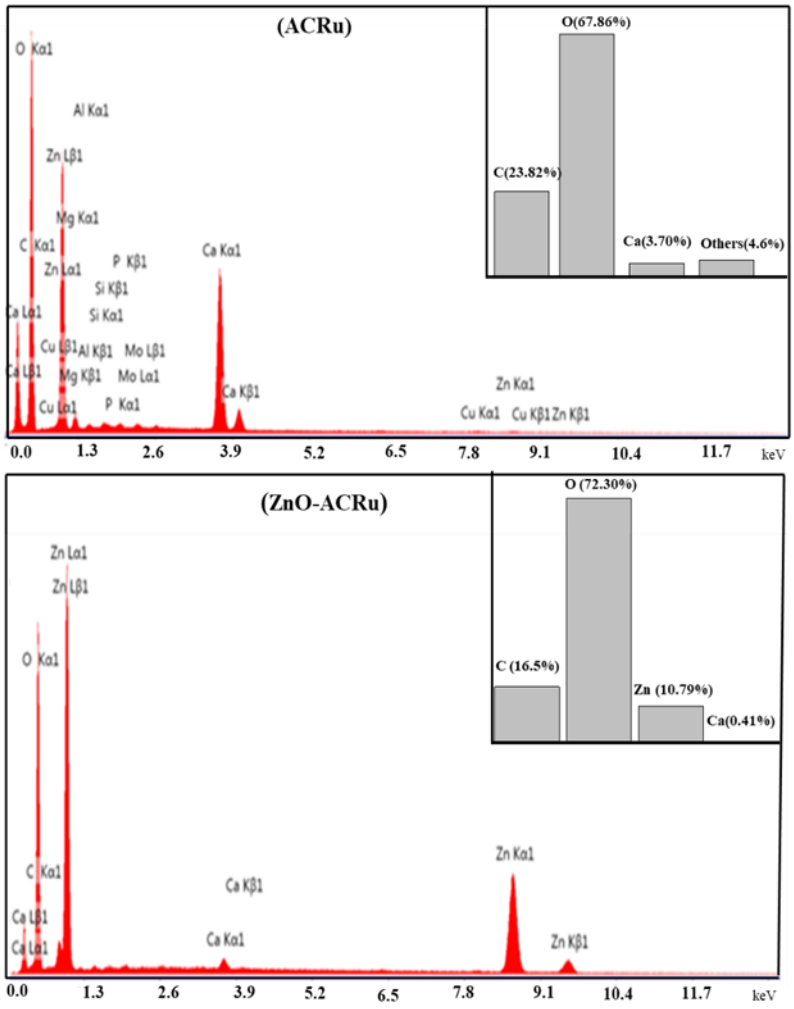

Figure IV.5. EDX elemental analysis of adsorbents ACRu and ZnO-ACRu

3.1.4. Thermogravimetric Analysis (TGA)

Thermogravimetric analysis (Figure IV.6) of the prepared adsorbents revealed contrasting thermal behavior patterns. In the first stage (25–200 °C), both materials exhibited similar mass losses of approximately 10%, attributed to the evaporation of physically adsorbed water molecules and volatile compounds typically present in porous carbon structures [7]. The second decomposition stage showed similar mass losses (20.51% for ACRu and 19.38% for ZnO-ACRu), although they occurred within different temperature ranges (200-537 °C versus 200-700 °C, respectively). This indicates that zinc modification expands the thermal stability range of functional groups on the ACRu surface, and that this weight loss in the second stage was primarily due to the decomposition of the cellulosic elements [8]. The most significant difference occurred in the final high-temperature stage, where ACRu lost 44.34% of its mass

between 537 and 1000°C, while ZnO-ACRu exhibited significantly improved thermal resistance with only a 15.54% mass loss between 700 and 1000°C. The incorporation of zinc fundamentally transforms thermally vulnerable functional groups into more stable structures.

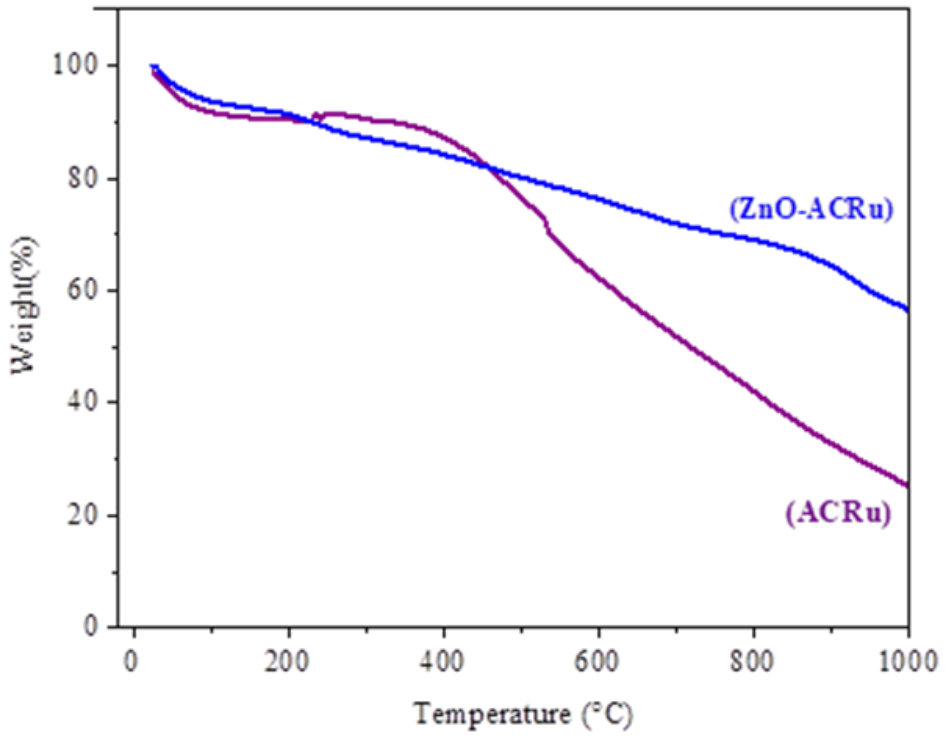

Figure IV.6. Thermogravimetric profiles of ACRu and ZnO-ACRu

3.1.5. Point of zero charge (pH_{pzc})

The point of zero charge (pH_{pzc}) values were 8.01 for ACRu and 8.10 for ZnO-ACRu, indicating only a slight upward shift after ZnO loading. Although EDX confirmed substantial zinc incorporation (≈11% Zn), the modest change in pH_{pzc} shows that the overall acid–base character of the carbon surface was largely preserved. When the solution pH is below pH_{pzc} , surface functional groups are protonated and the surface carries a net positive charge, which tends to attract anionic species and electrostatically repel cations. Above pH_{pzc} , deprotonation generates a net negative surface, favoring uptake of cationic species. Because ZnO-ACRu has a slightly higher pH_{pzc} than ACRu, it will remain positively charged over a marginally broader acidic-to-neutral pH window, and the transition to a net negative surface will occur at a slightly higher pH relative to the unmodified material.

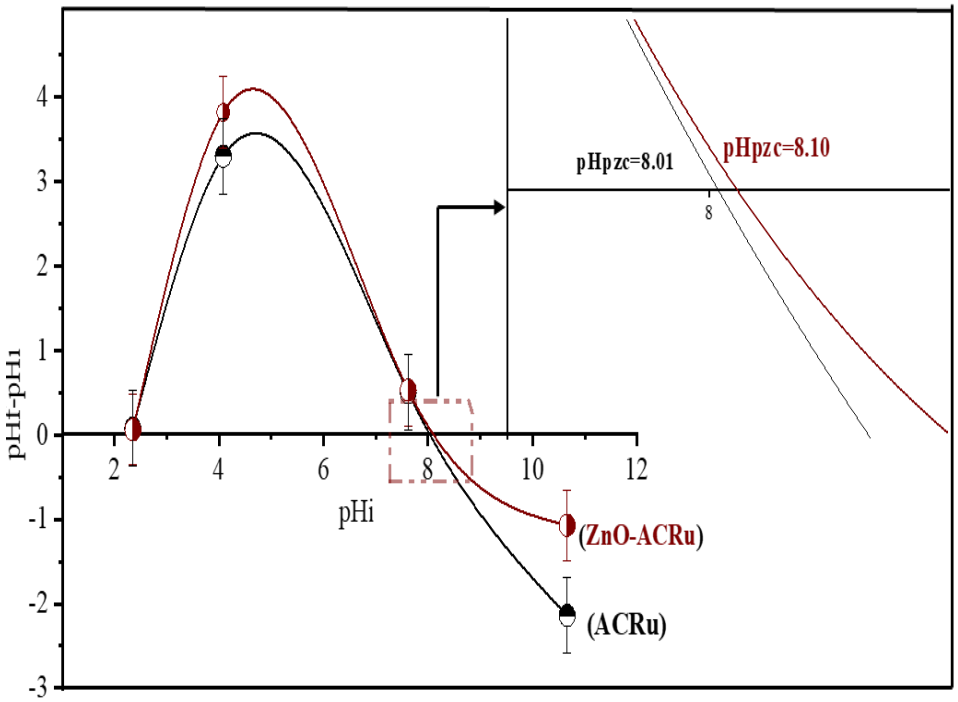

Figure IV. 7. The point of zero charge for ACRu and ZnO-ACRu

3.2. Adsorption results

3.2.1. Determining the Optimal Material for Congo Red Removal

Kinetic experiments of CR adsorption onto different adsorbents were carried out to determine the most efficient material for CR removal under neutral conditions (unmodified CR, pH = 7). As shown in Figure IV.8, ZnO-ACRu exhibited superior performance, achieving a remarkable removal efficiency of 83.56% within an equilibrium time of only 40 min. In comparison, ACRu reached a lower removal efficiency of 62.72% and required a significantly longer equilibrium time of 180 min. This notable enhancement, an increase of 20.84% in removal efficiency and a 3.6-fold reduction in equilibrium time, clearly highlights the superior performance of ZnO-ACRu. Consequently, all subsequent investigations on parameters affecting the adsorption capacity of CR were focused exclusively on ZnO-ACRu.

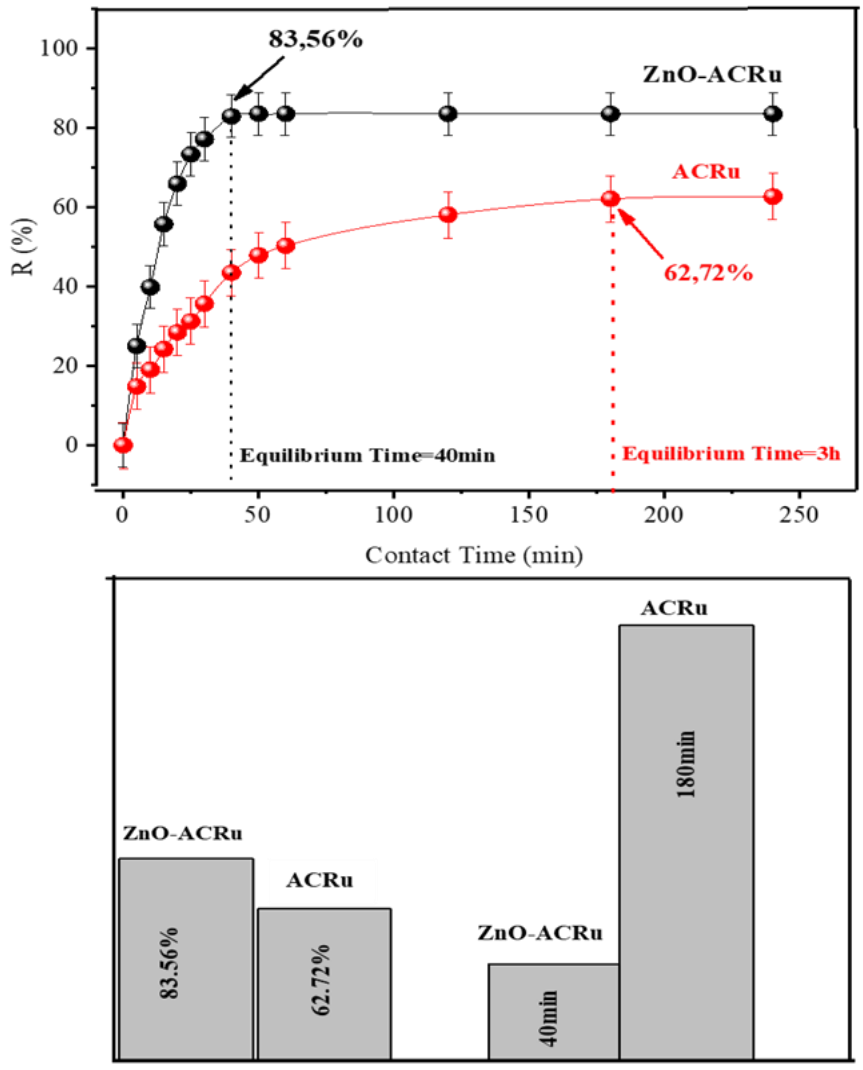

Figure IV.8. Evolution comparison of CR adsorption efficiency on ACRu and ZnO-ACRu over time (Dose=1g/L, C_0 =10mg/L, unmodified medium pH=7)

3.2.2. Determination of the Optimal pH for Enhanced CR Removal by ZnO-ACRu

The influence of pH on the adsorption performance of ZnO-ACRu toward CR was systematically examined (Figure IV.9), revealing a strong pH dependence. Under acidic conditions (pH = 2), ZnO-ACRu achieved the highest efficiency, removing 93.38% of CR within only 20 minutes at a dosage of 400 mg/L. This exceptional performance is primarily due to the pronounced electrostatic attraction between the positively charged surface of ZnO-ACRu (pH < pH_{pzc}= 8.10) and the negatively charged sulfonate groups of CR molecules. At neutral

conditions (pH = 7), which still fall below the pH_{pzc}, the adsorbent retained a positive surface charge but exhibited slightly reduced efficiency, reaching 83.56% removal in 40 min. Interestingly, even in alkaline conditions (pH = 9), where the surface charge becomes negative (pH > pH_{pzc}), the material was able to remove 76.55% of CR in 50 min using a higher dosage of 600 mg/L. This indicates that, aside from electrostatic attraction, other mechanisms such as hydrogen bonding, π–π interactions, or surface complexation might contribute to CR adsorption [9]. Therefore, due to the superior removal performance at pH = 2, all further experiments were carried out under acidic conditions.

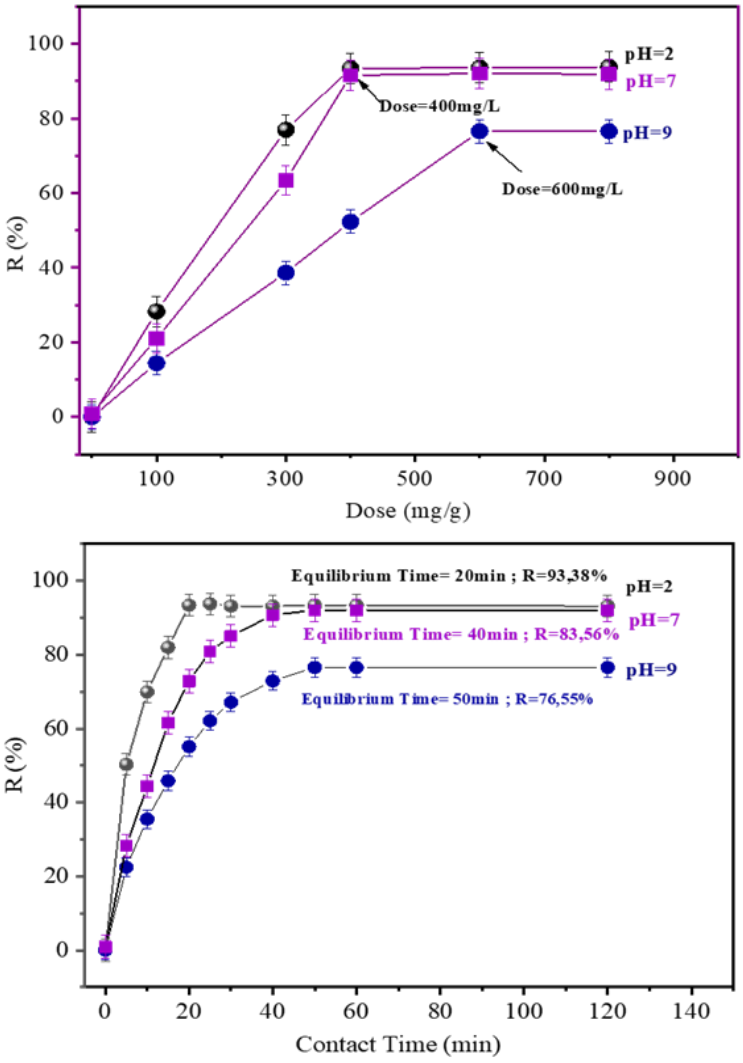

Figure IV.9. Time and dose-dependent study of CR adsorption efficiency on ZnO-ACRu in various media. (C_0 =10mg/L, pH=2,7,9)

3.2.3. Kinetic Modeling of CR Adsorption on ZnO-ACRu at pH = 2

To better understand the adsorption mechanism and kinetics of CR on ZnO-ACRu, the experimental data were analyzed using pseudo-first order (PFO), pseudo-second order (PSO), and Elovich models (Figure IV.10a), with the corresponding parameters summarized in Table IV.1. The PSO model was found to provide the best fit, as evidenced by its highest R^2 value (0.99), lowest relative error (E_r=0.01), and close agreement between calculated and experimental adsorption capacities. This suggests that chemisorption, involving strong chemical interactions between the adsorbate and the active sites of the adsorbent, governs the process [10]. Furthermore, intraparticle diffusion analysis (Figure IV.10b) revealed two distinct adsorption stages. The initial stage ($\sqrt{t}$< 3) corresponds to the rapid uptake of CR onto the external surface of ZnO-ACRu, while the second stage (3 ≤ $\sqrt{t}$≤ 11) reflects the gradual diffusion of CR molecules into the internal pore structure until equilibrium is reached. These findings highlight the combined influence of surface adsorption and intraparticle diffusion in controlling the overall kinetics of CR removal [11].

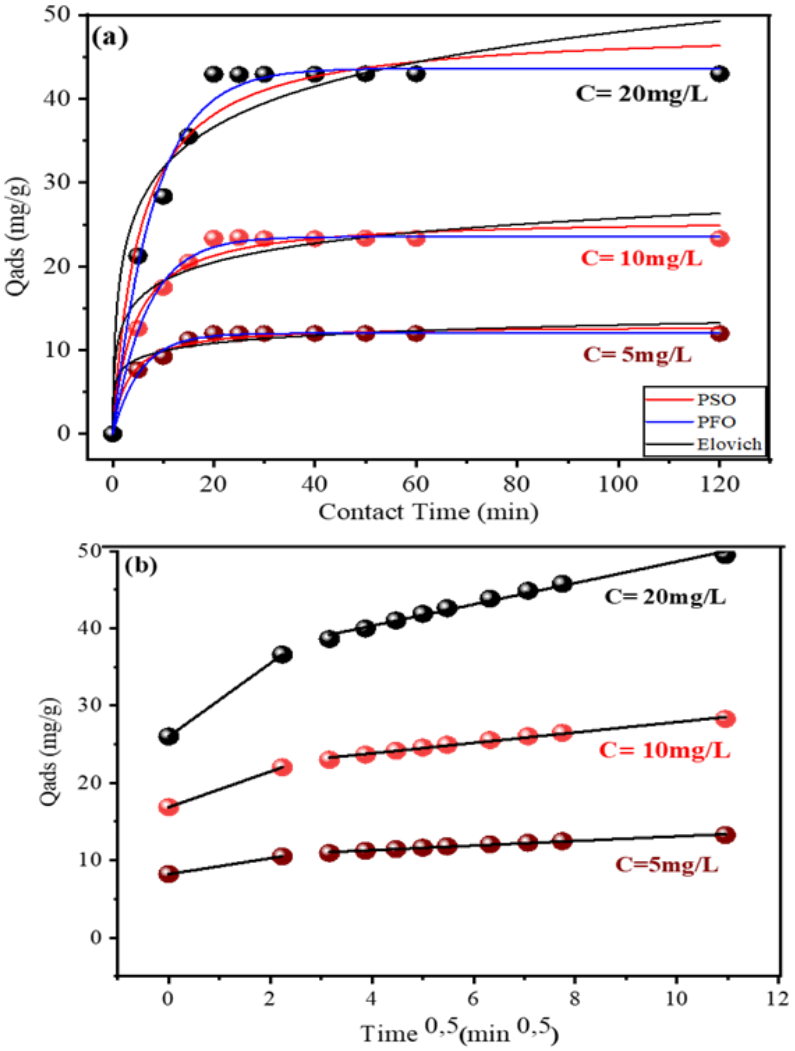

Figure IV.10. Kinetic analysis of CR adsorption onto ZnO-ACRu using (a) PFO, PSO, Elovich, and (b) intraparticle diffusion models.

Table IV.1. Kinetic parameters of PFO, PSO, and Elovich models for CR adsorption on ZnO-ACRu

	Parameters	$5mg/L$	$10\ mg/L$	$20mg/L$
PFO	$Q_e\ (mg/g)$	5.99	11.49	21.41
	$Q_{cal}\ (mg/g)$	5.93	11.34	21.41
	K_1	0.24	0.13	0.11
	R^2	0.997	0.994	0.992
	E_r	0.016	0.021	0.031
PSO	$Q_e\ (mg/g)$	11.99	23.29	42.98
	$Q_{cal}(mg/g)$	12.02	23.54	43.63
	K_2	0.02	0.009	0.003
	R^2	0.99	0.99	0.98
	E_r	0.027	0.036	0.046
Elovich	A	209.88	87.37	62.45
	B	0.74	0.30	0.14
	R^2	0.94	0.92	0.91
	E_r	0.068	0.082	0.095
Intra-particle diffusion	K_{int}	0.29	0.67	1.33
	C	10.10	21.12	35.14
	R^2	0.99	0.99	0.99
	E_r	0.060	0.113	0.135

3.2.4. Adsorption Isotherm Modeling

The equilibrium adsorption data obtained in this study were evaluated using four isotherm models: Langmuir, Freundlich, Redlich–Peterson, and Sips. The experimental data were fitted to these models, as illustrated in Figure IV.11 and summarized in Table IV.2. Among them, the Langmuir isotherm provided the best fit, as indicated by its highest determination coefficient (R^2), confirming its suitability for describing the adsorption behavior. Mechanistically, this implies that CR adsorption onto ZnO-ACRu occurs predominantly through monolayer formation on a homogeneous surface. The Langmuir model assumes that all adsorption sites are energetically equivalent, that there are no interactions between adsorbed molecules, and that a finite maximum adsorption capacity is achieved once the monolayer is complete [12].

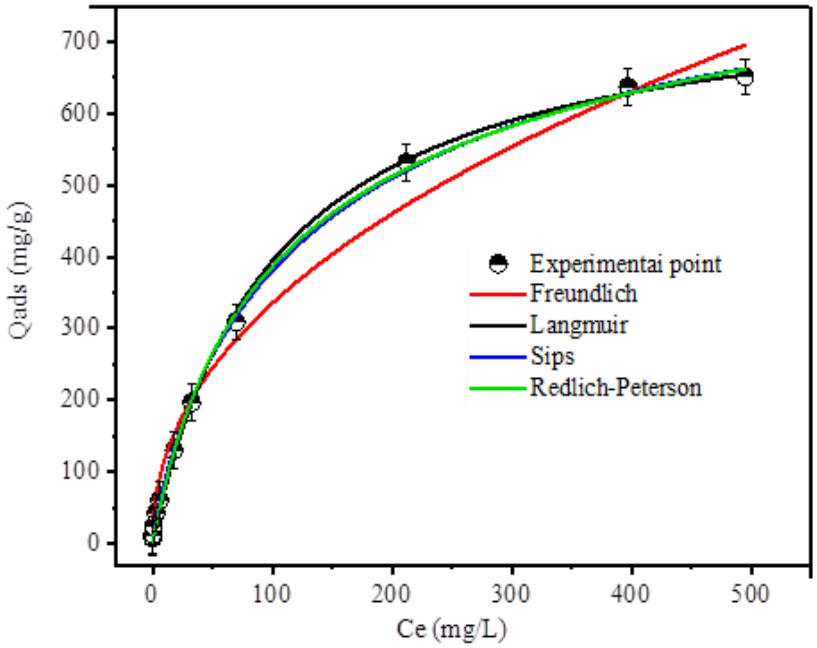

Figure IV.11. The equilibrium adsorption behavior of CR on ZnO-ACRu was described using Freundlich, Langmuir, Redlich-Peterson, and Sips models.

Table IV.2. ZnO-ACRu adsorption isotherm model parameters

Langmuir	$Q_{max}(mg/g)$	K_L (L/mg)		R^2	E_r
	785.38	0.01		0.998	0.285
Freundlich	K_f $(mg/g)/mg/L)^{\frac{1}{n}}$	**n**		R^2	E_r
	40.96	0.45		0.988	0.283
Redlich-Peterson	$K(L/g)$	**α (L/mg)**	**β**	R^2	E_r
	9.28	0.022	0.90	0.997	0.275
Sips	Q_s (mg/g)	b (L/mg)	**n**	R^2	E_r
	903.06	0.015	0.834	0.97	0.111

3.2.5. Thermodynamic study of adsorption

The thermodynamic parameters determined at different temperatures (293, 303, and 313 K) provide important insights into the adsorption mechanism of CR onto ZnO-ACRu. The negative values of Gibbs free energy (ΔG°) confirm that the adsorption process is spontaneous and thermodynamically favorable at all studied temperatures. The negative enthalpy change (ΔH°

< 0) indicates that the adsorption is exothermic in nature, meaning that heat is released during the interaction between CR molecules and the active sites of ZnO-ACRu. This suggests that the adsorption process is energetically favorable and does not require external energy input. Furthermore, the positive entropy change ($\Delta S° > 0$) reflects an increase in randomness at the solid–liquid interface, which may be attributed to the displacement of water molecules and structural rearrangements occurring during adsorption [13]. The dimensionless equilibrium constant (K_C) was calculated by multiplying the Langmuir constant (K_L) (Figure IV.12) by 55.5 × 10^3 and the molar mass of CR (696.663 g/mol), following methodologies reported by several researchers [14–16].

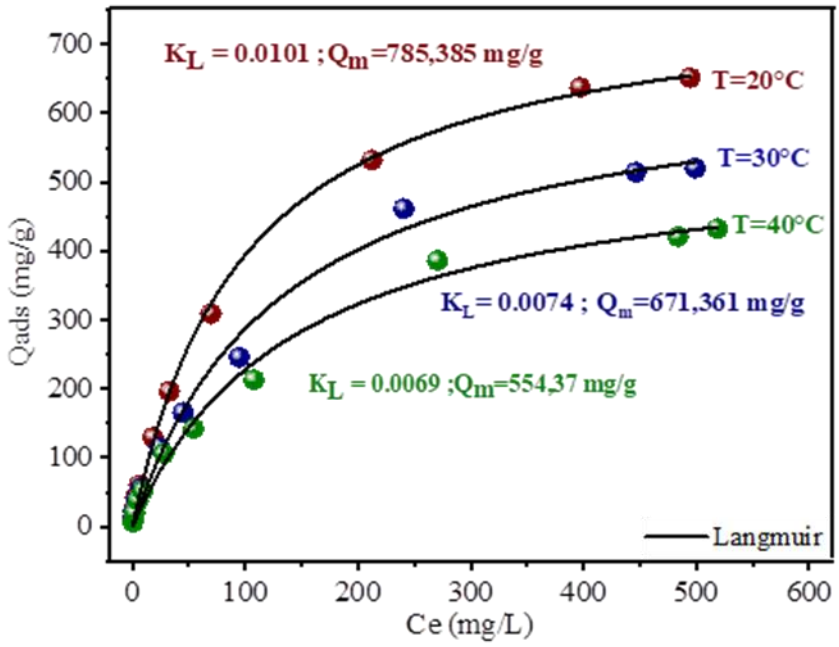

Figure IV.12. Nonlinear Langmuir isotherm analysis of CR experimental data collected at different temperature conditions.

Table IV.3. Thermodynamic analysis parameters of CR adsorption onto ZnO-ACRu.

$T(K)$	$K_L\ (L/mg)$	$K_C = K_L \times M_{adsorbate}\ 55.5 \times 10^3$	$\Delta G° = -RT\ln(K_C)(kJ/mol)$
293	0.0101	390514.445	-31.364062
303	0.0074	286119.494	-31.650915
313	0.0059	228122.299	-32.106011
$\ln(K_c) = -\frac{\Delta H°}{R}\frac{1}{T} + \frac{\Delta S°}{R}$		$\Delta H°(kJ/mol)$	$\Delta S°(J/K.mol)$
$\ln(K_c) = -2468.428\frac{1}{T} + 4.439$		-20.522511	36.912

3.2.6. Regeneration of ZnO-ACRu

Regeneration is essential for the economic viability and sustainable application of adsorption materials. As shown in Figure IV.13, the cyclic performance of ZnO-ACRu in CR removal declined progressively with reuse: removal efficiency decreased from 86% in the first cycle to 52.6% by the sixth cycle, indicating gradual saturation and loss of accessible active sites. This deterioration is likely due to the accumulation of strongly bound or poorly desorbed CR molecules that remain on the ZnO-ACRu surface after each regeneration step, leading to partial site blockage and reduced uptake capacity in subsequent cycles.

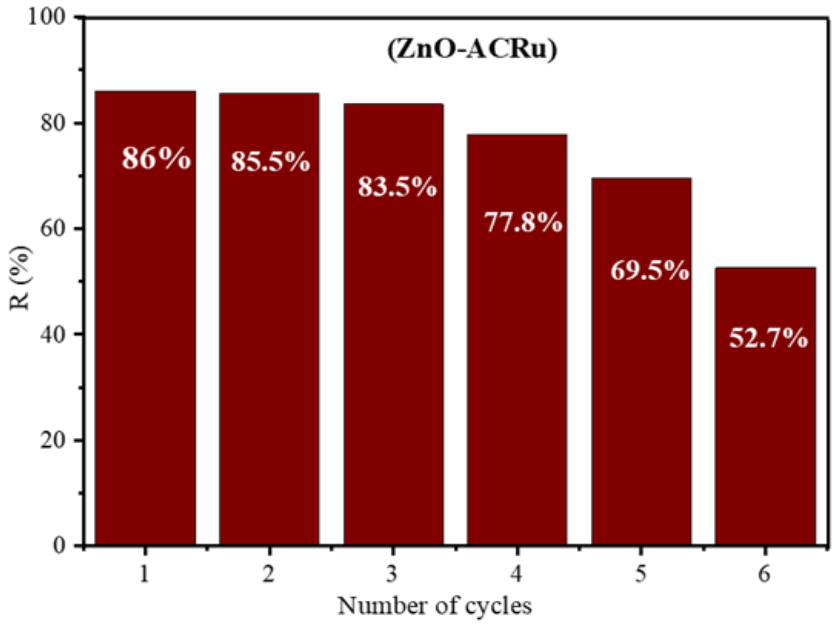

Figure IV.13. CR adsorption capacity of ZnO-ACRu throughout regeneration cycles

4. Conclusion

This study focused on the development of an efficient adsorbent by incorporating zinc oxide nanoparticles into activated and calcined Ruta graveolens (ZnO-ACRu). The resulting material exhibited outstanding adsorption performance, achieving 83.56% removal of Congo Red (CR) in an unmodified medium within just 40 min. A series of experiments investigating the effects of adsorbent dosage and contact time were conducted under varying pH conditions, with pH = 2

identified as the optimal medium for CR removal. Consequently, all subsequent adsorption studies were carried out at this pH. Kinetic modeling indicated that the pseudo-second order (PSO) model best described the adsorption behavior, suggesting that the adsorption follows PSO kinetics, which may indicate strong interactions between adsorbate and adsorbent. Furthermore, equilibrium data were found to fit the Langmuir isotherm, implying monolayer adsorption on a homogeneous surface. Thermodynamic analysis confirmed that the adsorption is spontaneous and exothermic. Notably, ZnO-ACRu maintained significant efficiency over six regeneration cycles, underscoring its potential for cost-effective and sustainable industrial applications.

Bibliographic references

[1] V.K. Gupta, Suhas, Application of low-cost adsorbents for dye removal – A review. Journal of Environmental Management, 90(8) (2009) 2313–2342.

[2] C. Wang, J. Li, J. Xu, Y. Xu, B. Pan, Environmental remediation of dye wastewater: A review. Chemosphere, 254 (2020) 126779.

[3] A. Bhatnagar, A.K. Jain, A comparative adsorption study with different industrial waste adsorbents for the removal of cationic dyes from water. Journal of Colloid and Interface Science, 281(1) (2005) 49–55.

[4] Y. Zhou, J. Lu, Y. Zhou, Y. Liu, Recent advances for dyes removal using novel adsorbents: A review. Environmental Pollution, 204 (2014) 201–210.

[5] Z. Hu, H. Chen, F. Ji, S. Yuan, Removal of azo dyes from aqueous solution by adsorption on modified rice husk. Journal of Hazardous Materials, 143(1–2) (2007) 56–64.

[6] N.S. Sayed, A.S. Ahmed, M.H. Abdallah, G.A. Gouda, ZnO@activated carbon derived from wood sawdust as an adsorbent for removal of methyl red and methyl orange from aqueous solutions. Scientific Reports, 14 (2024) 5384.

[7] A. Nasrullah, B. Saad, A.H. Bhat, A.S. Khan, M. Danish, M.H. Isa, A. Naeem, Mangosteen peel waste as a sustainable precursor for high surface area mesoporous activated carbon: Characterization and application for methylene blue removal. Journal of Cleaner Production, 211 (2019) 1190–1200.

[8] A. Guediri, A. Bouguettoucha, D. Chebli, N. Chafai, A. Amrane, Molecular dynamics simulation and DFT computational studies on the adsorption performances of methylene blue in aqueous solutions by orange peel modified with phosphoric acid. Journal of Molecular Structure, 1202 (2020) 127290.

[9] A. Guediri, A. Bouguettoucha, D. Chebli, A. Amrane, The use of encapsulation as a proposed solution to avoid problems encountered with conventional materials in powder form: Application in methylene blue removal from aqueous solutions. Journal of Molecular Liquids, 316 (2020) 113841.

[10] S. Sahnoun, M. Boutahala, Adsorption removal of tartrazine by chitosan/polyaniline composite: Kinetics and equilibrium studies. International Journal of Biological Macromolecules, 114 (2018) 1345–1353.

[11] F. Benamraoui, H. Boudiaf, A. Bouhank, L. Bencheikh, R. Bourzami, A. Gil, M. Boutahala, Methylene blue removal using black cumin seed waste: Experimental study and molecular dynamics simulation. Desalination and Water Treatment, 300 (2023) 167–177.

[12] G. Moussavi, M. Mahmoudi, Removal of azo and anthraquinone reactive dyes from industrial wastewaters using MgO nanoparticles. Journal of Hazardous Materials, 168(2–3) (2009) 806–812.

[13] K. Noufel, N. Djebri, N. Boukhalfa, M. Boutahala, A. Dakhouche, Removal of bisphenol A and trichlorophenol from aqueous solutions by adsorption with organically modified bentonite–activated carbon composites: A comparative study in single and binary systems. Groundwater for Sustainable Development, 11 (2020) 100477.

[14] I. Anastopoulos, G.Z. Kyzas, Are the thermodynamic parameters correctly estimated in liquid-phase adsorption phenomena? Journal of Molecular Liquids, 218 (2016) 174–185.

[15] H.N. Tran, S.J. You, H.P. Chao, Thermodynamic parameters of cadmium adsorption onto orange peel calculated from various methods: A comparison study. Journal of Environmental Chemical Engineering, 4 (2016) 2671–2682.

[16] S.P. Ghosal, A.K. Gupta, Determination of thermodynamic parameters from Langmuir isotherm constant – revisited. Journal of Molecular Liquids, 225 (2017) 137–146.

Chapiter V

Preparation and Characterization of Fish Bone-Based Adsorbents for Congo Red Dye Removal

Summary

GRAPHICAL ABSTRACT

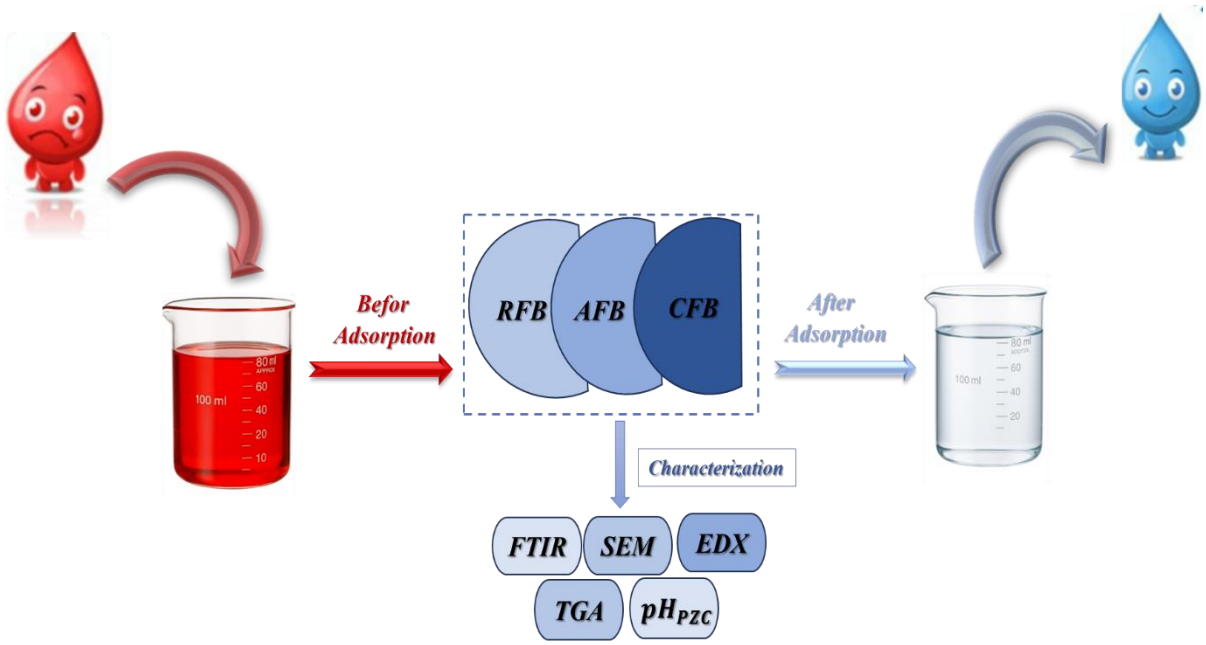

1. Introduction

In recent years, the search for cost-effective, sustainable, and environmentally friendly adsorbents has intensified due to growing concerns over industrial pollution and limited access to clean water. Biomass-derived materials have gained considerable interest owing to their natural abundance, low cost, and potential for surface modification. Agricultural and marine waste offer a dual advantage: they reduce environmental burdens associated with waste disposal

while simultaneously serving as low-cost raw materials for adsorbent production [1]. Among these, fish bones, a by-product of the seafood processing industry, have demonstrated remarkable potential. Typically discarded as waste, fish bones are rich in hydroxyapatite ($Ca_{10}(PO_4)_6(OH)_2$) and organic matrix components such as collagen and proteins [2]. This natural composition provides fish bones with intrinsic sorption sites and structural characteristics favorable for the adsorption of various pollutants.

Fish bone-derived materials exhibit good mechanical stability, high biocompatibility, and a naturally porous structure. These characteristics can be further enhanced through physical and chemical modifications. Raw fish bones can be utilized directly, but their adsorption performance is often limited by low surface area and insufficient active sites. To improve these properties, activation, a process involving chemical treatment or high-temperature pyrolysis in a controlled environment, is employed to increase surface porosity and modify surface functional groups [3]. Similarly, calcination, which involves thermal treatment at elevated temperatures, alters the crystalline structure and surface reactivity by decomposing organic components and enhancing the exposure of the inorganic hydroxyapatite phase [4,5].

This research explores the comparative performance of raw, activated, and calcinated fish bones as adsorbents. Emphasis is placed on how structural and surface chemistry changes resulting from thermal or chemical treatments influencing the adsorption behavior. By understanding these effects, the potential of fish bone-derived materials as low-cost alternatives to conventional adsorbents is critically assessed.

2. Experimental Method

2.1. Method for preparing RFB, AFB, and CFB

Fish bones were initially separated from the meat and thoroughly washed with distilled water to eliminate residual impurities. The cleaned bones were then air-dried at 80 °C for 24 h. Once completely dried, the bones were ground and sieved to obtain a fine powder, referred to as raw fish bone (RFB). To prepare the activated fish bone (AFB) adsorbent, a portion of the RFB powder was chemically activated by mixing with phosphoric acid (H_3PO_4, 85%) at a weight-to-volume ratio of (1:1). This mixture was left to impregnate at room temperature for 24 h, after which it was neutralized using 0.1 M sodium hydroxide (NaOH), and thoroughly rinsed with distilled water until the filtrate reached a neutral and stable pH. The resulting product was then dried, yielding the chemically activated form. For the calcined fish bone (CFB) adsorbent,

another portion of the RFB powder was subjected to thermal treatment by calcination in a muffle furnace at 600 °C for 2 h, leading to the formation of a thermally modified material.

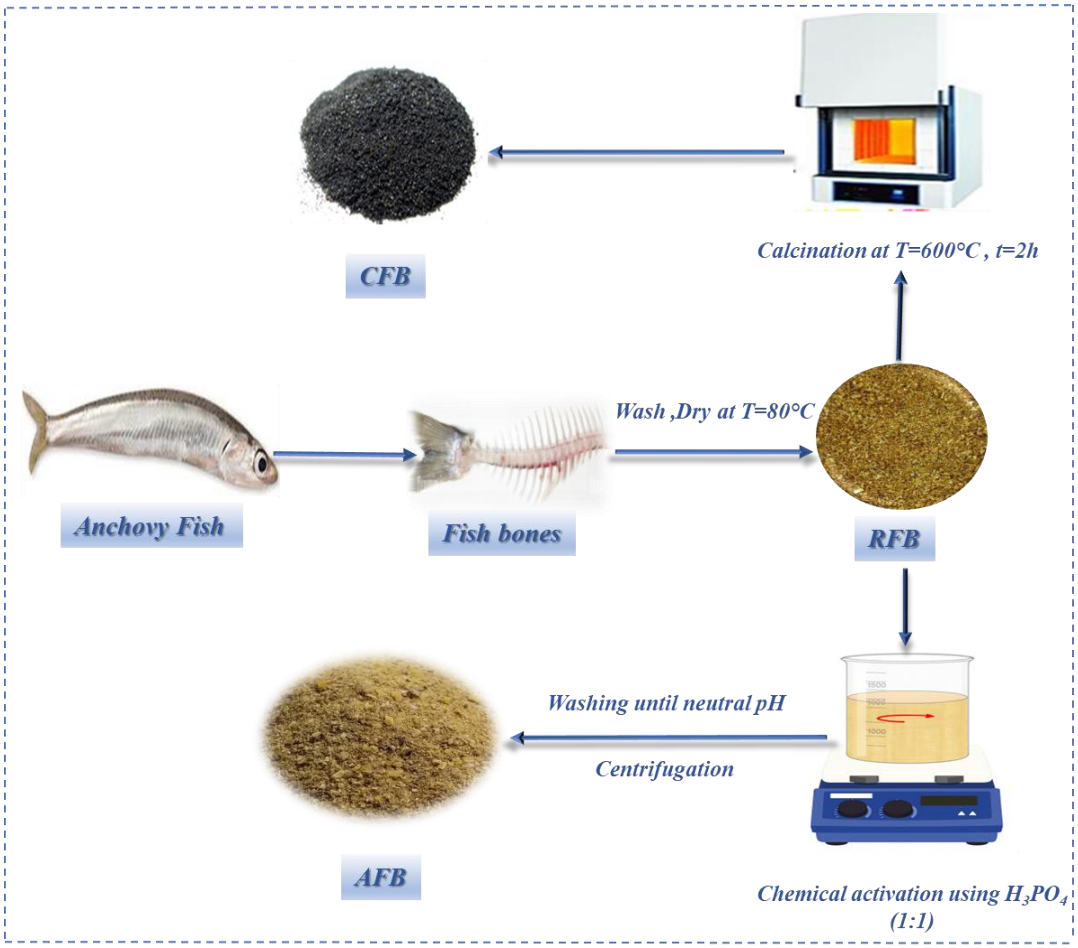

Figure V.1. Preparation methods of RFB, AFB, and CFB

3. Results

3.1. Evaluation of Adsorbent Characteristics

3.1.1. Fourier-transform infrared spectroscopy (FTIR)

The FT-IR spectra of RFB, AFB, and CFB (Figure V.2) display several characteristic peaks corresponding to key functional groups, confirming chemical transformations during each treatment step. Broad bands observed near 3300 cm^{-1} and around 1631 cm^{-1} are attributed to O–H stretching and bending vibrations, respectively, indicating the presence of hydroxyl groups, which are more pronounced in RFB due to moisture and organic content. The aliphatic $–CH_2$ stretching vibrations at 2920 and 2850 cm^{-1}, prominent in RFB, reflect residual organic

compounds naturally present in untreated fish bones. A distinct peak at 1788 cm^{-1} corresponds to carbonyl (C=O) groups, likely arising from fatty acids and lipid components in the raw material [6]. Upon chemical activation (AFB), a noticeable reduction in organic-related peaks is observed, indicating the effective removal of a portion of the organic matter. The appearance of a band around 1430 cm^{-1} in both AFB and CFB confirms the formation or retention of carbonate groups, which are characteristic of bone mineral components such as calcium carbonate. Peaks in the 1013–1142 cm^{-1} range and near 559 cm^{-1} observed in all three adsorbents are indicative of phosphate groups [7], primarily associated with hydroxyapatite, the main inorganic constituent of bone. The persistence of these phosphate-related bands after thermal calcination (CFB) suggests that the fundamental mineral structure is preserved, which is crucial for enhancing the adsorption performance of the prepared materials.

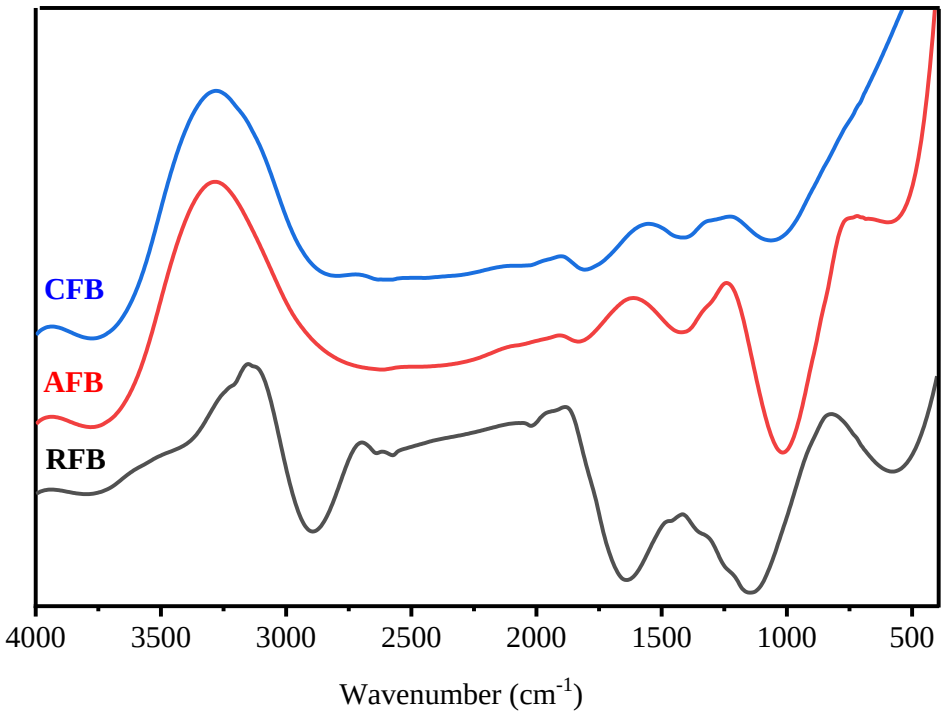

Figure V.2. FTIR characterization of RFB, AFB, and CFB

3.1.2. Scanning electron microscopy (SEM)

Scanning Electron Microscopy (SEM) analysis provides vital insights into the surface morphology and microstructural evolution of the RFB, AFB, and CFB. As illustrated in Figure V.3, all three samples exhibit irregular, fractured surfaces with heterogeneous pore distributions. The RFB displays a relatively compact surface with smaller and fewer pores, typical of

untreated biological material that still contains organic matter and residual tissues [8]. Following chemical activation (AFB), the surface undergoes a substantial transformation. SEM images reveal a dramatic increase in surface roughness and the emergence of well-defined pores with larger diameters. This enhanced porosity is likely due to the partial removal of organic compounds and the development of voids during acid treatment [9]. These morphological changes are highly beneficial, as they increase the available surface area for adsorption and facilitate greater accessibility to active sites [10]. In contrast, the calcinated fish bones (CFB) demonstrate a markedly different surface profile. Thermal treatment at high temperatures leads to sintering effects, causing particle aggregation and partial collapse of the porous network [11]. The resulting structure appears smoother with reduced pore density and altered particle dimensions. This loss of porosity may negatively impact adsorption capacity but could improve thermal stability and crystallinity, which are advantageous in certain applications [12]. Overall, the SEM analysis confirms that both chemical activation and calcination significantly influence the textural and morphological properties of the adsorbents.

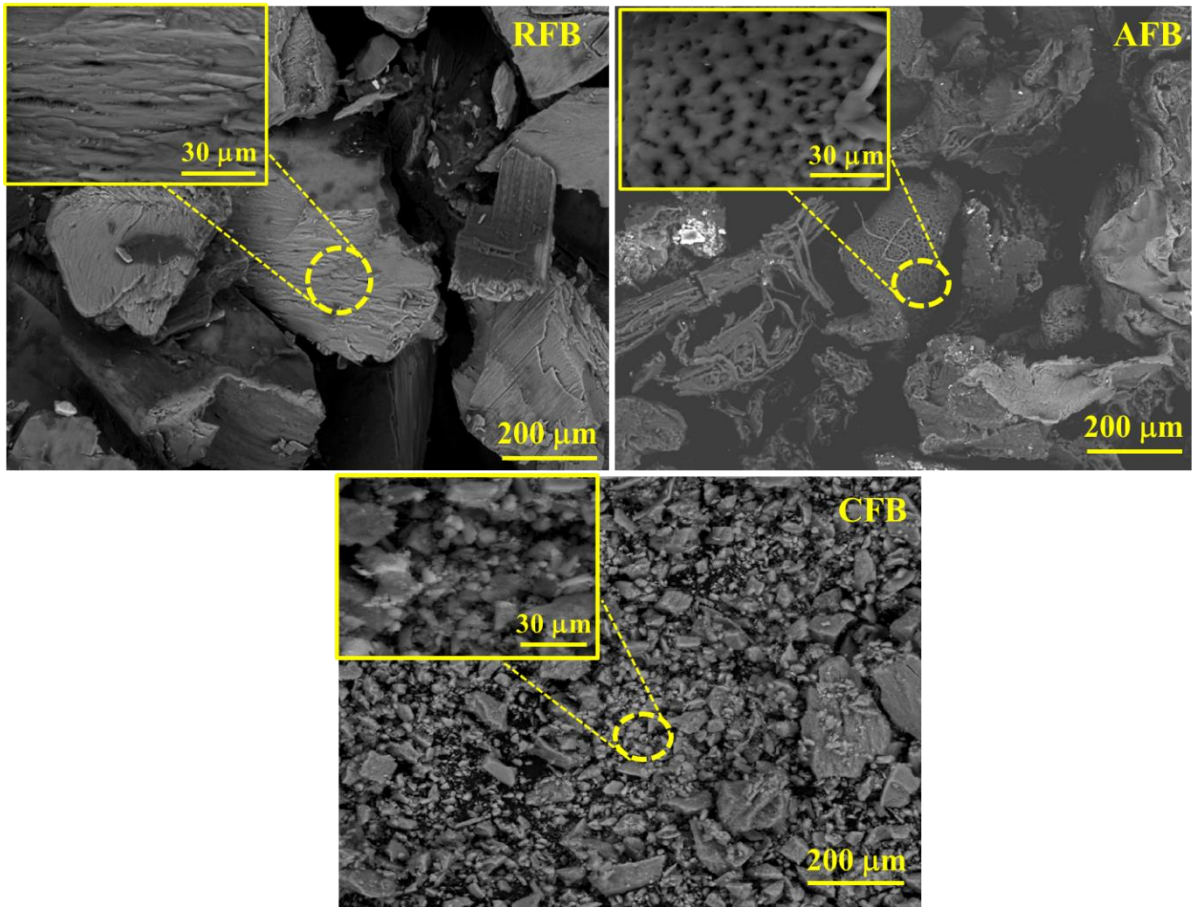

Figure V.3. SEM images of RFB,AFB,and CFB

3.1.3. Energy-dispersive X-ray spectroscopy (EDX)

Energy-dispersive X-ray (EDX) spectroscopy was employed to analyze the elemental composition of RFB, AFB, and CFB samples. The quantitative data indicates that all samples predominantly consist of carbon (C), oxygen (O), calcium (Ca), and phosphorus (P), which are typical constituents of biological apatite derived from fish bones. In the case of RFB, a relatively high carbon content was detected, which is attributed to the presence of residual organic matter such as collagen, fats, and other biological tissues that remain in the untreated fish bone matrix. After chemical activation with phosphoric acid, the AFB sample shows a marked increase in calcium and phosphorus concentrations, accompanied by a significant reduction in carbon content. This trend suggests that the acid treatment effectively removes much of the organic material, allowing the enrichment of inorganic phases such as hydroxyapatite ($Ca_{10}(PO_4)_6(OH)_2$). Moreover, the added phosphate groups from H_3PO_4 may facilitate the conversion or stabilization of hydroxyapatite within the bone structure [13].

The CFB sample exhibits even lower levels of carbon, due to the thermal degradation and volatilization of carbon-containing compounds. Concurrently, the percentages of phosphorus and oxygen increase compared to RFB. This is consistent with the known behavior of bone material during calcination, where organic constituents are eliminated and inorganic minerals, especially calcium phosphates, become more concentrated [14]. Overall, the EDX findings confirm the progressive removal of organics and the enrichment of mineral content during both activation and calcination.

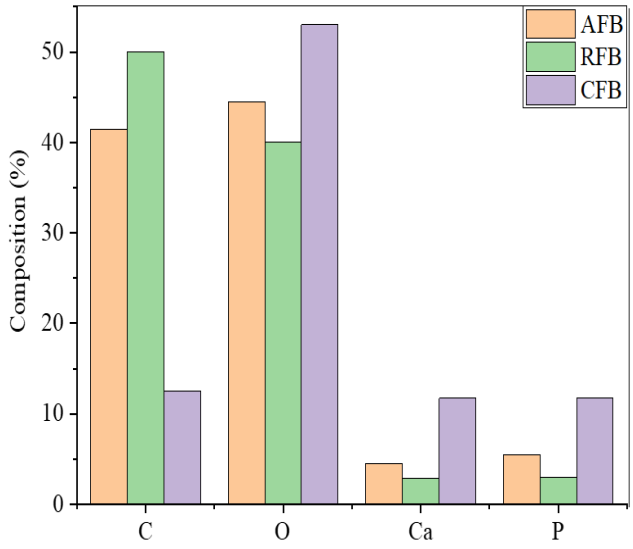

Element	RFB	AFB	CFB
C	50.86	41.48	12.54
O	40.85	44.75	53.55
Ca	2.91	4.40	11.70
P	3.59	5.25	11.88
Mg	1.30	_	2.99
Na	_	3.71	4.18
Others	0.49	0.41	3.16

Figure V.4. EDX elemental analysis of adsorbents

3.1.4. Thermogravimetric Analysis (TGA)

Thermogravimetric analysis (TGA) was performed on the raw (RFB), activated (AFB), and calcinated (CFB) fish bone samples to investigate their thermal stability and decomposition behavior within a temperature range of 25 to 1000 °C. The results revealed distinct decomposition patterns that reflect the different chemical compositions and structural changes induced by activation and calcination processes. For both RFB and AFB, the thermal decomposition proceeded in three characteristic stages. The first stage, occurring between 25 °C and 200 °C, was marked by initial weight losses of 13.25% for RFB and 10.92% for AFB. This phase corresponds to the evaporation of physically adsorbed water and low-molecular-weight volatile compounds present on the surface or within the pores of the material [15]. The second stage, from approximately 200 °C to 592 °C for RFB and up to 500 °C for AFB, exhibited significant mass losses of 34.1% and 60.72%, respectively. These substantial reductions are attributed to the decomposition of organic constituents such as collagen, proteins, and residual lipids inherent in the raw bone matrix [16]. Notably, the higher mass loss in AFB suggests a greater presence of acid-fragmented organic material, which decomposes more readily due to the activation process. The thermal degradation of these organics releases gases like CO_2, CO, and NH_3, consistent with previous findings in bone-based adsorbents [14]. The final stage involves the gradual breakdown of thermally stable components such as lignin and carbonaceous residues, continuing up to 800-1000 °C. This slow mass decline corresponds to the carbonization and eventual burnout of resistant organic matter, stabilizing into a final residual mass predominantly composed of inorganic minerals like hydroxyapatite [17]. In contrast, the TGA profile of CFB revealed a simpler decomposition pattern. An initial minor weight loss of 2.85% below 200 °C was attributed to moisture evaporation. Beyond this, a small additional weight loss of around 3% was observed between 282 °C and 975 °C, indicating the presence of trace organic residues that survived the calcination process. The low overall mass loss confirms the efficiency of the high-temperature treatment in removing most organic matter, leaving behind a thermally stable, predominantly inorganic matrix [18].

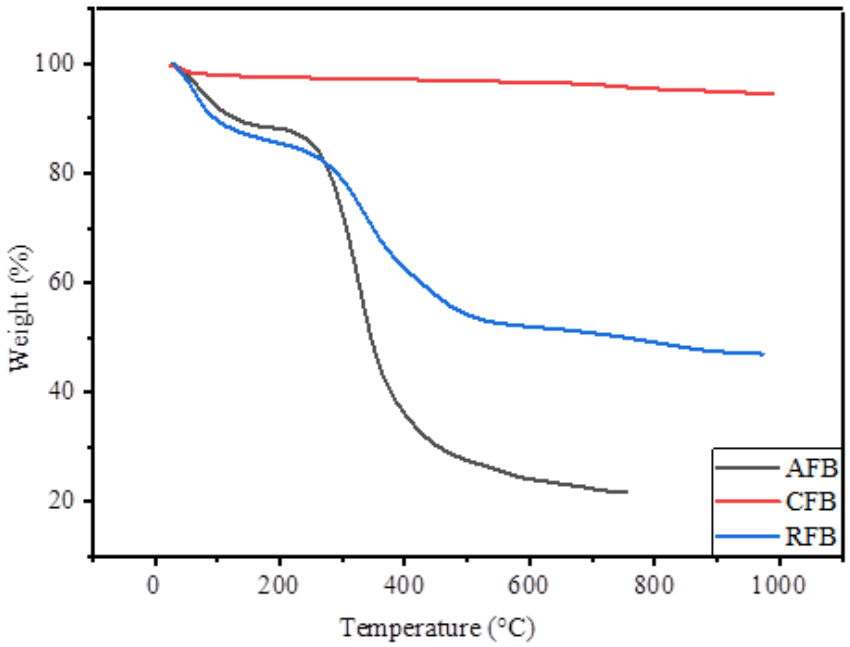

Figure V.5. Thermogravimetric profiles of RFB, AFB, and CFB

3.1.5. Point of zero charge (pH_{pzc})

The point of zero charge (pH_{pzc}) for RFB, AFB, and CFB was determined to be 7.1, 6.3, and 6.7, respectively. These values suggest that AFB has a more acidic surface, likely due to chemical activation with phosphoric acid, which introduces acidic functional groups. In contrast, RFB retains a more basic character due to its natural composition, mainly calcium phosphate. The intermediate pH_{pzc} of CFB reflects the effect of thermal treatment. These variations affect adsorption behavior; for example, at $pH > pH_{pzc}$, the surface is negatively charged, enhancing the adsorption of positively charged species.

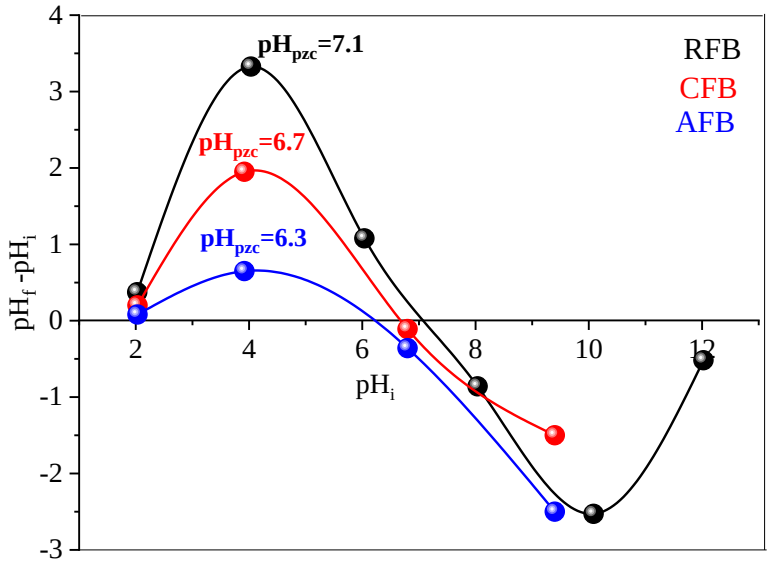

Figure V.6. The point of zero charge for RFB, AFB, and CFB

3.2. Adsorption results

3.2.1. Selection of the Optimal Adsorbent for Congo Red Elimination

Kinetic studies were performed to evaluate the adsorption behavior of Congo Red (CR) onto three types of fish bone–based materials: raw (RFB), activated (AFB), and calcinated (CFB), under neutral conditions. The results obtained, presented in Figure V.7, revealed a marked variation in adsorption performance among the different adsorbents. The activated fish bone (AFB) exhibited the best adsorption capacity, attaining a high removal efficiency of 92% within 40 min. The calcinated fish bone (CFB) followed, with an efficiency of 85.57% after 1 h, while the raw material (RFB) showed the lowest removal rate of 71.94% after 2 h. These findings confirm that activation and calcination significantly improve the surface reactivity and functional properties of fish bone materials. Consequently, the subsequent investigations on parameters influencing CR adsorption were focused mainly on the activated fish bone (AFB) due to its superior performance.

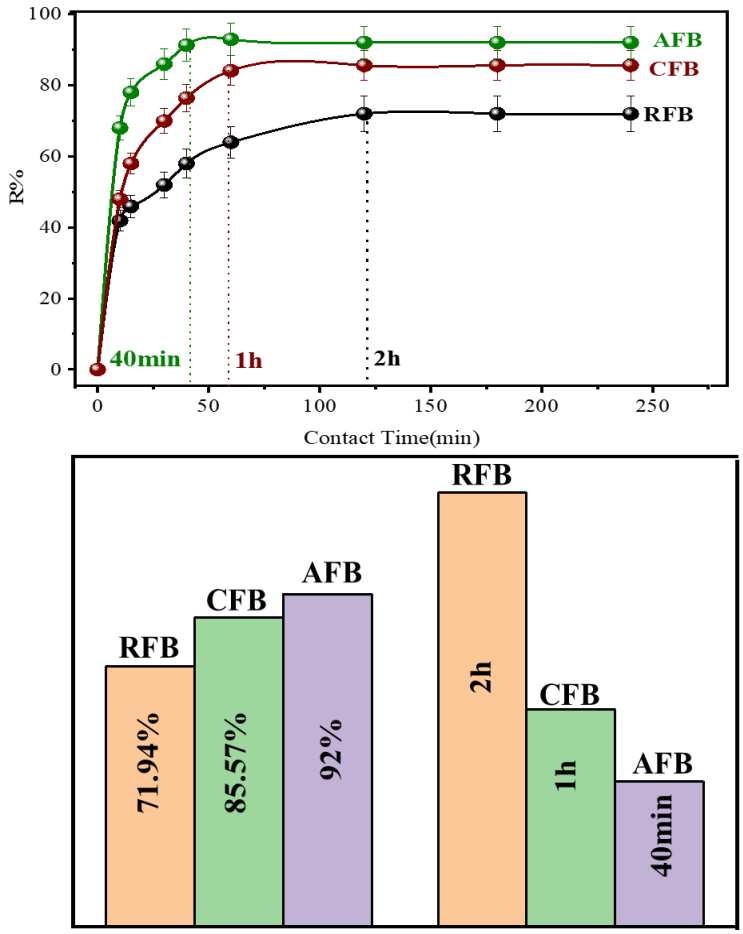

Figure V.7. Comparative evolution of CR adsorption efficiency on RFB, CFB, and AFB as a function of contact time

$$(C_0 = 10\ mg/L\ ;\ pH = 7\ ;\ Dose_{RFB,AFB,CFB} = 800 mg/L; t = 24h)$$

3.2.2. Effect of adsorbent dose (AFB)

The effect of AFB dosage on Congo Red (CR) removal efficiency is depicted in Figure V.8. The results indicate that increasing the AFB dose enhances CR removal, with maximum efficiency reaching 92% at 800 mg/L. This trend is primarily due to the greater availability of active adsorption sites as more adsorbent is introduced. However, beyond the optimal dose, further increases did not significantly improve removal efficiency, suggesting that most CR molecules had already been captured, and additional active sites remained unutilized. On the other hand, the equilibrium adsorption capacity showed a decreasing trend from 127.85 mg/g at 100 mg/L to 7.66 mg/g at 1200 mg/L as the dose increased. This inverse relationship is commonly

observed and can be attributed to the overlapping of adsorption sites and unsaturated active surfaces at higher adsorbent concentrations, leading to a dilution effect.

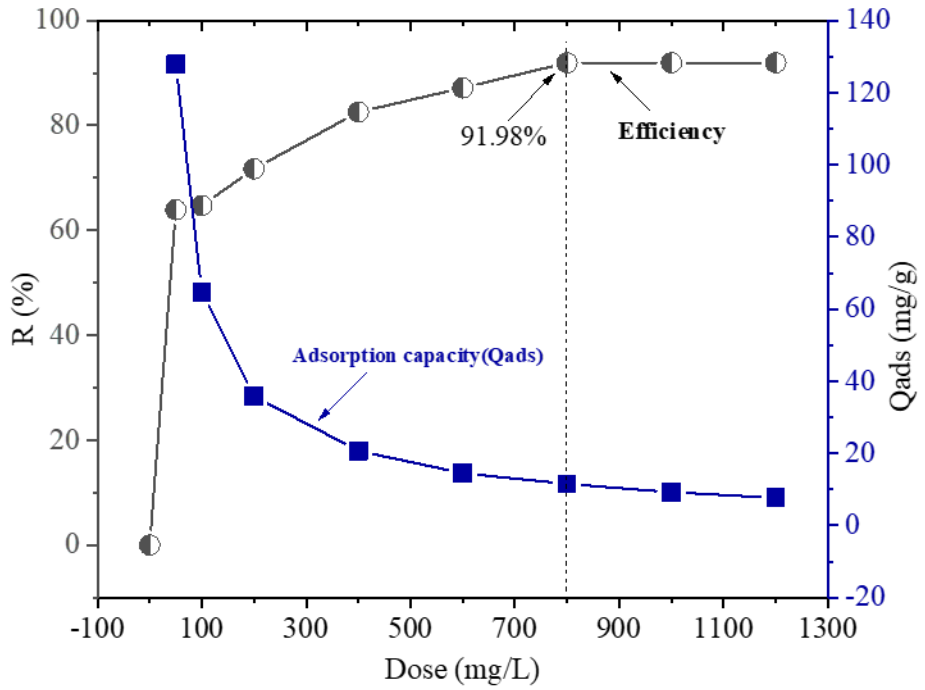

Figure V.8. Influence of AFB dosage on CR adsorption capacity and removal efficiency ($C_0 = 10\,mg/L\,;\ pH = 7\,;t = 24h$)

3.2.3. Initial pH effect

The adsorption performance of the AFB adsorbent was significantly influenced by the pH of the solution, as shown in Figure V.9. The highest removal efficiency was observed under acidic conditions, while adsorption declined in alkaline media**.** This behavior can be explained by the material's point of zero charge (pH_{pzc}= 6.3)**.** At solution pH values below the pH_{pzc}, the surface of the adsorbent becomes positively charged**,** which enhances the electrostatic attraction with the negatively charged Congo Red (CR) dye molecules. In contrast, at pH values above the pH_{pzc}, the surface acquires a negative charge**,** resulting in electrostatic repulsion and reduced CR uptake. Therefore, the strong adsorption observed in acidic environments is primarily driven by favorable electrostatic interactions between the AFB surface and CR anions, while the decline in basic conditions confirms the sensitivity of adsorption efficiency to surface charge behavior.

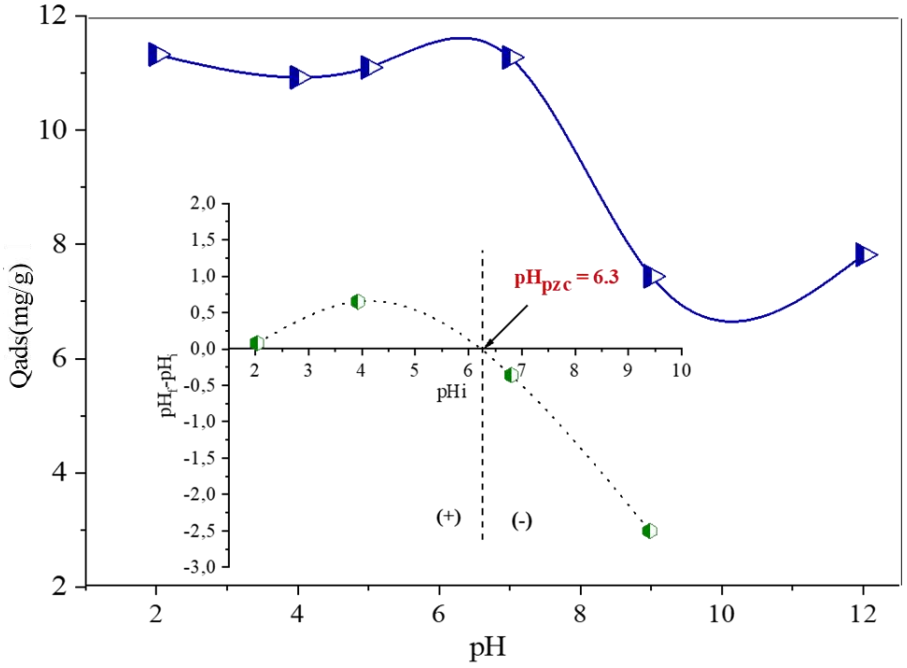

Figure V.9. Influence of pH on the adsorption of CR onto AFB

($C_0 = 10\,mg/L\,;\ Dose_{(AFB)} = 800mg/L\,;t = 24h$)

3.2.4. Kinetic Evaluation of Congo Red Adsorption on AFB

To gain deeper insight into the adsorption mechanism and kinetic behavior of Congo Red (CR) on activated fish bone (AFB), the experimental data were interpreted using three well-established kinetic models: the pseudo-first order (PFO), pseudo-second order (PSO), and Elovich models (Figure V.10). The calculated kinetic parameters are presented in Table V.1. Among the tested models, the PSO model exhibited the best correlation with the experimental results, as evidenced by its higher determination coefficient and the strong agreement between the experimental and theoretical adsorption capacities, suggesting strong interactions between CR and the active sites, involving the formation of strong interactions or chemical bonds between the dye molecules and the active functional sites on the adsorbent surface. Such behavior may indicate possible electron sharing or exchange during the adsorption process, confirming the high affinity of AFB toward Congo Red molecules [19]. In addition, the intraparticle diffusion model (Figure V.10) was applied to further elucidate the rate-controlling steps of CR adsorption onto activated fish bone (AFB). The obtained plot exhibited a multilinear profile, indicating the presence of two successive adsorption stages. The first, sharper region

corresponds to the rapid external adsorption of dye molecules onto the readily available active sites on the AFB surface. This stage is mainly governed by boundary layer diffusion, where the concentration gradient between the solution and the adsorbent surface drives a fast mass transfer. The second, slower linear portion represents the progressive diffusion of CR molecules into the internal pores of the adsorbent, continuing until equilibrium is established [20].

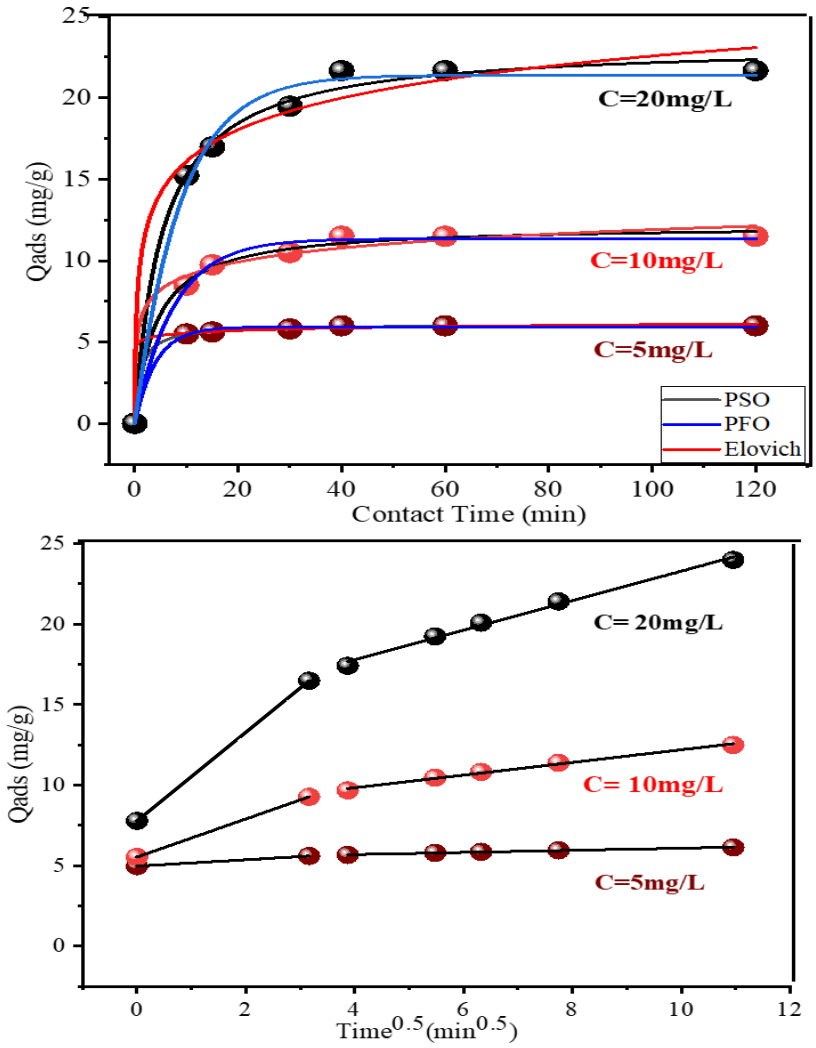

Figure V.10. Kinetic modeling of CR adsorption onto AFB using PFO, PSO, Elovich, and intraparticle diffusion models

Table V.1. Kinetic parameters obtained from PFO, PSO, and Elovich models for CR adsorption onto AFB.

	Parameters	$5mg/L$	$10\ mg/L$	$20mg/L$
PFO	$Q_e\ (mg/g)$	5.99	11.49	21.41
	$Q_{cal}\ (mg/g)$	5.93	11.34	21.41
	K_1	0.24	0.13	0.11
	R^2	0.997	0.994	0.992
	E_r	0.016	0.021	0.031
PSO	$Q_e\ (mg/g)$	5.99	11.49	21.41
	$Q_{cal}(mg/g)$	6.032	12.17	23.31
	K_2	0.16	0.02	0.008
	R^2	0.999	0.996	0.994
	E_r	0.008	0.022	0.020
Elovich	A	211215.56	176.79	74.06
	B	2.89	0.80	0.34
	R^2	0.996	0.986	0.983
	E_r	0.017	0.038	0.041
Intra-particle diffusion	K_{int}	0.35	2.10	4.89
	C	4.96	5.53	7.77
	R^2	0.988	0.910	0.897
	E_r	0.013	0.043	0.052

3.2.5. Evaluation of Adsorption Isotherm Parameters

The equilibrium adsorption data for Congo Red (CR) on activated fish bone (AFB) were analyzed using four classical isotherm models: Langmuir, Freundlich, Redlich–Peterson, and Sips. The experimental results were fitted to these models, as illustrated in Figure V.11 and summarized in Table V.2. Among them, the Freundlich isotherm showed the best correlation with the experimental data, indicating that this model most accurately describes the adsorption process. The superior fitting of the Freundlich model ($R^2 = 0.998$) suggests that CR adsorption on AFB occurs on a heterogeneous surface. The value of n ($0.47 < 1$) indicates high surface heterogeneity and strong adsorbate–adsorbent interactions, particularly at low dye concentrations. According to the Freundlich model, the adsorption capacity increases with dye

concentration, but the process is not restricted to the formation of a single layer, reflecting the complex nature of the adsorbent surface [21].

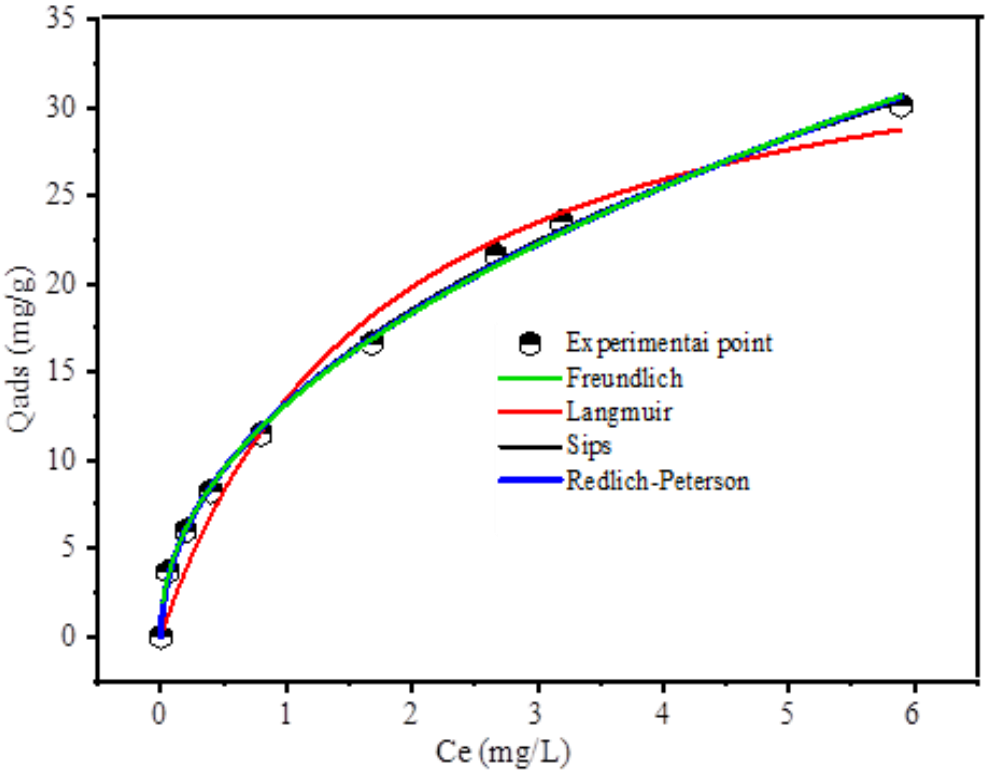

Figure V.11. Adsorption isotherms of CR on AFB fitted to Freundlich, Langmuir, Redlich–Peterson, and Sips models.

Table V.2. Isotherm model parameters for CR adsorption onto AFB.

Langmuir	$Q_{max}(mg/g)$	K_L (L/mg)		R^2	E_r
	37.45	0.56		0.978	0.156
Freundlich	$K_f\,(mg/g)/mg/L)^{\frac{1}{n}}$	**n**		R^2	E_r
	13.18	0.47		0.998	0.026
Redlich-Peterson	$K(L/g)$	**α (L/mg)**	**β**	R^2	E_r
	29.51	1.187	0.77	0.987	0.122
Sips	Q_s (mg/g)	b (L/mg)	**n**	R^2	E_r
	52.066	0.232	0.715	0.993	0.074

3.2.6. Thermodynamic Analysis of the Adsorption Process

The thermodynamic parameters obtained for the adsorption of Congo Red (CR) onto activated fish bone (AFB) revealed negative values of ΔH°, ΔS°, and ΔG°, providing important insights into the adsorption mechanism. The negative enthalpy change (ΔH° < 0) confirms that the adsorption process is exothermic, indicating that energy is released when CR molecules interact with the active sites on AFB. This suggests the involvement of physical interactions and possibly weak chemical contributions such as hydrogen bonding and van der Waals forces [21]. The negative entropy value (ΔS° < 0) reflects a decrease in randomness at the solid–solution interface during adsorption, as dye molecules become more ordered when immobilized on the adsorbent surface [22]. Furthermore, the negative Gibbs free energy values (ΔG° < 0) at all studied temperatures indicate that the adsorption process occurs spontaneously and favorably under the given experimental conditions [23]. Overall, these thermodynamic findings demonstrate that CR adsorption onto AFB is a spontaneous and exothermic process, characterized by decreased system disorder and strong adsorbate–adsorbent interactions.

Table V.3. Thermodynamic parameters for CR adsorption onto AFB.

$T(K)$	$k = Q_e / C_e$ (L/g)	$\Delta G° = -RT\ln(K)(kJ/mol)$
293	12.9261	-6.23434
303	8.0597	-5.25713
313	4.9875	-4.18169
$\ln(K) = -\frac{\Delta H°}{R}\frac{1}{T} + \frac{\Delta S°}{R}$	$\Delta H°(kJ/mol)$	$\Delta S°(J/K.mol)$
$\ln(k) = -4364.8\frac{1}{T} - 12.332$	-36.28894	-102.528

4. Conclusion

In this work, fish bone–derived materials were explored as promising and low-cost adsorbents for the elimination of Congo Red (CR) dye from aqueous media. Three adsorbents were prepared and compared: raw fish bone (RFB), activated fish bone (AFB), and calcinated fish bone (CFB). The results demonstrated that surface activation significantly enhanced the adsorption efficiency, with AFB achieving the highest removal rate of 92% within 40 min under neutral conditions. Parametric studies involving contact time, pH, and adsorbent dosage were conducted to optimize the process. The adsorption kinetics followed the pseudo-second-order

model, suggesting significant interactions between CR and the active sites of AFB. The equilibrium data were best represented by the Freundlich isotherm, revealing that adsorption occurs on a heterogeneous surface through multilayer formation. Thermodynamic evaluation confirmed that the process is spontaneous and exothermic, accompanied by a decrease in randomness at the solid–liquid interface. Overall, these findings demonstrate that activated fish bone (AFB) possesses excellent adsorption characteristics and can serve as an efficient, sustainable, and environmentally friendly material for wastewater treatment applications.

Bibliographic references

[1] M.A. Abdel-Khalek, G.O. El-Sayed, H.M.H. Gad, Removal of heavy metals from aqueous solution using rice husk ash. Environmental Science and Pollution Research, 24 (2017) 21484–21495.

[2] P. Mondal, S. George, Removal of fluoride by hydroxyapatite synthesized from fish bone. Desalination and Water Treatment, 54 (2015) 198–208.

[3] R. Tovar-Gómez, J. Alvarado, Enhancement of hydroxyapatite from fish bone by thermal activation for the adsorption of pollutants. Materials Chemistry and Physics, 262 (2021) 124306.

[4] R. Rehman, et al., A review on calcined biomass materials for pollutant adsorption: Mechanisms and applications. Journal of Environmental Management, 267 (2022) 110622.

[5] E.B. Arikan, et al., Characterization and adsorption performance of calcined bone-derived hydroxyapatite for heavy metals. Journal of Cleaner Production, 356 (2022) 131835.

[6] H.K. Lim, T.T. Teng, M.H. Ibrahim, A. Ahmad, H.T. Chee, Adsorption and removal of zinc (II) from aqueous solution using powdered fish bones. APCBEE Procedia, 1 (2012) 96–102.

[7] E.A. Ofudje, K.M. Al-Ahmary, I.F. Alshdoukhi, et al., Nano round polycrystalline adsorbent of chicken bone origin for Congo red dye adsorption. Scientific Reports, 14 (2024) 7809.

[8] Y. Chen, et al., Preparation and characterization of activated carbon from fish bone by chemical activation. Journal of Analytical and Applied Pyrolysis, 92 (2011) 303–308.

[9] K.Y. Foo, B.H. Hameed, A review on activated carbon adsorption for the removal of synthetic dyes. Journal of Hazardous Materials, 170 (2012) 552–559.

[10] M. Ghaedi, et al., Application of activated carbon prepared from fish bone waste for removal of dyes and heavy metals. Desalination and Water Treatment, 52 (2014) 6665–6674.

[11] J. Rivera-Utrilla, et al., Activated carbon modifications to enhance adsorption of organic contaminants from water. Journal of Hazardous Materials, 187 (2011) 1–23.

[12] D. Mohan, et al., Thermal behavior and textural development of biochar derived from wood and fish bone waste for environmental applications. Bioresource Technology, 160 (2014) 191–202.

[13] C. Rey, et al., Bone mineral: Update on chemical composition and structure. Osteoporosis International, 20 (2009) 1013–1021.

[14] S. Mondal, et al., Effect of calcination temperature on the structure and properties of hydroxyapatite derived from fish bone. Ceramics International, 38 (2012) 111–117.

[15] V.K. Gupta, et al., Preparation and characterization of activated carbon from agricultural waste for dye removal: Thermogravimetric study. Journal of Hazardous Materials, 162 (2009) 365–372.

[16] S. Wang, Y. Peng, Natural and engineered adsorbents for removal of pollutants from water: A review. Chemical Engineering Journal, 156 (2010) 11–24.

[17] Z. Al-Qodah, R. Shawabkah, Production and characterization of granular activated carbon from activated sludge. Brazilian Journal of Chemical Engineering, 26 (2009) 127–136.

[18] D. Mohan, et al., Biochar production and characterization: Thermal behavior and structural evolution of bone-derived biochar. Bioresource Technology, 160 (2014) 191–202.

[19] S. Sahnoun, M. Boutahala, Adsorption removal of tartrazine by chitosan/polyaniline composite: Kinetics and equilibrium studies. International Journal of Biological Macromolecules, 114 (2018) 1345–1353.

[20] F. Benamraoui, H. Boudiaf, A. Bouhank, L. Bencheikh, R. Bourzami, A. Gil, M. Boutahala, Methylene blue removal using black cumin seed waste: Experimental study and molecular dynamics simulation. Desalination and Water Treatment, 300 (2023) 167–177.

[21] K.Y. Foo, B.H. Hameed. Insights into the modeling of adsorption isotherm systems, Chem. Eng. J, 156 (2010) 2–10.

[22] I. Langmuir. The adsorption of gases on plane surfaces of glass, mica and platinum. Journal of the American Chemical Society, 40.9(1918), 1361–1403.

[23] Y. Liu. Is the free energy change of adsorption correctly calculated. Journal of Chemical & Engineering Data, 54.7(2009), 1981–1985.

General conclusions

General conclusions

This thesis investigates the preparation and synthesis of bio-based materials derived from agricultural and biological residues for application in wastewater treatment. Entitled "Preparation and Characterization of Biomaterials for Application in Wastewater Treatment," the research was carried out at the Laboratory of Chemical Process Engineering (LGPC), University of Sétif 1. The principal objective was to develop environmentally friendly adsorbents capable of removing synthetic dyes from aqueous effluents. Emphasis was placed on minimizing environmental impact while maintaining high adsorption performance through the adoption of green synthesis approaches, including plant extracts and wet chemical methods. Through a series of experimental investigations, various natural materials including rosemary, Ruta graveolens, and fish bones were transformed into activated carbon or nanoparticles and evaluated for their dye adsorption efficiency. These materials were selected due to their availability, low cost, rich surface chemistry, and documented potential for adsorption applications. The obtained results demonstrate significant potential for sustainable, low-cost materials in contributing to effective wastewater purification. They also highlight the relevance of green chemistry strategies in advancing sustainable water treatment technologies.

In the first part of this research, the focus was on exploring the adsorption capabilities of activated rosemary (AR) and iron oxide nanoparticles (Fe-P) synthesized via green chemistry. The nanoparticles were prepared using an aqueous extract of rosemary, highlighting an environmentally friendly synthesis route.

* Both materials were thoroughly characterized using a range of analytical techniques, including Scanning Electron Microscopy (SEM), Energy Dispersive X-ray Spectroscopy (EDX), Fourier Transform Infrared Spectroscopy (FTIR), and X-ray Diffraction (XRD), to confirm their structural, morphological, and chemical properties. These analyses provided essential information about surface functionality, crystallinity, and elemental composition, which directly influence adsorption efficiency.

* The adsorption experiments revealed that activated rosemary achieved a Methylene Blue removal efficiency of 94% within 40 min under basic conditions. In comparison, iron oxide nanoparticles exhibited a removal efficiency of 84% in just 20 min and showed high performance in both acidic and basic environments, indicating their versatility as adsorbents. Additionally, the reusability of AR was tested over six adsorption–desorption cycles, and the material retained a significant portion of its efficiency, confirming its stability and suitability for real-world wastewater treatment applications.

General conclusions

In the second phase of this study, Ruta graveolens was subjected to a two-step process involving chemical activation followed by calcination to enhance its adsorptive properties. This treatment was designed to improve surface area development and to increase the availability of active adsorption sites. Simultaneously, zinc oxide nanoparticles (ZnO-ACRu) were synthesized using the wet chemical method, a simple and cost-effective approach. Both the activated biomass and the synthesized nanoparticles were extensively characterized using SEM, EDX, and FTIR to evaluate their surface morphology, elemental composition, and functional groups.

*The experimental results revealed that the ZnO-modified adsorbent (ZnO-ACRu) achieved a Congo Red dye removal efficiency of 83.56% within 40 min under standard conditions. By optimizing key operational parameters, particularly solution pH and contact time, the removal efficiency was further improved to 93.38% within just 20 min under acidic conditions. This improvement emphasizes the critical role of operational parameter optimization in maximizing adsorption performance.

*These findings highlight the strong adsorption capacity and rapid kinetics of ZnO-ACRu. Moreover, the material demonstrated excellent recyclability over six adsorption–desorption cycles, indicating its chemical stability and practical potential for repeated use in wastewater treatment processes.

In the final stage of this research, fish bones were used as a low-cost, sustainable raw material to develop three types of adsorbents: raw fish bones (RFB), activated fish bones (AFB), and calcinated fish bones (CFB).

*The preparation involved chemical activation and thermal calcination, aimed at enhancing the surface properties and adsorption potential of the materials. These treatments significantly modified porosity, mineral composition, and surface functionality. These biosorbents were thoroughly characterized using the techniques previously mentioned (SEM, EDX, FTIR, XRD), confirming the structural and chemical modifications achieved through the treatment processes.

*Among the three materials, the activated fish bones (AFB) exhibited the highest removal efficiency, successfully adsorbing 92% of Congo Red dye within 5 h under neutral pH conditions. This high performance is attributed to the increased surface area and functional group availability resulting from the activation process. Although the raw and calcinated

forms also showed notable adsorption capacities, they were comparatively less efficient than AFB.

*This part of the study further demonstrates that biowaste materials, when properly processed, can be transformed into highly effective adsorbents for organic dye removal. The findings support the feasibility of using fish bone waste as a valuable resource in environmental applications, particularly in the treatment of industrial dye effluents.

Overall, this thesis contributes to the development of sustainable, low-cost, and efficient bio-derived adsorbents, offering viable alternatives to conventional materials in wastewater treatment applications.

Perspectives

Broaden Pollutant Scope: Future research may focus on evaluating the synthesized materials against a broader spectrum of pollutants, including heavy metals, pharmaceuticals, and other industrial contaminants, to evaluate their versatility and effectiveness under varying environmental conditions.

Exploration of New Green Precursors: Further exploration of plant-based extracts as natural precursors or reducing agents may lead to more sustainable and less toxic synthesis methods, thus reinforcing the environmental friendliness of the materials used.

Integration of Artificial Intelligence: The introduction of artificial intelligence (AI) and machine learning tools could be employed to optimize synthesis conditions, predict adsorption behavior, and improve overall system performance. This approach could enable real-time monitoring and adjustment of operational parameters for maximum efficiency.

Abstract

Safeguarding the environment and addressing ecological challenges are crucial steps toward improving quality of life and achieving sustainable development goals. Among the various water treatment methods, adsorption using renewable bio-based materials and nanostructured composites has emerged as a promising, environmentally friendly solution for removing persistent pollutants from wastewater. This research presents the development and detailed characterization of high-performance adsorbents produced from plant-based biomass and fish bone waste, enhanced with metal oxide nanoparticles, using environmentally friendly synthesis methods to minimize environmental impact. Three adsorption systems were developed and evaluated: activated rosemary for the removal of methylene blue, activated *Ruta graveolens* modified with ZnO nanoparticles for the removal of Congo Red, and raw, activated, and calcined fish bones for Congo Red adsorption. Experimental results revealed outstanding removal efficiencies, with activated rosemary (AR) achieving 94% methylene blue removal within 40 min, ZnO-ACRu composites reaching 93.38% Congo Red removal in just 20 min, and activated fish bones (AFB) removing 92% of Congo Red in 40 min. These findings demonstrate that low-cost, sustainable adsorbents prepared from waste materials can serve as effective alternatives for dye removal, offering both environmental and economic benefits for future wastewater treatment applications

Keywords: Adsorption, Biomass, Metal oxide nanoparticles, Green synthesis, Organic dyes, AR, ZnO-ACRu, AFB.

Résumé

La protection de l'environnement et la réponse aux défis écologiques constituent des étapes cruciales pour améliorer la qualité de vie et atteindre les objectifs de développement durable. Parmi les différentes méthodes de traitement de l'eau, l'adsorption à l'aide de matériaux biosourcés renouvelables et de composites nanostructurés s'est imposée comme une solution prometteuse et respectueuse de l'environnement pour éliminer les polluants persistants des eaux usées. Cette recherche présente le développement et la caractérisation détaillée d'adsorbants haute performance produits à partir de biomasse végétale et de déchets d'arêtes de poisson, enrichis en nanoparticules d'oxydes métalliques, en utilisant des méthodes de synthèse respectueuses de l'environnement afin de minimiser l'impact environnemental. Trois systèmes d'adsorption ont été développés et évalués : le romarin activé pour l'élimination du bleu de méthylène, le Ruta graveolens activé modifié par des nanoparticules de ZnO pour l'élimination du rouge Congo, et les arêtes de poisson brutes, activées et calcinées pour l'adsorption du Rouge Congo. Les résultats expérimentaux ont révélé des efficacités d'élimination remarquables : le romarin activé (AR) a permis d'éliminer 94 % du Bleu de Méthylène en 40 min, les composites ZnO-ACRu ont atteint 93,38 % du Rouge Congo en seulement 20 min, et les arêtes de poisson activées (AFB) ont éliminé 92 % du Rouge Congo en 40 min. Ces résultats démontrent que des adsorbants économiques et durables préparés à partir de déchets peuvent constituer des alternatives efficaces pour l'élimination des colorants, offrant des avantages environnementaux et économiques pour de futures applications de traitement des eaux usées.

Mots-clés : Adsorption, Biomasse, Nanoparticules d'oxydes métalliques, Synthèse verte, Colorants organiques, AR, ZnO-ACRu, AFB.

الملخص

يُعدّ الحفاظ على البيئة ومواجهة التحديات البيئية من الركائز الأساسية لتحسين جودة الحياة وتحقيق أهداف التنمية المستدامة .ومن بين مختلف تقنيات معالجة المياه، برزت تقنية الامتزاز باستخدام مواد حيوية متجددة ومركّبات نانوية كحلّ واعد وصديق للبيئة لإزالة الملوّثات المستعصية من المياه العادمة .يقدّم هذا البحث تطويرًا ودراسةً تفصيليةً لمواد ماصّة عالية الأداء محضّرة من الكتلة الحيوية النباتية ونفايات عظام الأسماك، ومدعّمة بجسيمات نانوية من أكاسيد المعادن، وذلك باستخدام طرق تخليق خضراء تهدف إلى تقليل الأثر البيئي. تم تطوير وتقييم ثلاثة أنظمة امتزاز مختلفة، شملت :الفحم المنشّط المحضّر من إكليل الجبل لإزالة صبغة أزرق الميثيلين، ونبتة السذاب المنشّطة والمعدّلة بجسيمات ZnO لإزالة صبغة الكونغو الأحمر، بالإضافة إلى عظام الأسماك الخام والمنشّطة والمكلّسة لاستخدامها في امتزاز صبغة الكونغو الأحمر.أظهرت النتائج التجريبية كفاءات إزالة مرتفعة ،حيث حقق الفحم المنشّط من إكليل الجبل (AR) نسبة إزالة بلغت 94٪ من أزرق الميثيلين خلال 40 دقيقة ، في حين بلغت كفاءة مركّب ZnO-ACRu حوالي 93.38٪ من الكونغو الأحمر خلال 20 دقيقة فقط، كما حققت عظام الأسماك المنشّطة (AFB) نسبة إزالة وصلت إلى 92٪ من صبغة الكونغو الأحمر خلال 40 دقيقة.تُبرز هذه النتائج الإمكانات الكبيرة لاستخدام مواد ماصّة منخفضة التكلفة ومستدامة، محضّرة من مخلفات طبيعية، كبدائل فعّالة لإزالة الأصباغ العضوية، مع ما توفره من فوائد بيئية واقتصادية واعدة لتطبيقات معالجة المياه العادمة مستقبلًا.

الكلمات المفتاحية: الامتزاز، الكتلة الحيوية، الجسيمات النانوية لأكاسيد المعادن، التخليق الأخضر، الأصباغ العضوية، AR، ZnO-ACRu، AFB.